

BRNO UNIVERSITY OF TECHNOLOGY

Faculty of Electrical Engineering
and Communication

DOCTORAL THESIS

Brno, 2019

Ing. Kryštof Zeman



BRNO UNIVERSITY OF TECHNOLOGY

VYSOKÉ UČENÍ TECHNICKÉ V BRNĚ

FACULTY OF ELECTRICAL ENGINEERING AND COMMUNICATION

FAKULTA ELEKTROTECHNIKY
A KOMUNIKAČNÍCH TECHNOLOGIÍ

DEPARTMENT OF TELECOMMUNICATIONS

ÚSTAV TELEKOMUNIKACÍ

MODELLING OF MMWAVE PROPAGATION CHANNEL FOR OFF-BODY COMMUNICATION SCENARIOS

MODELOVÁNÍ PROPAGAČNÍHO KANÁLU PRO OFF-BODY KOMUNIKACI V OBLASTI MILIMETROVÝCH
VLN

DOCTORAL THESIS

DIZERTAČNÍ PRÁCE

AUTHOR

AUTOR PRÁCE

Ing. Kryštof Zeman

SUPERVISOR

ŠKOLITEL

doc. Ing. Jiří Hošek, Ph.D.

BRNO 2019

ABSTRACT

This thesis addresses the „Modeling of mmWave Propagation Channel for Off-body Communication Scenarios“. Despite the advancements in the body area wireless networks, the 5G systems are still struggling with not enough bandwidth and large latency due to inefficient utilization of radio spectrum. This issue calls for immediate action and therefore the main aim of this Ph.D. thesis is to propose a novel mmWave off-body channel, which will enable its users to more effectively simulate the signal propagation. The proposed model is further optimized and verified against state-of-the-art measurements from the literature. Finally, the developed model is implemented into the NS-3 simulator and utilized for plethora of simulation scenarios. The main output of this thesis is the verified developed model as well as the implementation inside the NS-3 simulator, which enables a wide society to use it.

KEYWORDS

Channel modeling, mmWave, NS-3, Simulation, 5G, BAN, Body shadowing, Signal propagation, Off-body communication

ABSTRAKT

Předkládaná disertační práce je zaměřena na „Modelování propagačního kanálu pro off-body komunikaci v oblasti milimetrových vln“. Navzdory pokrokům v rámci bezdrátových sítí v přímé blízkosti člověka stále systémy 5. generace postrádají dostatečnou šířku pásma a dostatečně nízkou odezvu. To je způsobeno neefektivním využíváním rádiového spektra. Tento nedostatek je potřeba co nejdříve odstranit a právě z tohoto důvodu je hlavním cílem této práce navrhnout vylepšený model rádiového kanálu pro off-body komunikaci. Úkolem tohoto modelu je umožnit uživatelům efektivněji a přesněji simulovat propagaci signálu v rámci daného prostředí. Navržený model je dále optimalizován a ověřen vůči nejnovějším měřením, získaným z literatury. Nakonec je tento model implementován do simulačního nástroje NS-3, pomocí kterého je následně využit k simulaci množství scénářů. Hlavním výstupem této práce je ověřený model přenosového kanálu pro off-body komunikaci v rámci milimetrových vln, společně s jeho implementací do simulačního nástroje NS-3, díky čemuž je dostupný pro širokou veřejnost.

KLÍČOVÁ SLOVA

Modelování přenosových kanálů, mmWave, NS-3, Simulace, BAN, Útlum lidského těla, Propagace signálu, Off-body komunikace

ZEMAN, Kryštof. *Modeling of mmWave Propagation Channel for Off-body Communication Scenarios*. Brno, 2019, 98 p. Doctoral thesis. Brno University of Technology, Faculty of Electrical Engineering and Communication, Department of Telecommunications. Advised by doc. Ing. Jiří Hošek, Ph.D.

DECLARATION

I declare that I have written the Doctoral Thesis titled “Modeling of mmWave Propagation Channel for Off-body Communication Scenarios” independently, under the guidance of the advisor and using exclusively the technical references and other sources of information cited in the thesis and listed in the comprehensive bibliography at the end of the thesis.

As the author I furthermore declare that, with respect to the creation of this Doctoral Thesis, I have not infringed any copyright or violated anyone’s personal and/or ownership rights. In this context, I am fully aware of the consequences of breaking Regulation § 11 of the Copyright Act No. 121/2000 Coll. of the Czech Republic, as amended, and of any breach of rights related to intellectual property or introduced within amendments to relevant Acts such as the Intellectual Property Act or the Criminal Code, Act No. 40/2009 Coll., Section 2, Head VI, Part 4.

Brno

.....

author's signature

ACKNOWLEDGEMENT

The research described in this thesis has been conducted at Department of Telecommunications, Faculty of Electrical Engineering and Communication, Brno University of Technology over the years 2015 - 2019. This manuscript is, to the best of my knowledge, original, and neither this nor substantially similar dissertation thesis has been submitted at any other university. As the financial stability is essential for every researcher, I would like to acknowledge the generous support received from the grants of Brno University of Technology, which enabled me to pursue my Ph.D. study.

I would like to express my deepest gratitude to my supervisor doc. Ing. Jiri Hosek, Ph.D. for his support and guidance during my Ph.D. study. I own him a greatest respect and gratitude for his constant motivation and inspiration through many aspects of my life. Doc. Ing. Jiri Hosek, Ph.D. is an exceptional person and great professional, always ready to share his invaluable opinion.

During my international internships, I haven been very fortunate to meet and work with Prof. Luis M. Correia who has been my mentor at Instituto Superior Técnico, Portugal where I conducted research internship in 2018. This opportunity was the most important turning point in my research carrier. I would like to express my deepest gratitude for his professional guidance during my stay and after, as well as his positive attitude, exceptional work and highly valuable opinions. Special thanks goes to the Kennan Turbic for his insightful comments and positive attitude. It has been my pleasure to have countless discussions with him on my research topics. His profound knowledge and systematic approach was always very admirable.

I want to express my sincerest thanks to all my colleagues and friend for creating a professional and positively-charged environment, stimulating my effort to persistently work hard. This includes among others (in alphabetical order) Sergey Andreev, Petr Cika, Olga Galinina, Pawel Kulakowski, Prof. Yevgeni Koucheryavy, Ondrej Krajša, Prof. Jiri Misurec, Pavel Masek, Petr Mlynek, Aleksandr Ometov, Jiri Pokorny, Alexander Pyattaev, Martin Stusek, and Prof. Kamil Vrba.

Finally, and most importantly, I take this opportunity to express my heartfelt gratitude to my family, my mother, my brother and my girlfriend for their unfailing support and overall understanding. I am grateful to my mother for always being there for me, at any time, in any situation and in any place. I am forever indebted to her for giving me the opportunities and experiences that have made me who I am.

Brno

.....

author's signature

Contents

1	Introduction	9
1.1	Motivation	9
1.2	Novelty and Research Goals	12
1.3	Structure of the Dissertation	13
2	Signal Propagation at mmWaves	15
2.1	Large-Scale Propagation Channel Effects	16
2.1.1	Log-Distance Path Loss Models	18
2.1.2	Atmospheric and Weather Effects	19
2.1.3	Diffraction, Reflection and Penetration	20
2.1.4	Scattering	21
2.2	Small-scale Propagation Channel Effects	21
2.2.1	Delay Spread	22
3	mmWave Propagation Models	23
3.1	Outdoor Propagation Models	23
3.1.1	3GPP-Style Outdoor Propagation Models	23
3.1.2	Vehicle-to-Vehicle Channel Models	25
3.2	Indoor Propagation Models	26
3.2.1	Ray-tracing Indoor Channel Models	26
3.2.2	Rayleigh, Rician and Multiwave Fading Models	27
3.2.3	IEEE 802.15.3c	28
3.2.4	IEEE 802.11ad	28
3.3	Simulation tools for mmWaves	30
3.3.1	WSnet Simulator	31
3.3.2	Riverbed Modeler	31
3.3.3	OMNeT++	32
3.3.4	Network Simulator 3 (NS3)	32
4	Body Area Networks Modeling	36
4.1	BAN Channels	36
4.1.1	On-Body Channel	37
4.1.2	Off-Body Channel	38
4.1.3	Body-to-body Channel	38
4.2	Human Blockage Modeling	39
4.2.1	Self Blockage	39
4.2.2	Third Person Blockage	40

4.3	BAN Antennas	41
5	Designed Channel Model for mmWaves	43
5.1	Reference Scenario	43
5.1.1	Scenario Layout	43
5.1.2	Antennas	45
5.1.3	Channel Model Implementation	45
5.1.4	Channel Model Optimization	47
5.1.5	Verification of the Model, Comparison with Other Publicly Available Models	52
6	Analysis of Channel Model Behavior Using the Custom Model	59
6.1	NS3 mmWave Module Description	59
6.1.1	mmWave Core Module Overview	60
6.1.2	Physical Layer of mmWave Module	61
6.1.3	MAC Layer of the mmWave Module	64
6.1.4	RLC Layer of mmWave Module	65
6.1.5	Advancements of the NS3 mmWave Module	65
6.1.6	Extension of the NS3 Propagation Model	67
6.2	Simulated Scenarios	67
6.2.1	Simulation Parameters	67
6.2.2	Different Room Dimensions	68
7	Conclusion	73
	Bibliography	76
	Abbreviations	94
	List of appendices	97
A	Attachments	98

List of Figures

1.1	Body-centric communication.	10
2.1	Added attenuation to free space propagation due to the air absorption	15
5.1	Blueprint of the sample room.	43
5.2	Antenna placement on the user's body.	44
5.3	Base station and user equipment positions utilized for the model op- timization.	47
5.4	Pathloss distribution inside a room of size 10x6 m.	51
5.5	Comparison of our proposed model with real-world measurements at Boise state university campus.	53
5.6	Comparison of our proposed model with real life measurements at Queen's University Belfast.	55
5.7	Comparison of our proposed model with real-world measurements at ECIT.	57
6.1	Class diagram of the end-to-end mmWave module.	61
6.2	Class diagram of the end-to-end mmWave module.	63
6.3	SINR values based on the distance for two Evolved Node Bs (eNBs)s and two blockage objects.	66
6.4	Simulation results of complex building.	66
6.5	Simulation results of complex building with different materials used for walls.	66
6.6	SINR value estimates based on our proposed channel model.	69
6.7	SINR value estimates based on our proposed channel model.	70
6.8	Throughput of scenario with one User Equipment (UE) and one Base Station (BS).	70
6.9	Round Trip Time (RTT) of scenario with one UE and one BS.	71
6.10	RTT of scenario with one UE and one BS.	72

List of Tables

3.1	IEEE 802.15.3c channel models for various indoor environments where a human is holding a portable device	29
3.2	Most well known simulators simulation capabilities	35
5.1	Distribution fitting of proposed model results	48
5.2	Pathloss and Rician coefficients for room size of 4x2 m with reflection coefficient of 0.4-0.6	49
5.3	Pathloss and Rician coefficients for room size of 4x2 m with reflection coefficient of 0.6-0.8	49
5.4	Pathloss and Rician coefficients for room size of 10x6 m with reflection coefficient of 0.4-0.6	50
5.5	Pathloss and Rician coefficients for room size of 10x6 m with reflection coefficient of 0.6-0.8	50
5.6	Pathloss and Rician coefficients for room size of 20x12 m with reflection coefficient of 0.4-0.6	50
5.7	Pathloss and Rician coefficients for room size of 20x12 m with reflection coefficient of 0.6-0.8	51
5.8	Boise scenarios measurement parameters	52
5.9	Comparison of pathloss exponents and pathloss at reference distance for Boise airport and university campus.	53
5.10	Queens university of Belfast measurement parameters	54
5.11	Comparison of pathloss exponents and pathloss at reference distance for Queen's University Belfast	56
5.12	Institute of Electronics measurement parameters	57
5.13	Comparison of pathloss parameters for ECIT	58
6.1	mmWave Physical Layer (PHY) configuration parameters	62
6.2	Simulation scenarios' parameters	68

1 Introduction

The first part of this section will be dedicated to the motivation of this thesis, where the current status of the Body Area Networks (BANs) is described. The focus will be given onto the novel areas that are arising and their specifics. Furthermore, second part of this section will continue with detailed description of current imperfections and challenges that will be further studied in this thesis. The area of interest, which was further divided into sub-goals is also described here. In the last part, the Section 1.3, structure of the whole thesis is described.

1.1 Motivation

The communication technologies have been rapidly evolving during the past decade raising the demand for reliable and high speed communication. This demand is driven by the never-ending search of better quality of life and the advancements in almost all technology fields. Even more, with the recent boom in the online High Definition (HD) content streaming and applications of Augmented Reality (AR) and Virtual Reality (VR), the demand for very high throughput over short distances had risen exponentially (for AR and VR technologies specifically, Cisco forecasts 12-fold increase in global throughput from 2017 to 2022 [1]). To cope with these changes, the communication technologies in Local Area Networks (LANs) and BANs are still undergoing transformation from wired to wireless solutions. This BANs idea currently comprehends a wide variety of devices ranging from the sensors deployed on a human body or in the clothes fabric, that are measuring vital signals of a human body and thus providing valuable information for medical diagnosis, sports statistics and other leisure as well as professional activity reports, to a more bulky wearable devices, such as AR and VR glasses that are providing entertainment, information and industrial applications. All these devices have one key requirement in common – the radio link between them and the remote concentrator / access point needs to be very robust to fulfill the Quality of Experience (QoE) and to allow seamless transition to the already ongoing “smart” revolution, which is currently represented by the idea of smart cities and smart households. The unique placement of the devices (see Fig. 1.1) implies the need for a study of the signal propagation aspects, more precisely a proper channel characterization. This dissertation thesis is motivated by this vision of futuristic wireless system, which will be most probably part of the upcoming 5G systems, where the devices will be deployed on a human body and their wireless connectivity will enhance the user capabilities and quality of life by allowing users to be online anytime, anywhere and instantly [2].

The BANs are described as an extension of Wide Area Networks (WANs) to a personal sphere. They can be further divided into four distinct types:

- **In-Body** communications that occur between two or more devices inside a human body. This communication is mostly between implanted medical sensors and majority of the transmission path is inside the human body.
- **On-Body** communications are happening within the networks and wearable systems in direct proximity of human body. That means both Transceiver (Tx) and Receiver (Rx) are located directly on or very near the human body. Most of the communication channel is characterized by the propagation on the surface of human body.
- **Body-to-Body** communications appear between antennas placed on two or more separated human bodies. The communication principle is similar to the off-body case, but in body-to-body communication the antennas are influenced by the user body on both ends.
- **Off-Body** communications are made between the devices placed on a human body and devices placed on a remote Access Point (AP). Most of the channel is therefore represented by free space propagation and off body link.

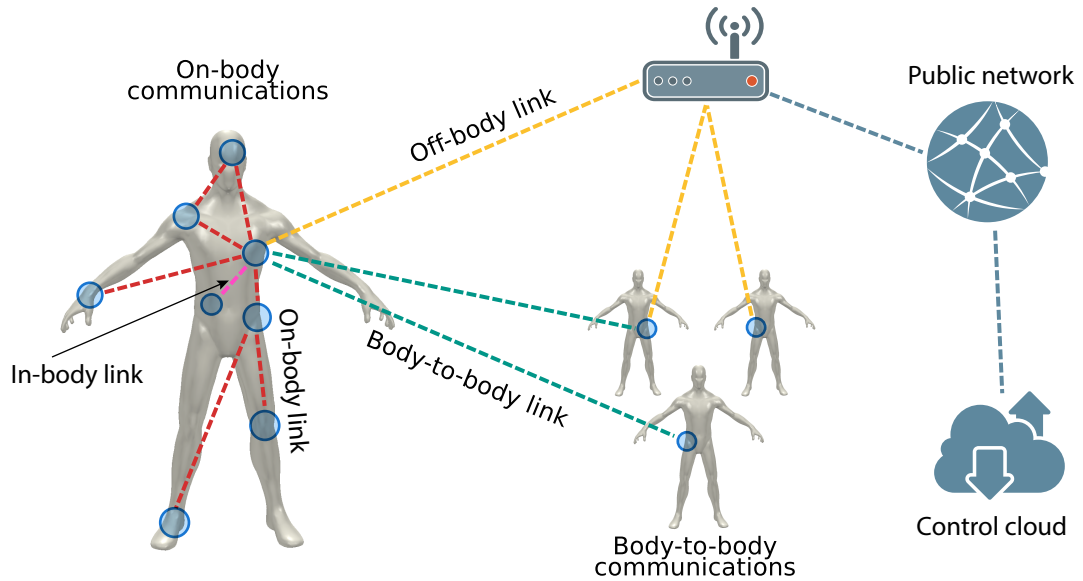


Fig. 1.1: Body-centric communication.

This thesis is focused on the off-body communication from the BAN domain. On-body and in-body communications are not covered as it would involve a comprehensive investigation of the insight of human body, which is clearly out of scope of this work.

As aforementioned, body centric communications are nowadays covering all fields of the market. The most known usages are in health-care, where BAN can be used to monitor health and motion information in real-time, sending the readings to the nearby diagnostic or storage devices, from which they can be further processed. This can not only significantly improve quality of life of patients that need constant monitoring of vital signals such as Electrocardiogram (ECG), Electroencephalography (EEG), respiratory rate, heart rate, etc., but also save time of medical personnel. Furthermore, with the rapid improvements in the hardware design, the devices are getting much smaller and some of the functions are being implemented in consumer-grade technologies (i.e., Apple Watch¹).

In military and emergency services, the wearable sensors can be used to track users motion, Global Positioning System (GPS) position, and vital signals. This can be further utilized to specialized suits that can monitor bullet wounds and share the position of the user with other soldiers [3] or, in case of firefighters, measure heat and toxicity levels together with providing important information about people and objects that cannot be seen due to the low visibility levels². For such cases, the communication link reliability is critical as any connection failure can be fatal.

For the secure authentication, BANs promise a new possibilities in form of biometric sensing. They can be used for both physiological and behavioral schemes creation, such as facial patterns, iris and fingerprints recognition. These techniques are recently being prone to forgery and duplicability, which motivated the investigations of new physical and behavioral characteristics of the human body, such as EEG and multimodal biometric systems. These authentication methods can also be used for daily life applications such as shopping (credit card authentication).

In sports, the BANs may be used for motion and vital signal monitoring. These measurements of fitness-related activities often include evaluation of heart rate, limbs position, energy consumption or fat percentage. Based on results from the measurements, data are displayed real-time to the user or are further evaluated by specialized software / personnel to optimize the athletes performance.

In both the entertainment and industrial applications, the trend is now clear – the multimedia future is wireless and belongs mostly to the AR and VR technologies. This means the communication requirements are vastly different from the aforementioned usages. The communication usually requires real-time high speed transfer of voice, video and data together, but on the contrary it is not so prone to packet loss and the security is also not so critical. Best example of this use case is the VR headset that is streaming high quality audio and video from the central unit to its inbuilt display and speakers.

¹<https://www.apple.com/apple-watch-series-4/health/> with integrated ECG

²<https://www.qwake.tech/>

In all aforementioned applications, the radio channel plays a key role in the overall system performance. The radio channel and signal propagation was extensively investigated over more than 2 decades. The technologies and standards underwent a big change during that time, evolving from the 2G, 3G and 4G to current 5G mobile communications. Together with the new standards, the supporting technologies also evolved, resulting in a myriad of channel models ranging from simple to sophisticated ones. Some of these models were results of European co-operation projects such as European Cooperation in Science and Technology (COST) 207, 231, 259, 273, 2100, IC 1004, or the European Telecommunications Standards Institute (ETSI), the Third Generation Partnership Project (3GPP) and Institute of Electrical and Electronics Engineers (IEEE) group 802 and therefore incorporated as part of them. Based on these projects, it can be concluded that there is quite profound knowledge of the outdoor channels (urban, suburban and rural) concerning the communication between mobile terminals and base stations. On the other side, most of these projects were done for the lower frequency bands of the Industrial, Scientific and Medical (ISM) spectrum. This means that there is still a lot of potential in the BANs and the higher frequency bands in the ISM spectra.

The goal of this thesis is to focus on BAN radio channeling issues, with accent given to the off-body communication at millimeter wave frequencies. The target is to create a channel model representing the communication link between the antenna on a user body and the antenna on the remote base station. The model will be further implemented into well-known NS3 to extend current model created by the New York University (NYU) and will enable more efficient and precise simulation of the indoor propagation.

1.2 Novelty and Research Goals

As it was mentioned in the Section. 1.1, the current evolution of high-speed wireless networks raised the demand for the higher throughput, lower latency networks. This sudden change increased the network scarcity that spread over multiple subgroups of devices which share the same transmission media – the wireless spectrum. The most interesting and up-to-date area of interest is the one comprised of BAN devices for VR and AR technologies and devices and applications alike [4]. Unfortunately, as aforementioned, these devices are demanding higher throughput and lower latency that the traditional ISM wireless networks can offer. To overcome these limits of the lower ISM frequency bands, there is undergoing shift to millimeter wave spectrum, which is still underutilized and able to offer two aforementioned key parameters: much wider bandwidths and lower latency [5]. Due to the complexity of this task, it has to be splitted into minor goals that will help to overcome a selected issue,

together forming a complete solution. One of this sub-tasks is to create a channel model that will help the scientific community to speed up the prototyping phase of new devices and planning of the devices / BS deployment. The main goals of this dissertation are therefore focused on the channel modeling issue, which is further divided into following sub-goals:

- Extensive study of currently available and researched high-speed wireless standards and technologies focused on the BAN.
- Evaluation of currently utilized mmWave network standards with a close attention given to the channel models.
- Based on the previous step, creation of mmWave BAN specific custom channel model to improve the simulation accuracy.
- Evaluation of the model against field measurements. Calibration of the parameters.
- Implementation of the created channel model into the NS3 simulator.
- Utilization of the NS3 simulator for a variety of simulation scenarios to provide an overview of the selected parameters impact on the signal propagation (i.e., different room sizes)

All of these tasks will be covered by this thesis, providing an comprehensive insight into the stated problem. Furthermore, the possible solutions for increasing the model accuracy and effectivity will be given together with an recommendations, how to extend it in the future.

1.3 Structure of the Dissertation

This dissertation thesis is composed of seven main chapters, which are covering author's research. These chapters are structured in logical order, providing an insight into all important parts of signal propagation modeling. The Introduction 1.1 provides a core motivation, closely followed by the research goals of this dissertation thesis. The Section 2 is dedicated to the state of art of the mmWave signal propagation. The key purpose of the this section is to lay out a complete picture of the signal propagation principles that are vital for the correct understanding and modeling of the mmWave channel. The Section 3 is providing an overview of two major groups of propagation models. For each group, the area of its usage and most commonly utilized models are described in detail. The indoor propagation models are described in more detail and greater amount of standards is discussed due to the orientation of this thesis. The last subsection is dedicated to the well-known simulation tools that can be utilized for the mmWave networks simulation. Further, in Section 4 the knowledge from previous sections is combined and extended to a BAN. This section is divided into three main subgroups. In the first one, the attention is

given to the body channels, more specifically three basic subgroups: (i) on-body, (ii) off-body and (iii) body-to-body channel modeling. The remaining two subsections are dedicated to human blockage and BAN antennas modeling, respectively. The Section 5 is dedicated to our proposed mmWave channel model. It is further divided into 5 subsections, each describing one of the key parts. Firstly, the reference scenario, which will be modeled, is described from the location point of view (i.e., room size, wall reflection coefficients, etc.), then the type of antennas and other parameters are defined. Based on this data, the model is created and implemented. Furthermore, the model is simulated for aforementioned scenarios and fitted to a log-distance model. Lastly, the resulted model is compared with field measurements from the literature. The Section 6 is providing an in-detail description of the proposed model implementation into the NS3 and its utilization for multiple scenario simulation. Firstly, the utilized mmWave module classes are described, to provide an insight into the module structure. Then the selected simulation scenarios results are discussed. Finally the conclusion is given in Section 7.

2 Signal Propagation at mmWaves

For complete understanding of the radio channel behavior (interference levels, expected communication range, transmitter power requirements, etc.) of the mmWave wireless communication links, it is necessary to start with the radio wave propagation. As it is understandable from the name, the wavelengths' size of mmWave frequencies are less than one centimeter. This translates to the fact, that everyday objects, such as cars, furniture or even humans are very big relative to the wavelengths. This induces a very pronounced phenomena, the signal blockage, when these objects are placed in the way between the transmitter and receiver. On the other hand, the scattering and reflections are enabling the possibility of keeping the wireless link active even when there is no direct Line of Sight (LOS) path between the transmitter and receiver, as long as there are implemented steerable antennas, which are able to find an object from which the signal will be reflected or scattered.

Furthermore, the wavelengths of the mmWave are so short, that even the molecules contained in the air are heavily affecting the free space propagation distance of the mmWave spectrum. The concrete numbers of the added attenuation to the well-known Friis distance-dependend free space pathloss formula for frequencies in sub-terahertz spectrum are depicted in Fig. 2.1.

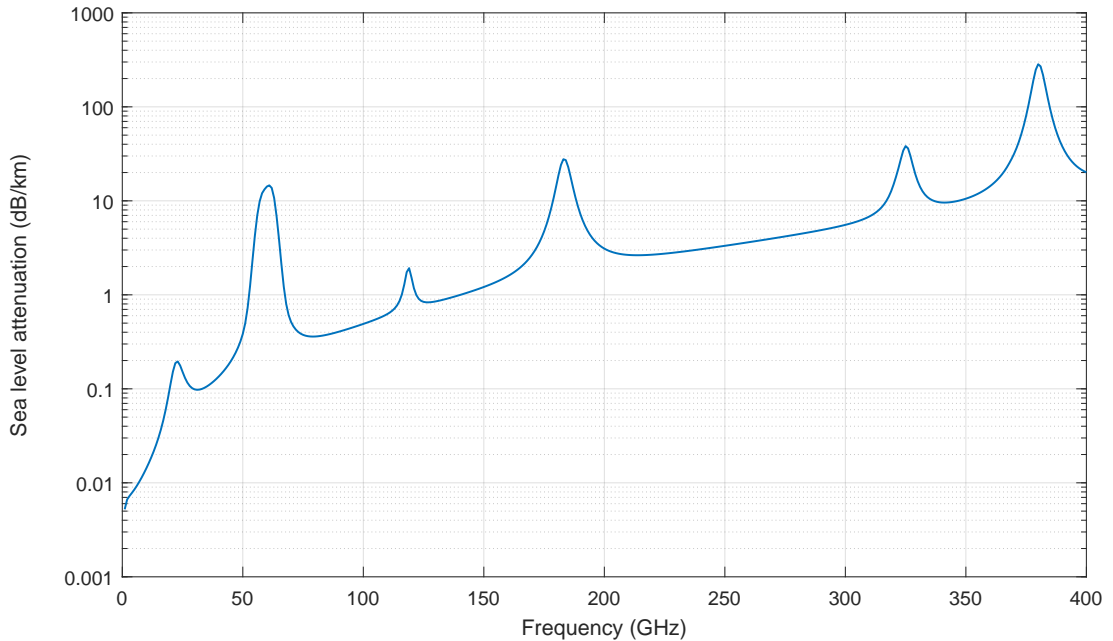


Fig. 2.1: Added attenuation to free space propagation due to the air absorption [6].

It can clearly be seen that at the frequencies of 60 GHz, 180 GHz and 320 GHz the attenuation is very high. At the first mentioned frequency, the attenuation is

caused by the interference with oxygen molecules, and in latter two it is the result of collisions with the water molecules [6]. These high-loss frequencies have very large potential for unlicensed networks that are mainly used for short range communications (up to tenths of meters), such as Wireless Local Area Networks (WLANs) that can be used for entertainment devices (AR, VR, video streaming, etc.) and similar applications. The reason is mainly the fact that the signal decay at this frequencies is very high and therefore there is much smaller possibility of interfering with adjacent networks. The atmospheric impact on frequencies ranging from the 0-50 GHz and 200-280 GHz, on the other hand, is very minor over the free space propagation loss, making them perfect enabler for the future mobile communication networks. They are feasible for both indoor and outdoor wireless networks, where large distances (hundreds or even thousands of meters) needs to be covered (i.e., backhaul links, macrocells, microcells and femtocells in emerging cellular networks). The reason why the Y axis in the Fig. 2.1 is referenced to the sea level is the fact, that the difference in altitudes greatly impact the amount of molecules interfering with the signals. For example, in the altitudes around 1 km above the sea level, the atmospheric attenuation can be 10-20 dB per km lower than at the altitudes directly above the sea level.

It is also worthwhile mentioning, that the atmospheric attenuation is not the only phenomena impacting the signal in terms of coverage or interference. For example the weather conditions, such as snow, rain or hail also introduce a great attenuation for certain frequencies. To overcome the atmospheric attenuation and weather-related losses, the future mmWave wireless systems will need to utilize adaptable antenna gain, beamwidth and beam-steering techniques. Furthermore it will enable the future technologies to minimize inter-network interference, which will be supported by utilizing aforementioned spectra and tiny antenna arrays.

From the Fig. 2.1 can also be seen, that for many of the mmWave frequencies, the additional attenuation for free space paths shorter than 1 km is reasonably small and comparable to current UHF wireless systems. Due to the fact, that the mmWave radio channel utilized by highly directional antennas is behaving differently than traditional wireless channels, especially for the BANs, this chapter starts with description of the macroscopic channel properties, known as large-scale channel effects.

2.1 Large-Scale Propagation Channel Effects

The electromagnetic wave propagation in free space is a perfect point to begin with the evaluation of large-scale wireless channel characteristics for situations, where the radiated signal power loss is characterized over distances from meters to thousands of meters. The first mathematical model of a propagation of electromagnetic waves in

free space, with no scatterers, reflections or obstructions is called free space path loss equation created by Harold T. Friis [7]. Based on this formula, the widely accepted power decay rate based on distance is 20 dB/decade.

On the contrary to this strong power decay, there is a hidden benefit for the mmWave propagation frequencies which can be deducted from the antenna aperture. Considering the fact that at the mmWave frequencies, the antenna arrays can be composed from very small directional antennas, the gain they are capable of delivering can be substantial and in some cases even produce lower overall pathloss. Even more, adaptive arrays can be used to create narrow beams (and therefore high-gain antennas) that can be steered to bounce off the surrounding scatterers and reflectors, concentrating the radiated energy only in directions that prove to be able to create a viable link for the communication path. This techniques combined with a Multiple Input Multiple Output (MIMO) and beam-combining principles, the channel pathloss can be reduced by a significant margin utilizing the possibilities of forming multiple beam paths in many different directions. If the Friis equation is extended to consider antenna arrays on both Tx and Rx, two very important notes can be concluded from the equation:

1. With mmWave carrier frequencies (i.e., 28 GHz and more), the creation of antenna arrays with dimensions that are on the order of or larger than the wavelength becomes very feasible. This is due to the fact, that the wavelength at frequencies of 60 GHz is 5 mm and 1 THz is only 0.3 mm. This not only allows engineering of very high gain antennas into small printed circuit boards, or onto a chip that can be easily fitted into modern cellphone devices (as opposite to the current mobile network antennas, where the wavelength is often much larger than the size of the whole device) but in cooperation with steerable high gain antennas also helps to overcome the great propagation path loss that comes within. In summary, the extended equation proves that the antenna array dimensions, while implemented both at transmitter and receiver sides, can help to overcome propagation path loss induced by the distance between Tx and Rx.
2. This extended Friis equation brings an entirely new design metric that can be exploited in the engineering of the size of new handheld devices. Also, the antenna systems, that are utilizing the beamsteering through selective excitement, electronic phasing and switching on and off the antenna array elements together with its small physical form factor, are the key aspects of mmWave communications.

In fact, the extended Friis equation proves that the physical size of the antennas induces a fourth-order increase in received power, thus diminishing the second-order power loss induced by the distance in free space. This was already proven by vari-

ous works presenting massive MIMO systems and steerable antenna arrays in very compact form factor [8, 9]. Also, thanks to the very new possibilities induced by the aforementioned form factor and high gain antennas, completely new wireless systems and architectures might arise [6, 10, 11].

2.1.1 Log-Distance Path Loss Models

Because the free space path loss model cited in [7] does hold for mmWave bandwidths only when the signal path is in the LOS region, that was further proven in [11, 12, 13, 14, 15], new models were created based on the 20 dB per decade decay in distance. These models are based on the generalization of the far field log-distance slope and can be described as:

$$P_r(d) = P_t K_{fs} \left(\frac{d_0}{d}\right)^\alpha \text{ for } d \geq d_0, \quad (2.1)$$

where P_t is transmitted power, K_{fs} is dimensionless constant used together with path loss exponent α to fit to the field measurements, d is the propagation distance, and d_0 (which must be $\gg \lambda$) is close-in free space path loss reference distance. Usually, in the the wireless communications and propagation analysis, the pathloss is represented by a decibel values. This is due to the ease of its use for the calculations, where the multiplication of linear (absolute) values becomes an addition in the decibel values. Furthermore, the decibels are more convenient to use for the propagation signal powers, as their range is very dynamic, changing by orders of magnitude over small distances. If the 2.1 is converted into decibel scale, it can be seen that the path loss becomes a function of the Pathloss Exponent (PLE) and the logarithm of the propagation distance, given by [16]:

$$P_r[\text{dBm}](d) = P_t[\text{dBm}] + 10 \log_{10} K_{fs} - 10\alpha \log\left(\frac{d}{d_0}\right). \quad (2.2)$$

By using the knowledge from 3.5, the received power P_r of given wireless system can be associated to the transmitted power P_t , the antenna gains G_r and G_t , and propagation pathloss of the channel. The received power P_r can than be expressed in a distance-dependent form using the decibel units by the transmitted power, antenna gains, and the pathloss exponent:

$$P_r(d)[\text{dBm}] = P_t(d)[\text{dBm}] + G_t[\text{dBi}] + G_r[\text{dBi}] + PL(d), \quad (2.3)$$

where the PL is represented as in 2.2, noting that typically the $\alpha > 2$. In special cases, where constructive interference or waveguiding happens, the $\alpha \leq 2$ can happen.

From the measurements done in the mmWave spectrum in indoor wireless channels with unobstructed line-of-sight path, the α proved to be varying in different environments such as laboratories, hallways and open spaces [17]. This varying was following an expected pattern, providing path loss exponent of $1.2 \leq \alpha \leq 1.32$ for the hallways, where the waveguiding can occur together with reflections from surrounding walls, floors and ceiling, altogether providing a constructive interference. In the open space scenarios, with very few reflectors, the $\alpha \approx 2.0$ and in laboratory environment, where the surroundings produce both constructive and destructive reflections, the path loss exponent was $1.71 \leq \alpha \leq 2.71$. By introducing the obstructions into the propagation path, the α dramatically rose to $2 \leq \alpha \leq 10$ [18]. In further measurements through the mmWave spectrum (at 28 GHz, 38 GHz, 60 GHz, and 73 GHz), the same trend continues resulting in $1.8 \leq \alpha \leq 2.2$ for LOS conditions and $\alpha \approx 5$ for Non Line Of Sight (NLOS) conditions and LOS conditions with antennas not properly facing each other. Interestingly, as the data from [19] shows, there is not much of a difference between omnidirectional mmWave channel path loss compared to current Ultra High Frequency (UHF) channels. Based on that data, it can be assumed that for LOS conditions, the Friis free space model [7] can provide adequate model, and similarly to current UHF systems, it is too optimistic for NLOS paths.

2.1.2 Atmospheric and Weather Effects

In previous Section, it was shown how the increased transmission frequency introduces additional path loss. Unfortunately, it is not the only factor – according to the [20], the signal degradation is also induced by atmospheric and rain attenuation, and path depolarization. This mainly affects the signals around the 60 GHz, where there is high oxygen absorption, as can be seen in Fig. 2.1. The atmospheric attenuation is therefore putting additional path loss (that is multiplicative in absolute terms and additive in decibel terms) to the [7] or 3.5. As it can be seen in the Fig. 2.1, this effect is occurring under normal conditions (temperature of 20°, 1 atm of atmospheric pressure and 7.5 g/cm³ water vapor density) at all the frequencies, but it becomes significant when the carrier frequency exceeds 50 GHz. In the Fig. 2.1, it is represented by a logarithmic power decrease per kilometer of transmission distance (dB/km) [6, 21].

Based on the measurements from [14], rain and hail introduce additional path loss of about 7 dB per km at frequency of 28 GHz, we can conclude that the attenuation from rain is not as high as might be expected (especially when combined with high gain steerable antenna arrays). On the other hand, measurements made in [22, 23] for two 38 GHz backhaul links, one of a 265 m length with obstructions in the path,

and the second of a 605 m with clear LOS, were less optimistic. For the former, the maximum attenuation is about 9 dB for 50 mm/hr rain rate, and the latter reach its maximum attenuation of about 16 dB for 200 mm/hr rain rate. Interestingly, the longer path suffered from multipath at heavy rains (created by the wet surfaces and water molecules in the air), creating the environment more reflective. This phenomena creates the situation, where the direct ray is more attenuated by the rain, but the reflected rays are getting stronger. Based on similar measurements, the International Telecommunication Union (ITU) approximates rain attenuation to the rain-rate R [mm/h] as described in:

$$\begin{aligned}\lambda_r(f[\text{GHz}], R) &= k(f)R^{a(f)}[\text{dB/km}], \\ k(f) &= 10^{1.203 \log(f) - 2.290}, \\ a(f) &= 1.703 - 0.493 \log(f).\end{aligned}\tag{2.4}$$

2.1.3 Diffraction, Reflection and Penetration

Diffraction on the mmWaves frequencies is becoming much bigger issue than in traditional wireless networks. Based on the information from [19], the observed signal difference is more than 40 dB, when a mobile receiver goes behind an elevator shaft and 10 dB, when the receiver moves around the hallway corner. This brings us to the conclusion, that the diffraction is the least reliable propagation mechanism for the mmWave mobile systems.

On the other hand, recent studies performed on the mmWave frequencies provide surprisingly good results for material in both indoor and outdoor environments. For example the measurements conducted in indoor and outdoor environments from 28 to 60 GHz provide a good comparison of the objects reflectivity in comparison to current microwave (1 to 6 GHz) networks. Works from [12, 14, 24] proves that human heads, metal garbage cans, lampposts and exterior walls of buildings are highly reflective with reflection coefficients more than 0.7 for most of the incident angles. This leads to the idea of overcoming the diffraction and propagation loss by utilizing highly directional antenna arrays that will be able to steer the beams to find the strongest signal components from different reflective surfaces (1st order reflections), direct and diffracted rays. Following this idea, the site-specific ray tracing methods seems to be currently the most important propagation modelling approach for planning and deployment of future indoor and outdoor mmWave wireless networks [11, 12, 25].

The aforementioned measurement campaigns also provided detailed measurements of the penetration loss of different materials. More precisely, the results from [24] prove that for the tinted glass (a glass surface with metal components

inside, usually used for outdoor windows) material, the penetration loss is about 10 dB per cm, but is only about 1 dB for clear glass material. Similar results were presented in [26], in which the penetration loss for indoor walls (such as cubicle walls, furniture, etc.) prove to be relatively low loss, i.e., 2-6 dB of loss per partition. As in [24], the loss for metal objects, such as elevator shafts, is about 40 dB.

As a conclusion from this section, we can say that for outdoor mmWave BAN signal propagation, the aforementioned phenomena will greatly influence the signal transmission. To overcome that, new usages of things such as creeping waves or body reflections would be needed. The indoor propagation scenarios, on the other side, might greatly benefit from the reflections of surrounding objects and thus providing a reliable link.

2.1.4 Scattering

At mmWave frequencies, the scattering becomes an important propagation mechanism. It causes the free space propagated power to be inversely proportional to d^4 . This means that in mmWave spectrum, some of the illuminated scatterers can reflect enough (occasionally even more) signal than reflected paths [11, 25]. Scattering models, combined with ray tracing algorithms are able to predict accurately the variations of interference and coverage by utilizing the surface roughness and Radar Cross Sections (RCSs) of objects in the channel. The RCS represents scattering objects in terms of an aperture with a specific area, which does not necessarily relate to the objects' physical area. Based on the well-known RCS model for received power from a scattered ray described in [16], we can deduce that the higher RCS, the higher received power is. This can be utilized to partially compensate for the decreased received power created by the nature of mmWaves. The smooth reflective surfaces such as lampposts and similar metallic objects proved to be valuable sources of multipath in mmWave outdoor environments [11, 14, 25]. Even though the rough surfaces such as large building facades, bricks or trees are less valuable multipath sources, some studies found out they still provide a strong scattering in various NLOS conditions [11], [14].

2.2 Small-scale Propagation Channel Effects

The evaluation of a channel also considers dramatic changes in the signal amplitude and phase that occurs after small changes (as small as a half wavelength) in the spatial positioning between Rx and Tx. These changes are referred as the small scale fading. In mmWaves, one of the most important aspect is the delay spread, which will be described further.

2.2.1 Delay Spread

Root mean square delay spread is representing a quantification of the temporal spreading effect caused by the multipath time dispersion of given channel. This simple channel parameter was observed to be relatively independent of the transmitter and receiver location inside a room [27]. The researches in this paper also measured, that the delay spread increases with the increasing room dimensions and wall reflections coefficient. Similar results were further observed in following works [28, 29, 30].

Measurements done in outdoor channels at the 28 and 38 GHz frequencies, shown different antenna beam widths impact on multipath delay spread. For the 28 GHz, the results indicate that for shorter distances, the wide beamwidths provided greater multipath delays spreads and smaller path loss exponents [11, 15]. Measurements on the 38 GHz done in New York City and Austin shown similar results, the larger multipath delay spreads for wider beamwidth steerable antennas over shorter distances. For longer LOS distances, the narrower beamwidth antennas are superior in terms of achieved gain in comparison to the multipath. This indicates the importance of implementing decision making logic into the future wireless systems that will be able to adapt the beam according to the particular multipath coefficients and received power based on the distance between the Tx and Rx [12, 25]. Based on aforementioned measurements, it is clearly visible that the directional antennas in mmWave frequencies will produce smaller multipath delay spreads and less frequency selective fading than currently utilized UHF systems that are using the omnidirectional antennas.

3 mmWave Propagation Models

This chapter is providing a basic overview of propagation models used for mmWave modeling. The most commonly used division for the models is by their targetted environment. The following sections are describing two main categories: (i) outdoor propagation models and (ii) indoor propagation models.

3.1 Outdoor Propagation Models

There are several methods used for outdoor mmWave propagation modeling. One of the most popular is the ray tracing, which utilizes geometric optics for simulation of the reflection and propagation of waves in an environment. In most cases, two to four reflections per each ray (wave) are considered, allowing usage of 2D approach if the Rx and Tx are at the same height and surrounded by much taller obstacles [31]. In notable amount of current cellular systems, a break-point models for LOS path loss with path loss exponent are utilized. These models share the same principle, having the path loss exponent of 2 (free space) for distances shorter than what is called the break-point distance, and path loss exponent of 4 for larger distances [16]. The break-point distance d_{bp} is defined as:

$$d_{bp} = \frac{20h_t h_r}{\lambda}, \quad (3.1)$$

where the h_t represents Tx height and h_r stands for Rx height. This equation indicates that with increasing frequency the break-point distance decreases. Using this equation for 60 GHz link between Tx and Rx of 1.5 m height we get a break-point distance of 9 km which is much longer that it will likely be in a real deployments. Therefore, for mmWave LOS links, the path loss is almost always anticipated to be very similar to a free space. This was found in [32] and later proofed in [13], where links on the 38 GHz and 60 GHz were measured. Furthermore, the results from [13] show that by using intelligent steering of the Tx/Rx antenna or adapting the gain/beamwidth of antenna according to the environmental conditions, the link quality can be significantly improved.

3.1.1 3GPP-Style Outdoor Propagation Models

To properly develop a global standards of future mmWave wireless systems, the engineering community requires various propagation models for evaluation of different aspects of wireless communication systems. Despite there are ongoing developments of standards for the indoor mmWave wireless networks, such as IEEE 802.11ad and

IEEE 802.15.3.c, no widely accepted models for the outdoor environments are available. This is mostly due to the fact that the technical community is still in early stages of formation, and the standard-setting activities are still in development. Currently the leading party in the outdoor model standardization is the 3GPP with its Technical Report (TR) 38.900 and TR 38.901. In this subsection we provide an overview of those two standards.

3GPP Statistical Channel Model

3GPP statistical channel model described in detail in [33] is defined for frequencies of 6-100 GHz with bandwidths up to 10 % of the carrier frequency. It also accounts for the mobility and offers multiple optional features that allow simulation of e.g., random blockage or spatial consistency. It also distinguishes three types of scenarios: (i) indoor, (ii) urban (further divided into the microcells and macrocells), and (iii) rural.

The pathloss for this model offers statistical characterization of the LOS and NLOS conditions, together with pathloss computation that is considering outdoor to indoor penetration loss [33]. The LOS/NLOS condition estimation is determined according to the positions of the UE, Base station called eNB and to the presence of buildings or obstacles in the environment. Furthermore, the model offers possibility to apply additional shadowing component.

For the small scale fading, the 3D statistical spatial approach is used. The channel is represented by a channel matrix $H(t, f)$, where t stands for time and f for frequency, of size $U \times S$, where U and S are denoting number of Tx and Rx antennas. Every entry is calculated according to the exponential power delay profile using $N \leq 20$ multipath components, called clusters, with different received powers and delays. Each cluster is further composed of 20 rays, each with its own departure and arrival angle in the horizontal and vertical planes.

The spatial consistency option is used for simulations, where the mobility is an important factor. It is further divided into two options, A and B, that are described in detail in [33]. Both options can be implemented for LOS and NLOS communication.

The last optional feature is the blockage model, that can be used to model attenuation in clusters based on their angle of arrival. It is further divided into two sub-models: (i) model A and (ii) model B. The former mentioned is utilizing the stochastic method for modeling human and vehicular blocking while the latter adopts a geometric method for the same purpose. Based on these information, it can be deducted that the blockage model A is more computationally efficient. In principle, it randomly generates $K + 1$ blocking regions, where K stands for

non-self-blocking regions and the 1 represents the self-blocking region with different parameters deducted from the UE orientation. The self-blocking attenuation is added as constant of 30 dB and the non-self-blocking one is determined based on the horizontal and vertical angles of arrival.

New York University Channel Model

New York University channel model described in [34] is based on extensive measurements of the 28 GHz and 73 GHz in New York City. These measurements were utilized to create a statistical channel model for urban areas for both LOS and NLOS paths. The NYU model also contains two pathloss models: (i) propagation loss model based on statistical characterization of the LOS state and (ii) buildings obstacle propagation loss model that is accounting for the obstacles in the path between the UE and eNB. The latter mentioned model can utilize deterministically or randomly deployed objects of different sizes to represent real-life blocking objects such as cars, buildings or even humans. To decide the LOS/NLOS state it then draws a virtual line between UE and eNB and if it intersects any of these objects, there is NLOS state. Afterwards the LOS/NLOS is decided, propagation loss is computed as in [34].

Because the channel matrices and beamforming vectors are not distance-dependent, the models implementation is utilizing pre-generated values to reduce the computation efficiency. In the beginning of each simulation, 100 instances of the spatial signature matrices together with beamforming vectors are loaded. The channel matrices are updated independently and in predefined period to simulate large-scale fading channels. On the other hand, the small-scale fading is calculated for every transmission. The rest of the parameters is assumed to be constant for the whole simulation as they are environment-dependent [34].

3.1.2 Vehicle-to-Vehicle Channel Models

Vehicle-to-vehicle communications are one of the newest and most commonly discussed applications for outdoor mmWave signals. Authors in [35] performed a measurements of 60 GHz intervehicle communications. The results from these trials show that a reliable communication using transmission powers of 2 W for distances up to 500 m is possible. Another trials made in [12] proved that LOS communication to vehicles from an outdoor Tx is possible at 60 GHz using highly directional antennas at both Rx and Tx sides with a slight attenuation. However, for the NLOS paths, the signal is greatly attenuated. Interestingly, the same study also shows that the Root Mean Square (RMS) delay spreads will be much lower than for the ones, where both Rx and Tx are in open spaces outside [12].

To correctly model the communications channels of vehicles, it has to be accounted for the impact of neighboring cars, as well as the traffic density and potential interference sources. Out of Band Emission (OOBE) scenarios and co-channel interference between satellite radio and cellular users in the 2 GHz band were explored in [36]. Similar techniques can be utilized in the future for estimating the capacity, coverage and interference for vehicle-to-vehicle communication systems. More thorough information on this topic can be found in [37], which focuses on underwater vehicle to underwater vehicle and more traditional vehicle-to-vehicle communications.

3.2 Indoor Propagation Models

To properly design the coverage, capacity or link budget, indoor channel models are needed. For frequencies above the 5 GHz, the site specific modeling is used as it is providing enough accuracy when estimating the received signal strengths, multipath components and their angles of arrival. For the development of the mmWave wireless standards, which main purpose is to unify the methodology for simulating bit error rates, PHY and MAC layer improvements, beam steering and cooperative communication methods, the statistical channel models are used. It is due to the ability of these models to account for both time delays and spatial multipath.

In the indoor environments, two major antenna characteristics can be observed for the signal multipath at the Rx: electromagnetic field polarization and antenna directivity. As the directive antennas are focusing certain directions, less space is excited and therefore energy from less space is captured. This allows directive antennas to be used for reducing of the multipath [38]. This effect can be very dramatic as shown in [39], where it reduced the RMS delay spread from 23 ns to 10 ns or in [40], where the reduction was even higher, going from 18 ns to 1 ns. On the other side, this directivity also brings issues with proper antenna alignment as the Rx and Tx antennas must point to each other.

As mentioned in Section 2.1.3, the reflection coefficients and penetration loss play a key role in proper mmWave indoor channels modeling [26, 41]. In further subsections, we present the most profound early works for mmWave indoor channel modeling of both small-scale statistical and large scale effects.

3.2.1 Ray-tracing Indoor Channel Models

Thanks to the dominance of the reflection and scattering effects combined with the lack of diffraction contributions in the mmWave propagation, ray tracing is a common and accurate method to simulate wireless channels. The main disadvantages

of this method are the need for an accurate physical model of the simulated environment and its deterministic approach [42], [43]. This approach renders the model highly site-specific and the simulation more time consuming. Statistical-based models, such as the Saleh-Valenzuela cluster model and the Rician fading, can model the environment of scenarios through stochastic parametrization and are therefore more general. These models will be described in next subsection.

It is also worth mentioning that as shown in [19, 44, 45, 46], the N-ray tracing models (where N is denoting the number of rays considered for propagation) are in general in good agreement with measurement data. Furthermore, only few reflections are necessary to take into account as the path loss is so severe that after more than a few reflections the signals do not contribute to the main signal anymore [47, 48].

3.2.2 Rayleigh, Rician and Multiwave Fading Models

The Rayleigh fading model, derived from a rich scattering channel response composed of many non-resolvable multipath components (in time or space), statistically describes the envelope of the received signal [16]. These models are usually used for the narrowband channels or low gain omnidirectional antenna systems, as these do not account for individual multipath components (common practice is to vectorially sum the randomly arriving signal energy). Each of these unresolved components is phased shifted by a tiny margin, resulting in Rayleigh distributed signal envelope. On the other side, if there is a dominant non-fading LOS multipath signal component, the signal envelope matches the Ricean distribution, where the dominant non-fading signal component serves as a baseline for the Rx signal characteristic. In the [49, 50, 51], the authors have measured the 60 GHz systems' adherence to Rayleigh/Rician fading. The authors from [49] determined, that for an outdoor urban environment covered with omnidirectional antennas, the outdoor channel does not have the richness that is needed for a highly varied fading distribution. They also discovered, that with the increasing distance between the Rx and Tx, the fading distribution grew closer to the Rayleigh fading. The results of [50] show that the Rician factor decreases logarithmically proportional to the distance. Based on that, it can be, as expected, concluded that the LOS component dominates if it is present and the strongest NLOS component is usually almost negligible, leading to the Ricean fading.

By utilizing the directional antennas at the mmWave frequencies, the need for new class of fading distributions is becoming critical. This distribution, developed by Drugin, Rappaport, and de Wolf, called Two Wave with Diffuse Power (TWDP) properly models the fading from the combination of a few strong multi-

path components above diffuse power or random noise. The TWDP distribution still contains the Rayleigh and Ricean fading distributions, that are used for special cases [52, 53, 54]. The Durgin distribution provides accurate closed form expressions for modeling impact of three specular waves combined with diffuse multipath and two specular waves. This expressions were further improved in [55]. The Durgin distribution is expected to be widely used in mmWave channels, where the strong multipath components exist in most cases due to the use of highly directional antennas [56].

3.2.3 IEEE 802.15.3c

The IEEE 802.15.3c channel model, further described in Tab. 3.1, is composed of 9 sub-models, each targeting different situation or environment [57, 58]. It is applicable for both LOS and NLOS channels and utilizing the modified Saleh-Valenzuela model for channel impulse responses simulation. The only difference is a separate LOS component representation [58]. Poisson random processes are used to model cluster arrivals and ray arrivals inside the clusters, and log-normal distributions are used for modeling the amplitudes. The cluster angles of arrival are presumed to be independent across the paths and uniformly distributed, while the angles of arrival of independent rays are Gaussian or Laplacian distributed.

The pathloss exponents are fitted for various environments, given by the tables in [58]. The path loss itself is calculated as:

$$PL = PL_0 + 20 \log_{10}(f) + 10n \log_{10}\left(\frac{d}{d_0}\right) + \chi_\sigma, \quad (3.2)$$

where the frequency dependent term is excluded for selected environments. The mean number of clusters in IEEE 802.15.3c ranges from 3 to 14, but usually lies between the 3 and 4 [59]. It is also worth mentioning, that authors from [18] discovered, that the amount of clusters do not follow specific distribution, but are highly environment-dependent with statistical nature.

3.2.4 IEEE 802.11ad

The IEEE 802.11ad model is comparable to the IEEE 802.15.3c, but is more precise thanks to the wide commercial activity that is surrounding the 60 GHz mmWave communications. As it was described in [60], the channel model primarily focuses on temporal and spatial effects together with capturing the amplitude, phase, and polarization channel impacts and characteristics.

Similarly to the aforementioned IEEE 802.15.3c, the IEEE 802.11ad channel model is exploiting the well-known Saleh-Valenzuela channel model and most of it

Tab. 3.1: IEEE 802.15.3c channel models for various indoor environments where a human is holding a portable device

Channel Model	Scenario	Environment	Description
CM1	LOS	Residential	Typical furnished home with multiple rooms. Similar size as a small office. Floor and walls are from concrete or wood, covered with paper or carpet. Windows and wooden doors are present.
CM2	NLOS		
CM3	LOS	Office	Typical office setup with multiple desks, chairs, and computers. Other furniture such as cabinets, whiteboards and bookshelves are present. Metal or concreted walls, covered by plasterboard or carpet. Windows and at least one door are present. Can be used to simulate cubicle, laboratory and open and closed office.
CM4	NLOS		
CM5	LOS	Library	Typical small sized library with multiple chairs, desks and book/-magazine filled metal bookshelves. Concrete walls. At least one side with windows and/or door.
CM6	NLOS		
CM7	LOS	Desktop	Typical office and computer clutter. Typically surrounded by cubicles.
CM8	NLOS		
CM9	LOS	Kiosk	Typical station in a public space such as mall. Users are intended to be positioned directly in front and close (1-2m) to the device.

was derived from a rigorous ray-tracing measurements of a conference room environment. The IEEE 802.11ad model exploits the Friis free space formula for LOS paths [59] and following equation for the NLOS paths:

$$\beta_i(dB) = 20 \log_{10} \left(\frac{g_i \lambda}{4\pi(d + R)} \right), \quad (3.3)$$

where the λ is the wavelength, g_i stands for reflection loss of the i^{th} path, d is the distance between Rx and Tx, and R represents the NLOS distance excluding the LOS path distance.

The IEEE 802.11ad channel model provides two use-cases: (i) Station-to-Station (STA-STA) and (ii) Station-to-Access Point (STA-AP) [60]. For these scenarios, both LOS and NLOS paths are further considered and based on the condition, the impact of selected number of reflections added. The average number of clusters for each scenario is based on the results from previously mentioned work [60].

3.3 Simulation tools for mmWaves

From the beginning of the wireless communication networks, there was a need for efficient planning and deployment. In recent years, the evolution of the networks sped up even more, introducing us to the 5G era. Although the hardware for the 5G and the mmWave deployment is already available at the market, its price is still very high for both testbeds and commercial deployments. As this fact is causing significant delays in the evolution and optimization of mmWave networks, protocols together with the deployment of the real hardware. To mitigate this, a variety of simulation tools arose. In this section, the overview of currently available BAN, mmWave or both-capable simulation tools together with the implementation details, is presented.

Despite the fact that there is a wide variety of simulators on the market, such as the WSNNet [61], OMNeT++ [62], Riverbed Modeler [63], NS3 [64] and NS3 [65], there is none, which directly supports full mmWave BAN simulation. On the contrary, most of them provide a certain level of user customization. This usually comes in form of module, library or program extensions, which enables users to create their own modules with desired functionality. The insight to what additional steps are needed to be taken in order to create the modules and enable full mmWave BAN simulation is given in following subsections.

3.3.1 WSnet Simulator

The WSnet simulator (currently in version 9.07) is a free, event-driven wireless network simulator. It is capable of network nodes simulation as an arbitrary assembly of blocks that represent software or hardware components or resource/behavior of the node. The big advantage of this simulator is its associated platform simulator WSIM, that enables users to perform a full hardware events simulation inside the nodes. Together, these two simulators can simulate complete sensor network. Furthermore, in the CORMORAN project [66], the WSnet simulator was interfaced with the PyLayers simulator [67], creating the first mobility-enabled physical simulator coupled with a packet-oriented simulator. Authors from [68] adapted the WSnet to fulfill upper layers' requirements by exploiting the PyLayers path loss, shadowing, fading, and interference simulation capabilities. They also utilized the Matlab Mobility Modeling Tool for modeling the bio-mechanical mobility. The resulted WSNet adaptation empowers users to simulate BAN channel models, radio link, and mobility models according to the IEEE 802.15.6 standard. Based on the above mentioned, it is possible to conclude that by changing the propagation model of this adaptation, it will be possible to simulate the mmWave-based BAN networks. It is also clear, that creation of such scenario will require a proficient knowledge of all the utilized programs and simulators, together with the peculiarities of mmWave propagation.

3.3.2 Riverbed Modeler

The Riverbed Modeler (currently in version 18.7.1 [69]) is also well-known and broadly used wireless network simulator. Formerly, it was known as the OPNET Simulator, and during its lifetime it evolved into licensed simulator with considerably large and active community. Its main strength lies in the support of huge amount of wired/wireless protocols and vendor devices, hierarchical modeling environment, and scalable wireless simulations incorporating terrain, path-loss and mobility models. In order to create accurate system level simulations of the mmWave BANs, utilization of all aforementioned parts is needed. Despite the Riverbed Modeler was used to simulate BAN-specific scenarios [70, 71], it does not take in account all of the BAN propagation aspects (i.e., human body mobility). On the other hand, according to the work done in [72], the Riverbed Modeler Wireless Suite can be modified in its pipeline stages to extend or create its propagation models [73]. This can be further bridged with the Wireless Body Area Network (WBAN) module¹ to produce a realistic BAN simulation. By leveraging the 3D Network Visualized (3DENV), the

¹<https://github.com/billryan/WBAN-OPNET-Simulation>

simulation can be even shown in 3D space [74, 75]. Riverbed Modeler was also used in [76], where authors proposed mmWave heterogeneous network architecture. Based on mentioned works, it seems possible to create mmWave BAN simulation module, but it will require utilization of all mentioned parts, and a lot of effort.

3.3.3 OMNeT++

OMNeT++ (currently in version 5.4.1) is an extensible, modular, component-based discrete event simulator written in C++ [62]. It supports several specifically designed frameworks for BAN simulation. The most well-known are Castalia [77] and INET [78] (previously known as MiXIM) [79]. Castalia was developed to support BAN and Wireless Sensor Network (WSN) simulation. Among others, it contains Media Access Control (MAC), radio and mobility models and utilizes log-normal shadowing model in its default settings [80]. This default model is operating in 2D space, but can be expanded to 3D if the computational difficulty is not an issue [80, 81]. The INET framework primarily focuses on the first layer of the well-known ISO-OSI model and on detailed models of radio wave propagation, interference estimation, radio transceiver power consumption and wireless MAC protocols [78]. It also integrates channel models, such as MoBAN, that further extends the accuracy of lower layers and therefore increases the realism of the simulations [82]. Both Castalia and INET are capable of the mmWave BAN simulations, but to do so, the channel and mobility models need to be updated.

3.3.4 NS3

The network simulators family (NS, NS-2, and NS3) started in 1989 [64]. The latest version, NS3 [65], is an open-source discrete-event simulator that under development since 2006. Even-though the NS3 is considered as a successor of the NS-2, and both are written in C++, they are not compatible. The reason for this lies in the fact, that NS3 was written from scratch to provide better performance and user experience, and therefore denying the backward compatibility. Concerning the BAN simulations, the NS3 was utilized in few studies, such as [83], which is targeting a mitigation of interference between multiple Time Division Multiple Access (TDMA)-based WBANs. In this study, authors omitted the impact of the mobility and channel models, and focused solely on the TDMA scheduling. Authors in [84] proposed a WBAN module for the NS3, which they further evaluated in terms of simulation speed and complexity against the NS-2 implementation. Their proposed model utilizes Carrier-Sense Multiple Access with Collision Avoidance (CSMA/CA) protocol together with PHY and MAC modules and therefore also not taking in the account all of the BAN communication peculiarities. If the model should be used

for complete BAN simulation, the realistic channel and mobility models will need to be added.

From all aforementioned (and currently available) simulators, the NS3 is the only free simulator that contains implementation of mmWave model. This implementation is done in the module called ns3-mmWave, which was designed by a NYU research team [85] and is heavily based on the Long Term Evolution (LTE)-Evolved Packet Core (EPC) Network Simulator (LENA) [86]. It consists of propagation and channel model coupled with physical and MAC layers. Currently, there are three different channel models included in the module: (i) 3GPP Statistical Channel Model [87], (ii) Ray-tracing-based (e.g., Winprop [88]) or Measurement Trace-based Model (e.g., Quadriga [89]) and (iii) NYU Statistical model [34, 85]. All those models suffer from specific imperfection that are based on the input assumptions made to simplify the simulation model and make the simulations less time consuming.

The NS3 mmWave NYU module currently provides a custom implementation of three different channel models. The reason to offer multiple models is to offer a trade-off between computational complexity, flexibility and accuracy of the results. The most flexible one, described in [90], is based on 3GPP channel model and operating in frequency bands ranging from 6 GHz to 100 GHz [87]. It allows outdoor to indoor communication modelling while providing a spatial consistency of mobility-based simulations and a random blockage model. The second model is utilizing the ray-tracing principle. This restricts the usage of the model only for simulations, where the ray traces from measurements or ray-tracing software are available [91]. This makes the model very accurate and realistic, but also bound to a limited number of ray-tracing routes. This usually leads to use of the other modules due to their higher versatility. The last available model is the statistical channel model based on pre-calculated MATLAB traces [34], that effectively reduces the computation complexity but also restrains the model only to the 28 GHz and 73 GHz frequencies. In following paragraphs, we provide a brief overview of aforementioned pathloss models:

1. 3GPP Statistical channel model described in [87], is applicable for bandwidths up to 10% of the carrier frequency and takes the mobility in account. The implementation of its pathloss model is in NS3 mmWave module's `MmWave3gppPropagationLossModel` class, which contains pathloss computation that accounts for the outdoor to indoor penetration loss as in [87]. It also contains a simple LOS/NLOS condition characterization algorithm. The `3gppBuildingPropagationLossModel` class is used to determine the LOS/NLOS condition based on the presence of buildings in the scenario and reciprocal position of eNB and UE. The utilized formula for the NLOS pathloss computation taken from [87] is:

$$PL = 35.3 \log_{10}(d_{3D}) + 22.4 + 21.3 \log_{10}(f_c) - 0.3 \cdot (h_{UE} - 1.5), \quad (3.4)$$

where d_{3D} denotes the 3D distance between eNB and UE, f_c is the center frequency and the h_{UE} is the height in which is the user terminal.

2. Ray-tracing model uses software-generated or measured traces for channel modeling. It can be used with data from any ray-tracing software (i.e., WinProp [92] or Wireless InSite [93]) that can generate trace samples with number of paths and angle of arrival or departure, delay and propagation loss for each of the paths. This renders the model very accurate but also constrains it in the way of flexibility – it is needed to choose the simulation scenario before the simulation starts. Also the scenario cannot be random since it has to be input into the ray-tracing software.
3. NYU Statistical model is based on a statistical models described in [34]. It contains two pathloss models differing in the way of computing the LOS/NLOS condition. The first leverages the statistical characterization of the LOS/NLOS state and the other is utilizing the NS3 buildings module to decide. In principle it draws a virtual line between the UE and eNB and if this line intersects any of the buildings there is NLOS, otherwise its LOS. The buildings can be placed randomly or deterministically to mimic the users, cars, buildings and other blocking objects. After the LOS/NLOS is determined, the actual path loss is calculated via following formula:

$$PL = \alpha + \beta \cdot 10 \log_{10}(d), \quad (3.5)$$

where α and β are constants taken from [34] and the d is distance between the UE and eNB.

All those models deal with the propagation loss in similar way – they do not account for the attenuation from objects based on their thickness. That results in very inaccurate simulations in scenarios with multiple sources of blockage or varying thickness of objects. To mitigate this issue, we present an enhanced penetration loss model described in the next section.

All of the aforementioned simulation tools are summarized in Tab. 3.2, providing not only overview of their characteristic parameters but also the information about their suitability for mmWave simulations. Based on this overview, it can be seen that even though there are simulators capable of either BAN or mmWave simulations, there is currently no simulator capable of native mmWave BAN simulation. However, with the aforementioned knowledge of the signal propagation principles and utilizing

Tab. 3.2: Most well known simulators simulation capabilities

Criteria	WSnet	Riverbed Modeler	OMNet++	NS3
Language	C++	C, C++	C++	C++
License Type	CeCILL	Paid	Academic public license	GNU GPLv2
Supported OS	Linux	Windows, Linux	Linux, macOS, Windows	Linux, macOS, Windows
GUI Support	Yes	Yes	Yes	Yes
BAN	✓	✓	✓	✓
mmWave	X	✓	X	✓
mmWave BAN	X	X	X	X

the developed model described in further chapters, the BAN simulation of certain scenarios will be possible.

4 Body Area Networks Modeling

As the technological advancement in mobile and wireless communications undergone a huge transformation of the well-known, massively deployed cellular systems (i.e., Global System for Mobile Communications (GSM), Universal Mobile Telecommunication System (UMTS), LTE), new subgroups of the networks, such as the BANs, emerged. They is a natural evolution of the wireless networks into the shorter range systems, that are needed for nowadays high-throughput requiring devices and services. The BANs are defined as networks in near proximity of the users, and therefore they have to take into account the influence of the human body on the signal. In this section, the state of the art of mmWave BANs modeling is provided.

4.1 BAN Channels

As the communication performance of the BANs primarily relies on the link quality between nodes, there is a need for optimized system design. To effectively design the systems, a precise channel models that are considering the peculiarities of the body-centric communications are needed. These models should take into account the frequency detuning, body blockage effects and the influence of human body dynamics. Thanks to the nature of the mmWave frequencies, the body dynamics of the wearable antennas also need to consider even the smallest body movements, such as the breathing.

Another issue known to affect the mmWave BANs is the need for lower Tx powers, which results in less strong Multipath Components (MPCs) from the surrounding environment coming to the Rx, virtually proving the Modulation and Coding Schemes (MCSs) from further objects negligible. In addition to that, the nature of the antenna position increases the probability of blockage effects coming from surrounding humans.

Thanks to the different dominant effects of the channel and its intrinsic characteristic, the BAN communications are divided into three sub-groups: (i) on-body, where both Tx and Rx antennas are placed on the surface of the same human body, (ii) off-body, where the Tx is on a surface of a human body and Rx is remote access point (i.e., on a wall), and (iii) body-to-body, where both Tx and Rx are placed on a surface of a human body, but each antenna is on a different user. In following paragraphs, these models will be described in more detail.

4.1.1 On-Body Channel

The on-body channel is characterizing communication that is happening in close proximity to the surface of a human body. Interestingly, most of the channel models focus on the unlicensed 60 GHz (V-band) and 94 GHz (W-band, unlicensed only for indoor use). These two bands are utilized thanks to their oxygen absorption levels, which makes them ideal candidates for on-body, short range, wearable networks. Most of the on-body propagation models are considering several on-body antennas locations (typically, head, torso, waist, arms, hips, feet, etc.), from which they derive stochastic models based on extensive measurements or mathematical electromagnetic models. Furthermore, researchers are focusing on various link topologies based on those locations, such as helmet-to-all body [94], head-to-shoulder [95, 96], waist-to-torso [96], etc. Even more interesting are the antenna placements that are utilizing the mmWave nature, such as skin-penetration (that should be around 0.5 mm [97]), offering possibilities to use implant antennas [94]. Even though, some studies are also considering the human body dynamics like a crawling [94] or even mixed regular daily activity [98], the most common scenario is still the standing pose [94].

From the viewpoint of the channel model complexity, the simplest mmWave channel models are generally represented by a simplified function of distance between the Tx and Rx, which is further augmented via a random component that is normally distributed with zero mean and standard deviation σ . The more complex models include separation of the short-term and long-term fading components, such as the fast fading approximation by the Cauchy-Lorentz distribution [99], where the long-term components were considered log-normal. Delay spread, that might be used as a prerequisite for the PHY-level algorithms or Doppler power spectral density (critical i.e., for respiration [100]) are also critical for accurate modeling. Another way of complex modeling is presented in [101], where the creeping wave theory is used for studying the propagation of vertically and horizontally polarized electromagnetic fields around a cylinder that has an electromagnetic properties of a human body.

Interestingly, the well known clustering models, such as Saleh-Valenzuela and its modifications are not yet applied to the on-body propagation modeling in mmWaves. However, they might be used in future for more detailed link-level simulations. Similarly, to the best of author's knowledge, there is only one study that derives a Markov process model for 60 GHz on-body communication link and provides the time periods distribution parameters in case of the received signal is stronger than threshold corresponding to 0.001 Bit Error Rate (BER) and when the communication is down.

4.1.2 Off-Body Channel

There are several studies of the off-body mmWave channels in the literature. Majority of them are based, as discussed in Section 3.1, on narrowband channel measurements and are exploiting the statistical channel models [102, 103, 104].

Authors in [102] presented a simple model with Mean Path Loss (MPL) parameters obtained from wearable antenna (placed on a users chest) indoor measurements conducted in a 60 GHz frequency band. The indoor environment was divided into two scenarios: (i) laboratory and (ii) seminar room. For each of the scenarios, the MPL parameters were measured based on the blockage / shadowing done by the user, creating a LOS/NLOS specific values. Furthermore, they investigate the MPL values spread around the models predictions, based on which they concluded the linear function of distance as a good model.

More comprehensive study was done in [103], where authors conducted measurements at 60 GHz in indoor, outdoor and anechoic chamber environments. The utilized scenario composed of user with antenna on his chest walking towards and away from the off-body antenna. The results of the measurements are a gamma distributed random variable for large-scale fading and Rice and Nakagami-m distributions for the small-scale variations in the LOS and NLOS cases, respectively. Similar measurements were further conducted in [105, 106], where the UE was placed in the pocket or held by its user against the head.

For the wideband off-body channels, authors in [107, 108] presented a simple ray-based model of the body blockage losses for 60 GHz indoor environment that utilizes the creeping wave propagation theory. The model is capable of deriving the amplitude distribution of the multipath components for the on-body antenna placed in the front and back shadowing regions, in the situations, where the TWDP model is suitable.

Another wideband model implementation is presented in [109], where authors utilize the well-known Saleh-Valenzuela model for the channel impulse response. The model parameters are estimated based on the results from 60 GHz indoor measurements with 4 Gb bandwidth for three wearable antenna locations: wrist, head and belt.

4.1.3 Body-to-body Channel

The Body to Body (B2B) body channel is still the least explored area of the BANs, and with respect to the mmWave frequencies, there are very little resources. Most of the available works are done by the Cotton et al., where authors analyze the B2B channel via the ray-tracing simulations [110, 111, 112].

Authors in [110] provided angular and delay characteristics of the B2B channel for a soldiers sweep and search operation in combined outdoor and indoor environments based on aforementioned simulations. In [111] they further investigated the channel, which resulted in observation of greater angular and delay dispersion inside the indoor environments.

In [112], a different look on the B2B channel is taken. Authors used the inter-BANs ray-tracing to analyze the interference between BANs operating on 60 GHz and 2.45 GHz. The results of this comparative analysis showed, as expected, that the 60 GHz frequencies allow coexistence of multiple BANs on the same areas.

As it can be seen from all the aforementioned sections, the need for BAN channel model capable of body shadowing simulation is still needed. The best way to satisfy this demand is to further develop the currently available models and propose an easy to use channel model, which can be implemented into well-known simulators. This approach was used in this thesis to create a new off-body channel model.

4.2 Human Blockage Modeling

As the human blockage (shadowing) is a severe problem that is affecting the wireless mmWave communications, many channel models take it into account [113, 114, 115]. Various types of models have been proposed to simulate the human blockage, such as knife-edges, cuboids or cylinders [114, 115, 116]. These models can also be described via the type of the blockage, that can be either self-blockage, which is induced by a shadowing of users body, or third-person blockage that is caused by people around the user. In this section we provide a basic overview of mentioned models.

4.2.1 Self Blockage

Thanks to the nature of the BAN antennas, which causes them to be in very close proximity to the human body surface, the blockage from the user yields higher losses when compared to the third-person blockage. This blockage is the most critical in the B2B communication, where both antennas are susceptible to the shadowing, which, in the worst case, can produce a double signal loss (shadowing from both users at the same time).

Interestingly, the self blockage at mmWave frequencies received very little attention, leaving the works in [117, 118] the only ones considering it. The proposed model is based on a simplified version of Uniform Theory of Diffraction (UTD) for mmWave frequency body-diffracted fields, derived for a cylinder representation of the body.

Other works available in the literature are using the common approach, where the user blockage is considered as a part of the radiation pattern [119, 120, 121, 122]. The simple model adopted in [119] uses a rectangular shadowing region in the angular azimuth-elevation domain, in which it applies additional 30 dB loss to all associated MPCs. This shadowing region is represented by its center point, height and width, where the values for landscape and portrait orientations of the mobile terminal are provided. Because the rectangular shadowing region is not ideal representation of the users body shadowing, authors in [120, 121] use more realistic approach, when the user blockage effect is directly incorporated into the radiation pattern of the mobile terminals antenna. The downside of this approach is the inability to account for user dynamics and the required equipment, which is needed for complex measurement procedures and is fairly expensive.

4.2.2 Third Person Blockage

A third person blockage models in mmWave is currently a hot topic thanks to its big impact on the transmission channel. Several different modeling approaches for this kind of modeling can be found in the literature, including the ray-based methods that are modeling the interaction of propagating waves and humans, and empirical models for the time-varying loss during body-blockage events.

Ray-based Methods

The ray-based methods are modeling the interaction between human body and propagating waves in a deterministic way. These methods usually utilize simplified geometric representations of the human body, and exploit diffraction theories, such as Knife-Edge Diffraction (KED) [123] or Geometrical Theory of Diffraction (GTD)/UTD [124, 125] for calculation losses added by the diffraction of signals around the human body.

The KED models typically utilize a perfectly absorbing flat screen as a representation of a body blockage profile of the human [126, 127] or its projection onto the perpendicular plane to LOS direction [128, 129]. The first KED model implementation of the body blockage was proposed in [126], and was soon adopted for mmWaves with a number of modifications in [127, 128, 129].

The alternative to the KED models are the GTD/UTD theories that can be utilized to calculate the field intensity diffracted around the human body [124, 125]. The most common way how to employ the GTD/UTD is to use the cylindrical representation of a human body [115, 116, 130, 131]. Based on the GTD/UTD research done in [132, 133] for the smooth curved surfaces, the incident field that is tangential to the cylinder excites two surface creeping waves, that travel along the

geodesic arc around both sides of the cylinder, while partially scattering the energy in tangential directions, and therefore into the shadowed region. Even though the cylinder diffraction GTD/UTD is a 3D method [116, 131], in general, it is simplified to a 2D problem by assuming horizontal propagation of the waves [115, 130, 134]. According to the [134], the shape of the cylinder is almost negligible for the blockage losses prediction, which further proves that the 2D simplification is a viable solution. It also needs to be stated, that the radius of the circular cylinder does impose a significant influence on the blockage losses at mmWaves. This means that the blockage losses are greatly dependent on the human body proportions and body part, that is obstructing the LOS [115].

Stochastic Geometry Based Models

Stochastic Geometry Based Models are generally used to model body blockage effects in crowded environments. This approach is using the distribution of people in the area around the Tx and Rx to derive the blockage probabilities [135, 136]. This blockage probability is commonly obtained for a cylindrical representation of the human body and for a people distribution inside the environment governed by a Poisson Point Process.

This method was used in [135], where authors derive the path loss based on the LOS blockage probability for normally distributed heights of people (based on typical population data) in a crowded environment around a base station. The results of the study are provided for both arbitrary and point assumptions of the Rx, corresponding to a single antenna and antenna array at the Rx, respectively.

It should be noted, that the stochastic geometry-based models are useful for general network planning purposes due to their results, which are provided as the average performance metrics (such as mean Signal to Interference plus Noise Ratio (SINR), average system throughput and outage probability). These models also do not account for the dynamics aspects of the body blockage effects, however the provided blockage probabilities can be utilized together with empirical blockage models to simulate the time varying channel behavior.

4.3 BAN Antennas

Wearable antennas are the essential components for the BAN communications. Genarally, they are either integrated into the fabrics (as shown in [137]), inside the garment accessories such as belts ([138]) or buttons ([139, 140]) or inside the handheld devices [141]. More recently, 3D printing technologies and Additive Manufacturing (AM) are being investigated as supporting techniques in fabrication of

wearable antennas [142, 143].

The AM manufacturing introduces new possibilities in terms of waste and cost reduction together with enabling designs that would be extremely difficult to realize through conventional methods. Interesting idea was presented in [144], where authors utilized inkjet printing to develop a co-planar waveguide fed antenna that can be used in unmanned paper vehicle applications. The AM was also recently presented in [145, 146], where the former 3D printing was used for circular polarized wideband mmWave antenna and in latter, authors propose three different 3D printed plastic antennas: flat lens, 3D lens, and a rod that can be used for different Radio Frequency (RF) sensing application on frequencies around 122 GHz. Similar work was done in [147], where authors propose 3D printed 28 GHz patch antenna for 5G wearable applications (i.e., to be put into medallions).

In contrast with aforementioned techniques, there are many works studying the possibilities of using of high gain directional antennas with beam steering capabilities [11]. These antenna arrays were studied in [90, 148], where authors focused on 5G mobile terminal applications. Furthermore, in [120, 122] focused on the user effects on the 28 GHz mobile terminal antennas and their results show that the user shadowing plays a key role in the antennas performance. On the other side, currently there are very little studies about users effects on the 28 GHz phased antennas arrays. Authors in [149] presented a finger ring phased antenna array for the 28 GHz frequency, which they further verified in free space. The results have shown that the coverage efficiency was of 70 % for 7 dBi gain.

5 Designed Channel Model for mmWaves

This chapter will focus on designed in-detail mmWave channel modeling scenario. The reason for this scenario is mainly the fact, that, as described in 4, there are very few works targeting the body shadowing modeling in off-body mmWave spectrum scenarios. Furthermore, most of these models are utilizing static transmitter and receiver or focus on communication between vehicles. Even fewer scientific works consider scenarios with mobile devices (such as hand-held phones) operated by dynamic users. They are further restricted to forward motion with constant velocity and do not account for body postures [121].

5.1 Reference Scenario

The reference scenario is focusing on indoor off-body communication, represented by a rectangular room with predefined measures as depicted in Fig. 5.1. The idea of this scenario is to model the propagation loss of mobile terminals and devices that are operating in near proximity of a human body (such as hand-held phones) or directly on it (AR/VR glasses, sensors, etc.) that are communicating with the static wall-mounted BS.

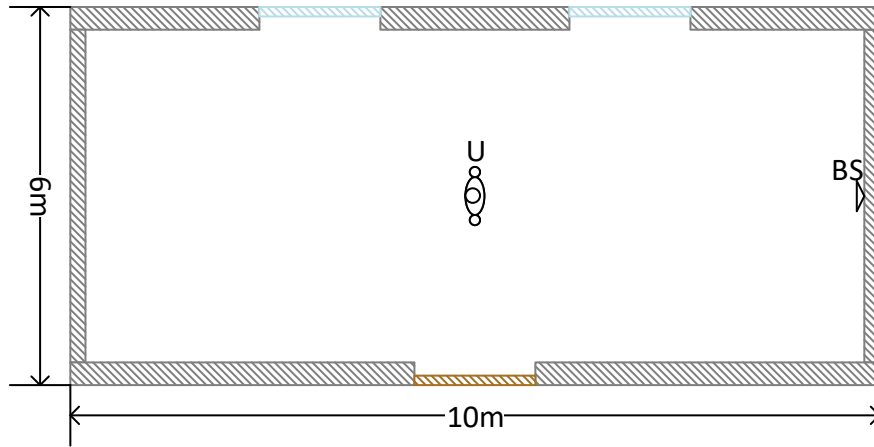


Fig. 5.1: Blueprint of the sample room.

5.1.1 Scenario Layout

As aforementioned, the footprint of the scenario was chosen to be rectangular, representing the most common room shapes. The measures of the room were further adjusted to simulate specific cases such as closet (4 x 2 m), study room (10 x 6 m),

and seminar room closet (12 x 20 m). As the inside objects of the room, such as wall-papers, posters, image frames, and other types of traditional room equipment are specific to each room, it was decided to simulate them using probability function. Other items inside the rooms are omitted for the time being, but are planned to be added in future work.

The position of the UE antenna is dynamic and can be placed at any location inside the room, therefore effectively simulating user movement. The BS position is fixed, representing a wall-mounted BS, as it would be in a real scenario. Similarly, the height of the UE antenna is 1.6 m from ground, which is the statistical average of human height. The height of the BS antenna is set to 2 m, which is the usual height of the antenna placed on the wall or near the ceiling. The UE antennas are further divided into several on-body locations (see Fig. 5.2):

- Head, where the antenna can be put either on left (He_L) or right side (He_R)
- Chest, where the antenna is placed directly on user's middle chest from the front (To_F) or back side (To_B)
- Wrist, where the antenna is situated at the right arm of the user (Wr_R)

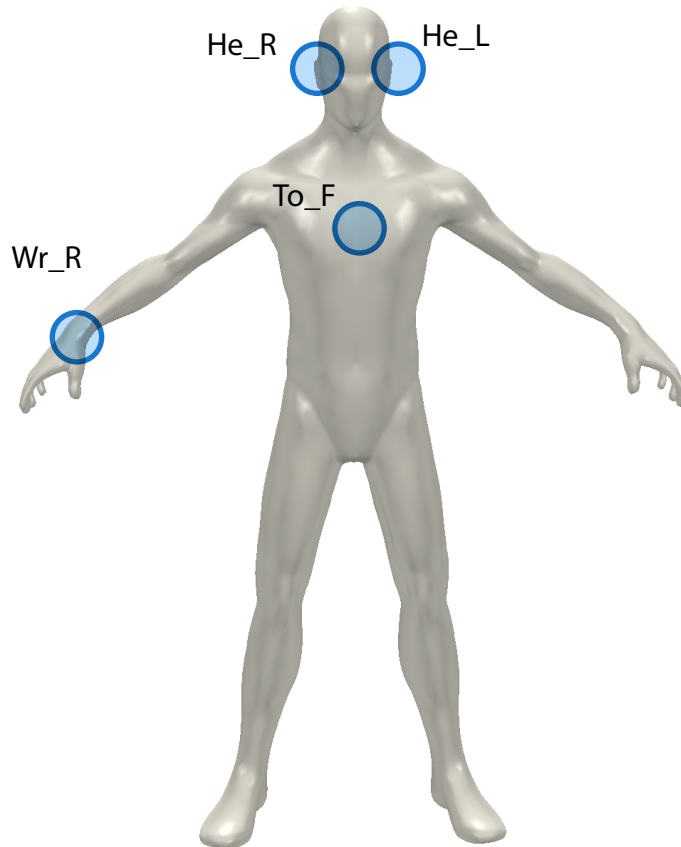


Fig. 5.2: Antenna placement on the user's body.

Based on the human dynamics, the UE antennas are always modeled as dynami-

cally moving (due to the subtle body movements such as breathing). This means the antenna elevation and azimuth angles are again modeled by a random distribution.

5.1.2 Antennas

As this thesis is focused on the millimeter wave propagation, the main operating frequency of the antennas was selected to be 60 GHz. This frequency was primarily selected due to the availability of measurement devices and its suitability for indoor usage (as of writing this thesis, the Czech Telecommunication Office (CTO) is still working on regulations on this frequency). Both the Tx and Rx antennas are modelled as an $N \times M$ antenna arrays, where N is the number of rows and M number of columns. The exact numbers for N and M can be selected according to the device that is modelled. The same approach is taken for the antenna gain, which is derived from the aforementioned physical aspects of the array.

5.1.3 Channel Model Implementation

The created channel model itself is divided into several parts that represent each of the phenomenons that influence the signal loss. The founding idea of this thesis is to create modularized model that incorporates the most influential large and small scale fading parameters. In this section we provide detailed description of each part to illustrate the complexity of the model and to provide better understanding of each part of the implementation.

The first part is dedicated to creation of the core of the model. Its main purpose is the path loss calculation. It accounts for four rays at total. First ray is the direct ray representing the line of sight connection between the transmitter and receiver. This can be defined by modified Free Space Path Loss (FSPL) formula:

$$H(t) = \frac{\lambda}{4\pi d} \sqrt{G_t G_r} e^{-j \frac{2\pi d}{\lambda}}, \quad (5.1)$$

where H represents the amplitude (transmittance), the λ is wavelength, d distance between the transmitter and receiver, G_t and G_r are transmitting and receiving gain, respectively, and the $e^{-j \frac{2\pi d}{\lambda}}$ accounts for the signal phase. The same principle is used for the other three rays, each of them representing reflection from one wall. In addition to the path loss generated by the aforementioned FSPL formula, the reflected rays are also attenuated by the reflection loss. This loss was added as:

$$|\Gamma| = U(0.6, 0.8), \quad (5.2)$$

where the $|\Gamma|$ represents the reflection loss and the U represents uniform distribution. This loss is material-dependent, usually in range from 0.6 to 0.8 for the mmWave

frequencies [150]. More information about the material dependency and reflection principles can be found in Section 2.1.3. Furthermore, the reflection on the incident object causes phase shift that can be generally added as random variable to the phase of the ray. This influence comes from the wavelength of the mmWave signals and the great variance of the phase coupled with it. Therefore the reflection randomness was added as:

$$Ref_{rand} = U(0, 2\pi). \quad (5.3)$$

The last part is dedicated to the body shadowing on the user side. This is one of the most neglected loss and also one of the most important losses when it comes to simulation of user mobility. Presented model utilizes the shadowing function created in [151]. This shadowing function was originally developed for lower frequencies, but we further adjusted it for millimeter waves. The body shadowing loss is modeled as:

$$S(d, \phi)_{[\text{dB}]} = S_m(d)_{[\text{dB}]} \frac{1}{2} \left(1 + \cos \frac{2\pi}{\Delta\phi} (\phi - \phi_0) \right), \quad (5.4)$$

where S_m is maximum body-shadowing loss, $\Delta\phi$ is the shadowing pattern width, ϕ is the azimuth angle of departure, ϕ_0 is azimuth angle of maximum loss represented as:

$$\phi_0 = \phi_a + \pi, \quad (5.5)$$

where ϕ_u is the maximum radiation antenna orientation angle in Global Coordinate System (GCS) and the π represents the exact opposite orientation, therefore providing the maximum loss angle. Together all aforementioned parts can be expressed as:

$$P_{r[\text{dBm}]} = P_{t[\text{dBm}]} - L_{sf[\text{dB}]}, \quad (5.6)$$

where the P_r and P_t are transmitting and received power respectively and the L_{path} is the shadowing loss expressed as:

$$L_{sf[\text{dB}]} = -20 \log_{10} \left| \sum_{i=0}^n H_i 10^{\frac{S(d, \phi)_{[\text{dB}]}}{-20}} |\Gamma| \right|, \quad (5.7)$$

where $S(d, \phi)_{[\text{dB}]}$ equals to:

$$S(d, \phi)_{[\text{dB}]} = S_m(d)_{[\text{dB}]} \frac{1}{2} \left(1 + \cos \frac{2\pi}{\Delta\phi} (\phi - \phi_0) \right), \quad (5.8)$$

where S_m is maximum body-shadowing loss, $\Delta\phi$ is the shadowing pattern width, ϕ is the azimuth angle of departure, ϕ_0 is azimuth angle of maximum loss. This

resulting formula can be used to simulate the complex propagation inside rooms of variable sizes.

5.1.4 Channel Model Optimization

The developed model, which was introduced in Section 5.1.3 was further utilized to simulate user movement inside three different rooms of predefined sizes (2x4 m, 6x10 m, 12x20 m). The goal was to approximate the propagation attenuation by less complex function and to approximate the fading by a distribution function. The methodology of fitting is described in further paragraphs.

For each of the aforementioned room sizes, three different base station positions were chosen: (i) in the middle of right room, (ii) top right corner, and (iii) middle of the top wall. The user's position was chosen to be on lanes positioned at $y/16$ increments to cover gradually increasing reflection angles and the accompanied prolonged propagation distances (see Fig. 5.3).

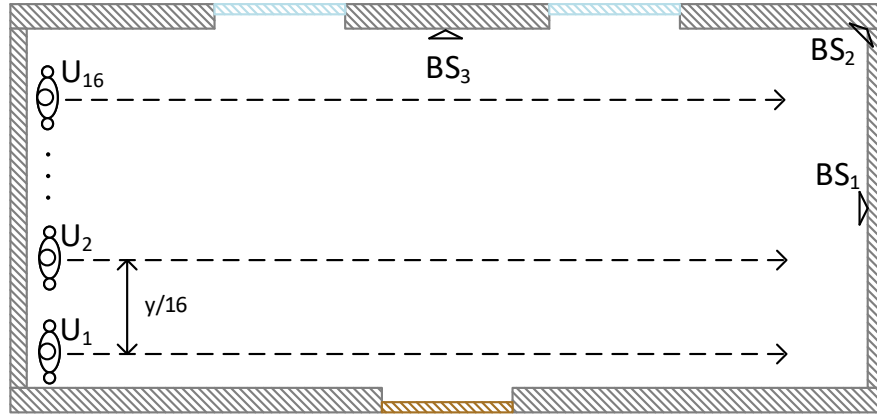


Fig. 5.3: Base station and user equipment positions utilized for the model optimization.

For each set of aforementioned data, the linear scale pathloss component was calculated using the 5.1, 5.2 and 5.3 formulas. Then for each lane, the pathloss was approximated by a curve using following formula:

$$y = \frac{\alpha}{x^\beta}, \quad (5.9)$$

where α and β are slope and shape coefficients, respectively and x is the distance in meters. Using the resulting curve, the shadowing variation was found. The shadowing was further fitted to a number of different distributions (Rician, Rayleigh, Stable, Normal, Logistic) in order to find the best correlation for each line segment in the room. To compare goodness of the fit of all aforementioned distributions,

standard evaluation metrics were used in following order: (i) Standard correlation statistics with threshold of 0.95 for first, quick sorting, and then (ii) Chi-squared statistics with 0.05 significance of goodness of the fit to further evaluate the goodness of the fitting process. After calculating the distribution coefficients per each line (y/16 m step) segment, the resulting data were averaged and used to generate the resulting coefficients used in the model for the shadowing.

Based on the overall averaged results provided in a sample Tab.5.1 (complete list of tables is provided the attachments), we can conclude that if we compare the goodness of the fit for selected distributions purely by the correlation coefficient, the Normal distribution provides best fit for the most cases with the average correlation coefficient of 0.796, closely followed by the Rice distribution. If we compare the goodness of the fit using more complex methods, such as χ^2 statistics, the Normal distribution is still the most satisfying, again very closely followed by Rice distribution.

Tab. 5.1: Distribution fitting of proposed model results

Distribution	χ^2 order	Corr order	χ^2 stat	χ^2 crit	χ^2 p value	Correlation
Normal	3.00	3.00	802.65	64.00	0.00	0.90
Rayleigh	7.00	7.00	9191.35	65.17	0.00	0.40
Logistic	5.00	5.00	1198.04	64.00	0.00	0.88
Stable	2.00	2.00	800.21	61.66	0.00	0.90
Rice	1.00	1.00	800.07	64.00	0.00	0.90
Nakagami	4.00	4.00	1039.85	64.00	0.00	0.89
Lognormal	6.00	6.00	2373.50	64.00	1.41	0.83

Based on the distributions provided in Annex.A, we consider a Rice distribution as the best one for further simulations. Furthermore, to be able to recreate the original signal, the curve got from 5.9 were converted into dB and fitted to common log-distance pathloss formula:

$$L_p = L_{p_{d_0}} + 10n \log_{10} \frac{d_i}{d_0} + L_{sf}, \quad (5.10)$$

where $L_{p_{d_0}}$ is pathloss at reference distance d_0 (1 m), n is the pathloss exponent, d_i is the distance in meters, and L_{sf} is the shadowing coefficient which was added after the fitting as:

$$L_{sf} = R(s, \sigma), \quad (5.11)$$

where $R(s, \sigma)$ is the Rician distribution with s standing for noncentrality parameter, modelled as a mean of all partial noncentrality parameters s_{part} that resulted

from the different y positions and the σ representing the shadowing variation. The resulting parameters used for further simulations are grouped for each room size, antenna position of the UE and BS and frequency:

Tab. 5.2: Pathloss and Rician coefficients for room size of 4x2m with reflection coefficient of 0.4-0.6

	BS position [m]									
Tx position	[4,1]					[4,2]				
	L_{pd_0} [dB]	n	s	sigma	corr	L_{pd_0} [dB]	n	s	sigma	corr
TO_F	67.84	1.92	0.96	0.29	0.94	67.84	1.89	0.94	0.33	0.93
HE_L	67.87	2.00	0.99	0.17	0.84	67.64	2.06	0.98	0.18	0.91
HE_R	67.96	2.00	0.99	0.12	0.90	67.87	2.01	0.99	0.13	0.89
WR_R	67.94	1.98	0.99	1.15	0.93	67.86	2.00	0.98	0.17	0.94
TO_B						68.04	1.96	0.99	0.18	0.97

Tab. 5.3: Pathloss and Rician coefficients for room size of 4x2m with reflection coefficient of 0.6-0.8

	BS position [m]									
Tx position	[4,1]					[4,2]				
	L_{pd_0} [dB]	n	s	sigma	corr	L_{pd_0} [dB]	n	s	sigma	corr
TO_F	67.74	1.84	0.93	0.38	0.93	67.78	1.77	0.88	0.44	0.90
HE_L	67.78	1.99	0.97	0.23	0.82	67.30	2.12	0.97	0.25	0.89
HE_R	67.87	2.00	0.99	0.16	0.87	67.78	2.01	0.98	0.19	0.88
WR_R	67.83	1.99	0.98	0.21	0.93	67.72	2.00	0.97	0.24	0.93
TO_B						67.80	1.77	0.88	0.44	0.90

Based on the tables 5.2, 5.3, 5.4, 5.5, 5.6, and 5.7 it can be seen that the rooms size does not play major role in the pathloss estimation. Oppositely, the BS location affects the pathloss more significantly. This can be seen for the cases, where the BS is shifted from the center right position of the room to upper right corner (the second column in all aforementioned Tables). Also, the antenna position can play an important role, when placed on specific locations such as TO_F and HE_L/HE_R . Interestingly, when utilizing the antenna position on the wrist (WR_R), the signal attenuation has generally having smaller pathloss exponent than the head antenna position. This is due to the fact, that the hand is periodically moving and therefore the body attenuation is not taking place all the time. Furthermore, to provide more

Tab. 5.4: Pathloss and Rician coefficients for room size of 10x6 m with reflection coefficient of 0.4-0.6

	BS position [m]									
Tx position	[10,3]					[10,6]				
	L_{pd_0} [dB]	n	s	sigma	corr	L_{pd_0} [dB]	n	s	sigma	corr
TO_F	68.18	1.93	0.97	0.26	0.94	68.53	1.87	0.95	0.32	0.93
HE_L	67.86	2.00	0.99	0.17	0.87	67.19	2.08	0.98	0.20	0.91
HE_R	67.96	2.00	0.99	0.12	0.91	67.82	2.01	0.99	0.14	0.89
WR_R	67.95	1.99	0.99	0.15	0.95	67.88	2.00	0.99	0.17	0.94
TO_B						68.22	1.96	0.99	0.18	0.97

Tab. 5.5: Pathloss and Rician coefficients for room size of 10x6 m with reflection coefficient of 0.6-0.8

	BS position [m]									
Tx position	[10,3]					[10,6]				
	L_{pd_0} [dB]	n	s	sigma	corr	L_{pd_0} [dB]	n	s	sigma	corr
TO_F	68.35	1.87	0.94	0.35	0.93	69.00	1.74	0.90	0.41	0.90
HE_L	67.76	2.00	0.97	0.23	0.84	66.40	2.16	0.96	0.27	0.88
HE_R	67.91	2.00	0.99	0.16	0.89	67.66	2.02	0.98	0.19	0.87
WR_R	67.94	1.98	0.98	0.21	0.94	67.74	2.00	0.97	0.24	0.94
TO_B						68.45	1.91	0.98	0.24	0.96

Tab. 5.6: Pathloss and Rician coefficients for room size of 20x12 m with reflection coefficient of 0.4-0.6

	BS position [m]									
Tx position	[20,6]					[20,12]				
	L_{pd_0} [dB]	n	s	sigma	corr	L_{pd_0} [dB]	n	s	sigma	corr
TO_F	68.38	1.93	0.97	0.26	0.93	68.88	1.87	0.95	0.31	0.93
HE_L	67.89	2.00	0.99	0.16	0.87	66.93	2.08	0.98	0.20	0.91
HE_R	67.95	2.00	0.99	0.12	0.92	67.82	2.01	0.99	0.14	0.89
WR_R	67.97	1.99	0.99	0.15	0.95	67.86	2.00	0.99	0.17	0.95
TO_B						68.34	1.96	0.99	0.17	0.97

Tab. 5.7: Pathloss and Rician coefficients for room size of 20x12m with reflection coefficient of 0.6-0.8

	BS position [m]									
Tx position	[20,6]					[20,12]				
	L_{pd_0} [dB]	n	s	sigma	corr	L_{pd_0} [dB]	n	s	sigma	corr
TO_F	68.75	1.87	0.94	0.35	0.93	69.65	1.75	0.89	0.41	0.91
HE_L	67.71	2.00	0.97	0.23	0.85	65.82	2.17	0.96	0.28	0.89
HE_R	67.91	2.00	0.99	0.16	0.90	65.56	2.02	0.98	0.19	0.87
WR_R	67.96	1.98	0.98	0.21	0.95	67.65	2.00	0.97	0.24	0.94
TO_B						68.64	1.92	0.98	0.24	0.97

graphical illustration of the channel model functionality, complex pathloss map for a room of size 10x6 m is provided in Fig. 5.4.

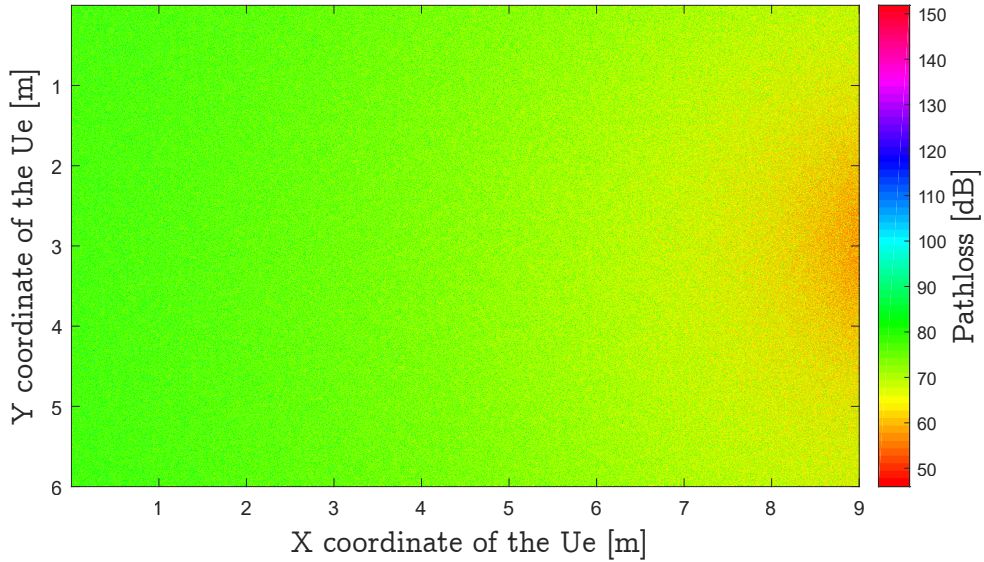


Fig. 5.4: Pathloss distribution inside a room of size 10x6 m.

As it can be seen in Fig. 5.4, the BS is static at [10,3] coordinates, while the theoretical UE can be at any point ranging from [0,0] to [9,6] coordinates. This effectively produces a map of all points inside the room (except the ones that are from 9 meters further apart), showing the complex propagation characteristics. The model presented in this section and its utilization for simulations is further published in [152].

5.1.5 Verification of the Model, Comparison with Other Publicly Available Models

The model described in Section 5 was created by utilizing mathematical models and formulas. To evaluate its accuracy and verify the results, three different real-world measurement campaigns were chosen: (i) Boise Airport Measurements, (ii) 60 GHz UE to eNB Measurements for Small Cell Deployments, and (iii) Path Loss Models for Indoor Off-body Communications at 60 GHz. These campaigns were chosen for their specific locations, all mostly targeting the indoor propagation. Also, they were further simulated using the developed model and the simulation results were verified with the data collected in referenced works. This section is focusing on these campaigns, describing the measurement setup and discussing the results.

Boise Airport Measurements

In the work [153] authors performed 60 GHz channel measurements on the premises of Boise Airport and Boise State University campus. The measurements were done in mostly LOS scenarios at four different places: (i) outdoor, (ii) airport gate area, (iii) airport baggage area, and (iv) hallway. The utilized measurement equipment parameters are summarized in Tab. 5.8.

Tab. 5.8: Boise scenarios measurement parameters

Parameter	Value
Carrier frequency	60 GHz
Bandwidth	1.3 GHz
Modulation scheme	BPSK
Tx antenna gain	25 dB
Rx antenna gain	25 dB
Tx and Rx antenna half power beamwidth in E-plane	7.92
Tx and Rx antenna half power beamwidth in H-plane	9.65
Maximum Tx power	-5 dBm

All the measurements were performed using horn antennas and the measured data were collected from the receiver side of the link. Unfortunately, authors only provide detailed description of the hallway measurement, with room size of 32mx2.2mx1.9m. The hallway was composed of walls made of sheetrock over metal studs, concrete ground and fiberboard-tiled ceiling. To provide as close as possible simulation results, we adjusted our model to this scenario and the results are further compared in Fig. 5.5.

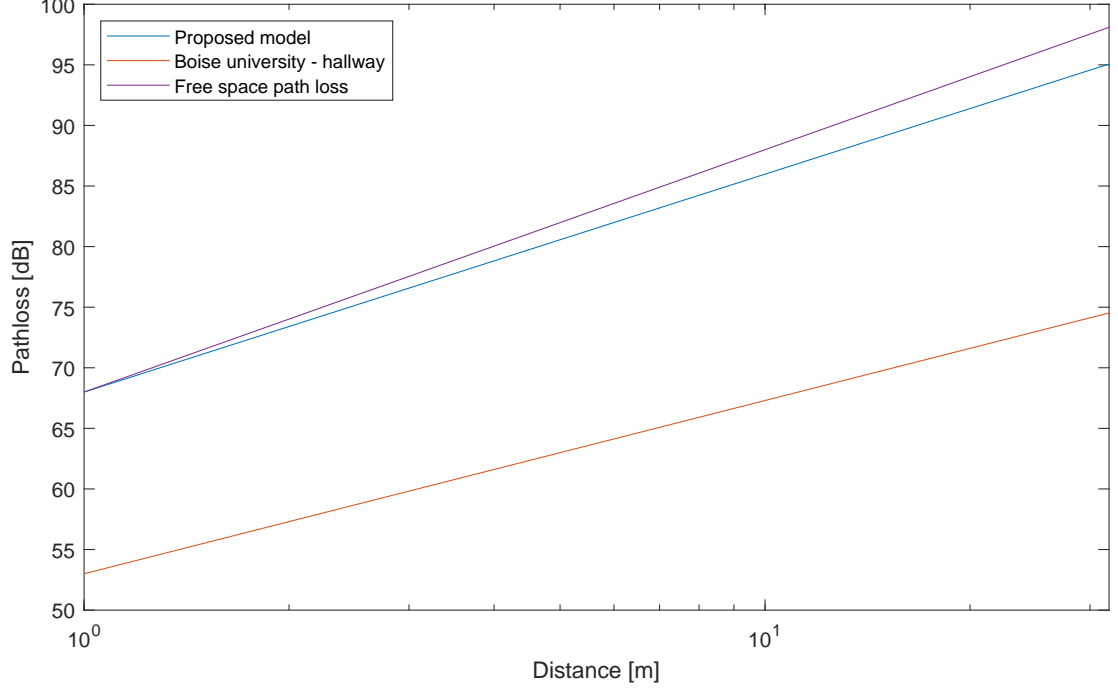


Fig. 5.5: Comparison of our proposed model with real-world measurements at Boise state university campus.

From the Fig.5.5 it can be clearly seen that there is an offset of about 11 dB between our model and the measured values from the referenced paper. The main reason for the offset is the the omitted self blockage that is taken into account in our proposed model, a strong wave-guiding effect that is definitely occurring inside the narrow room and a lot of reflections coming from the strongly reflective materials of the walls. To further demonstrate the difference, in Tab. 5.9, we provide log-distance model coefficients for FSPL, our proposed model and all the Boise measurements:

Tab. 5.9: Comparison of pathloss exponents and pathloss at reference distance for Boise airport and university campus.

Model	$P_0[\text{dB}]$	n
Free space pathloss	68.00	2.00
Proposed TO_F	67.99	1.80
Boise airport - gate	56.00	2.13
Boise airport - baggage	57.00	1.70
Boise university - hallway	53.00	1.43

As it can be seen from the Tab.5.9, the difference between our proposed model and measured results is similar in terms of the pathloss at reference distance, but

the pathloss exponent is changing more rapidly. These changes are caused by the environments difference, more specifically the airport gate was the largest room and the measurements were made when people were walking through. These conditions together caused higher attenuation because of the longer distances the multipath components needed to travel and also they faced much higher possibility of being blocked by the moving people. The baggage area, on the other hand, was much closer to the hallway scenario thanks to the narrower size of the measurement area, which was created by wall from one side and the baggage carousels on the other. These objects have higher reflection loss and also offer scatterers, resulting in better pathloss exponent.

60 GHz UE to eNB Measurements for Small Cell Deployments

In the work [154], authors conducted measurements of 60 GHz wireless channel at the premises of Queen's University Belfast. The utilized hallway's size was $17.38\text{ m} \times 1.40\text{ m}$ and the size of the open office area was $10.62\text{ m} \times 12.23\text{ m}$. Both locations featured metal studded dry walls with a metal tiled floor covered with a polypropylene-fiber, rubber backed carpet tiles, and a ceiling with mineral fiber tiles and recessed louvered luminaries suspended 2.7 m above floor level. Furthermore, the open office area contained a number of PCs, chairs, desks, cabinets, and soft partitions. The measurement modules utilized Rx and Tx antennas with a 7.5 dBi gain. The Rx module was positioned on a non-conductive PVC stand 2.38 m above the floor level, while the Tx module was placed at adult male of height of 1.83 m and weight of 78 kg. The continuous-wave measurements were performed for three different Tx antenna positions: (i) hand, effectively simulating a SMS texting, (ii) head, simulating phone call and (iii) pocket, simulating a carrying of the device. The measurement parameters are summarized in Tab. 5.10

Tab. 5.10: Queens university of Belfast measurement parameters

Parameter	Value
Carrier frequency	60.1 GHz
Bandwidth	continuous wave
Tx antenna gain	7.5 dBi
Rx antenna gain	7.5 dBi

According to the authors, the pathloss parameters P_0 and n were extracted from the measurements by removing the Equivalent Isotropically Radiated Power (EIRP) (of 21.1 dBm) and gain at the Rx from the signal power that was received by the Vector Network Analyzer (VNA) and further by performing a linear regression on

the resulted data. In the following Fig. 5.6, we provide comparison of our proposed model, which was fitted to match the room parameters and the results from aforementioned measurements.

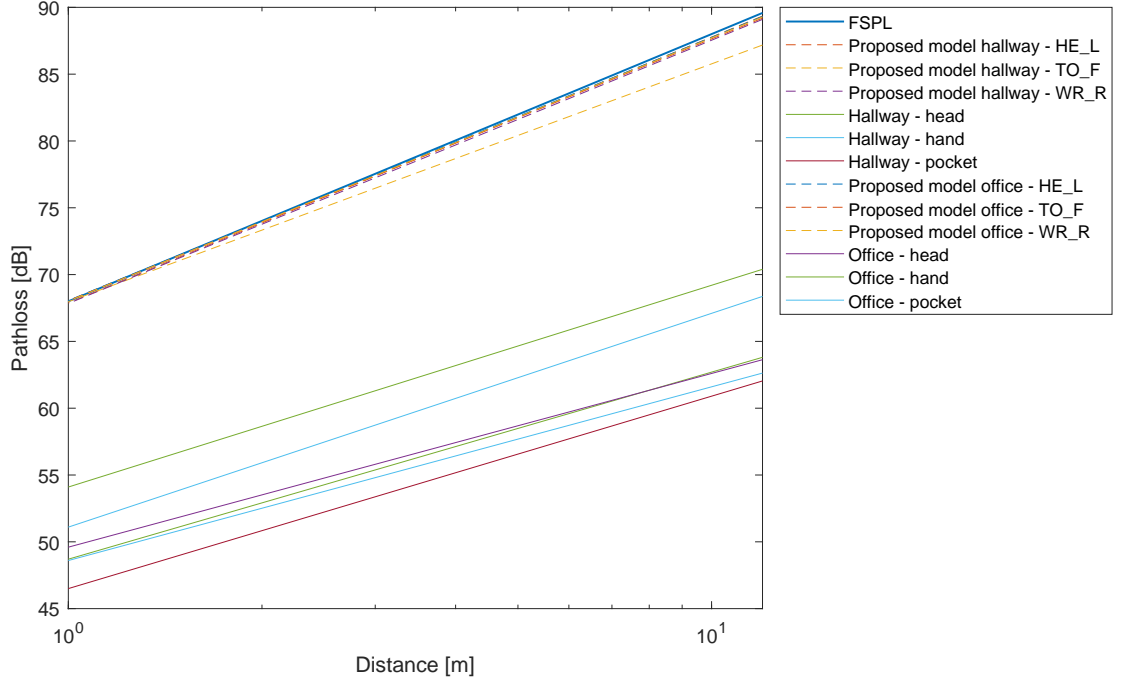


Fig. 5.6: Comparison of our proposed model with real life measurements at Queen’s University Belfast.

From the Fig. 5.6 can clearly be seen that our model provides overly pessimistic results for all the scenarios. For the hallway scenario, our model is generating almost same results as a free space model in the HE_L and WR_R scenarios, which is most probably due to the antenna orientation and its limitation into first order reflections. The reason for significantly better results, gained within the discussed measurements, is the wave-guiding effect of narrow nature of the hallway combined with the high amount of multipath components. Also, authors do not describe how exactly they subtract the antenna gains, which could possibly also lead to much better n parameter values. Very similar situation is visible in the office scenarios, where our model is producing even worse pathloss exponent values, which are most probably the result of not accounting for furniture inside the room. This can create a huge difference as the MPC’s path distance can be significantly reduced while reflected from objects in user close proximity. This is also the only logical explanation, why the office performance of measured data is always better than the hallway one, when referring to the n parameter. The pathloss parameters are further summarized in Tab. 5.11.

Tab. 5.11: Comparison of pathloss exponents and pathloss at reference distance for Queen’s University Belfast

Model	$P_0[\text{dB}]$	n
Free space pathloss	68.00	2.00
Proposed hallway - HE_L	67.87	1.99
Proposed hallway - TO_F	67.97	1.78
Proposed hallway - WR_R	67.84	1.97
Hallway - head	48.7	1.40
Hallway - hand	51.1	1.60
Hallway - pocket	46.5	1.44
Proposed office - HE_L	68.06	1.97
Proposed office - TO_F	68.04	1.96
Proposed office - WR_R	68.02	1.97
Office - head	49.6	1.30
Office - hand	54.1	1.51
Office - pocket	48.6	1.30

Path Loss Models for Indoor Off-body Communications at 60 GHz

Authors in [155] conducted measurements at 60 GHz at the Institute of Electronics, Communications and Information Technology (ECIT) at Queen’s University Belfast. Two different rooms were utilized: (i) medium-sized laboratory (4.75 m \times 9.14 m) and (ii) larger seminar room (7.91 m \times 12.58 m). Both locations were constructed from metal studded dry walls, metal tiled floor covered with polypropylene-fiber, rubber backed carpet tiles and metal ceiling with mineral fiber tiles and recessed louvered luminaries. The laboratory was equipped with chairs, boxes, lab equipment, metal cabinets and desks composed of medium density fibreboards. The seminar rooms was furnished with a large number of chairs and desks, a white board and a projector. One of the external facing boundary walls was constructed entirely from glass with metallic supporting pillars [155]. Both Tx and Rx antennas were on-chip, low profile antennas with 7.5 dBi gain, with 23.5 dBm EIRP. All the measurements were taken with stationary user and BS. The main measurement equipment parameters are shown in Tab. 5.12.

The measurement results were further logarithmically transformed into the signal power and the pathloss was calculated. Further, the linear regression was performed to obtain the estimates for P_0 and n . Unfortunately, authors did not provide any information about the antenna gain separation and therefore it can be estimated that this step was omitted. Fig. 5.7 shows the FSPL, our proposed model with

Tab. 5.12: Institute of Electronics measurement parameters

Parameter	Value
Carrier frequency	60 GHz
Bandwidth	continuous wave
Tx antenna gain	7.5 dBi
Rx antenna gain	7.5 dBi

tuned parameters to match the scenario dimensions and the measured P_0 and n values.

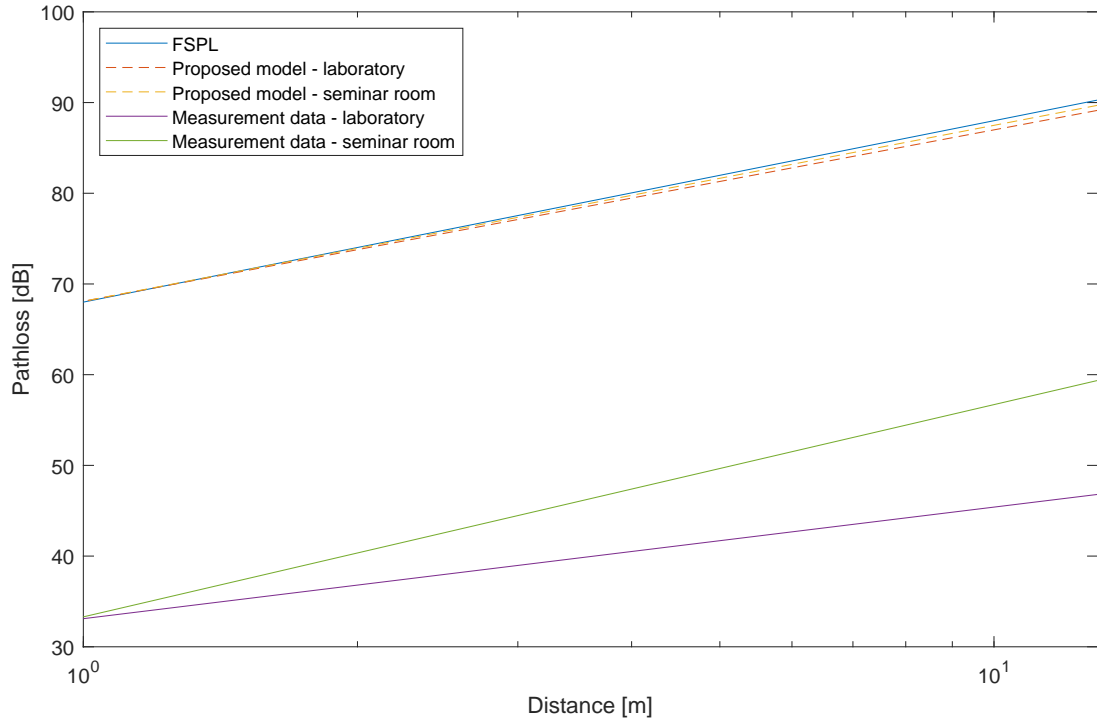


Fig. 5.7: Comparison of our proposed model with real-world measurements at ECIT.

The results shown in Fig. 5.7 show again the offset between our proposed model and the measurements. This offset is again most probably due to the inclusion of antenna gains in the measurement results. The pathloss coefficient for the laboratory LOS measurements is much better than the free space, which means that strong multipath influence is present. Furthermore for the seminar room, this exponent is 2.34, which is expected due to the larger room footprint and less reflective surfaces that can be utilized for multipath propagation. As we discussed in previous sections, our model is currently accounting only for first order reflections from walls, effectively ignoring the closer objects such as cabinets. This surely affects the accuracy and

therefore will be added in future iterations. The summarizing comparison of pathloss parameters is provided in Tab. 5.13.

Tab. 5.13: Comparison of pathloss parameters for ECIT

Model	$P_0[\text{dB}]$	n
Free space pathloss	68.00	2.00
Proposed - laboratory	68.09	1.89
Proposed - seminar room	68.09	1.94
Laboratory - LOS	33.1	1.23
Seminar room - LOS	33.3	2.34

Based on all three above mentioned correlation tests, we are confident to say that our model is accurate for indoor mmWave off-body simulations at 60 GHz frequency. We are also aware, that reaching more accurate results will definitely need extension of the model to account for phenomena like body shadowing or higher order reflections. In the next chapter, case-specific simulations utilizing our created model will be presented.

6 Analysis of Channel Model Behavior Using the Custom Model

The model created in Section 5 and further evaluated in Section 5.1.5 is utilized to analyze the channel behavior in this section. The idea of further described scenarios is to provide a detailed analysis of the signal propagation in indoor environment that consists of static obstacles (walls) and dynamic user with mobile antenna. The model is further implemented into the NS3 simulator, but thanks to its mathematical nature, it can be easily implemented into any other simulation tool. In the first section of this chapter, brief introduction into the structure of utilized NS3 module is given. In latter sections, the simulated scenarios and results are discussed.

6.1 NS3 mmWave Module Description

This section provides a basic overview of the NS3 simulator, with closer attention given to the NYU mmmWave module. This module was chosen because it is the only freely available module, which can be easily modified and has a strong community support. The NS3 discrete-event network simulator is very powerful simulation tool for analyzing complex systems and developing new protocols [65]. It is a successor to a well-known NS-2 simulator that has been tested and utilized by the community for over a decade. It is an open-source, community-backed tool that is actively maintained by both industry and scientific communities, which enriched the core of the simulator with several modules that enabled the tool to simulate a wide variety of wired and wireless protocols and algorithms.

The NS3 simulator repository is divided into folders based on their functionality. The `src` folder contains a collection of C++ classes that implement broad amount of modular simulation models and network protocols. These modules can be combined and instantiated to create complex network scenarios, effectively making NS3 an ideal tool for cross-layer simulation and analysis. This modularity together with object-oriented design patterns allow fast prototyping and implementation of new algorithms for testing purposes. Each module is further divided into subfolders that are composed of the model source code (`model` folder), helpers (`helper` folder), tests (`test` folder), examples (`example` folder) and documentation (`doc` folder). The helpers are very handy tools to have as they are combining multiple functionalities into one (such as assigning Internet Protocol (IP) addresses, setting up different protocol classes together, etc.) and therefore effectively “shielding” users from the configuration complexity of such tasks. The `build` folder consists of the model binaries, and the `scratch` folder is unique folder used solely for the scripts that can

be run on-the-fly there. The mmWave module for NS3 will be described in similar fashion in the following sections.

6.1.1 mmWave Core Module Overview

The NS3 mmWave module was created to perform 3GPP-style end-to-end cellular network simulations. Its architecture is heavily based on the LTE-EPC Network Simulator (LENA) module from which it leverages the implementation of the LTE/EPC protocols and adds custom PHY and MAC layers [91]. Furthermore, it provides a possibility of interconnection with a patched version of Direct Code Execution (DCE) that allows utilization of Linux Transport Control Protocol/Internet Protocol (TCP/IP) stack as NS3 nodes' stack as well as execution of Portable Operating System Interface (POSIX) socket-based applications (i.e., iPerf, tttcp, etc.). This structure can be seen in Fig. 6.1, where the high-level composition of the `MmWaveUeNetDevice` and `MmWaveEnbNetDevice` classes, that are representations of the mmWave Ue and eNB radio stacks, are depicted. The last class representation for the network devices is `McUeNetDevice`, which is a special type of `NetDevice` capable of dual stack (mmWave and LTE) connection. Furthermore, the Fig. 6.1 provides a perspective on the end-to-end structure of the mmWave module [91].

The MAC layer is represented by `MmWaveUeMac` and `MmWaveEnbMac` classes that implement Service Access Point (SAP) provider and user interfaces from the LTE module. These interfaces enable inter-operation with the LTE Radio Link Control (RLC) layer. The MAC and scheduler classes (i.e., `MeWaveMacScheduler`) are providing support for Acknowledged Mode (AM), Unacknowledged Mode (UM), Saturation Mode (SM) and Transparent Mode (TM). The MAC scheduler also provides a `LteEnbRrc` SAP interface for LTE Radio Resource Control (RRC) layer configuration. All aforementioned components together enables users to establish EPC connections [91].

The directional transmission and reception of the UL and DL data and control channels based on the control messages from the MAC layers is processed by `MmWavePhy` classes. As the PHY layer communication is inspired from the LTE module, each PHY instance is communicating through the channel using an instance of `MmWaveSpectrumPhy` class [91]. This class is shared for both Uplink (UL) and Downlink (DL) due to the utilization of the Time Division Duplex (TDD). All of the PHY-layer models instances: `MmWaveInterference` for interference calculation, `MmWaveSinrChunkProcessor` for SINR calculation, `MmWaveMiErrorModel` for Mutual Information (MI)-based packet error probability calculation, and `MmWaveHarqPhy` Hybrid Automatic Repeat Request (HARQ) PHY-layer entity for soft combining are encapsulated by the `MmWaveSpectrumPhy` instances [91].

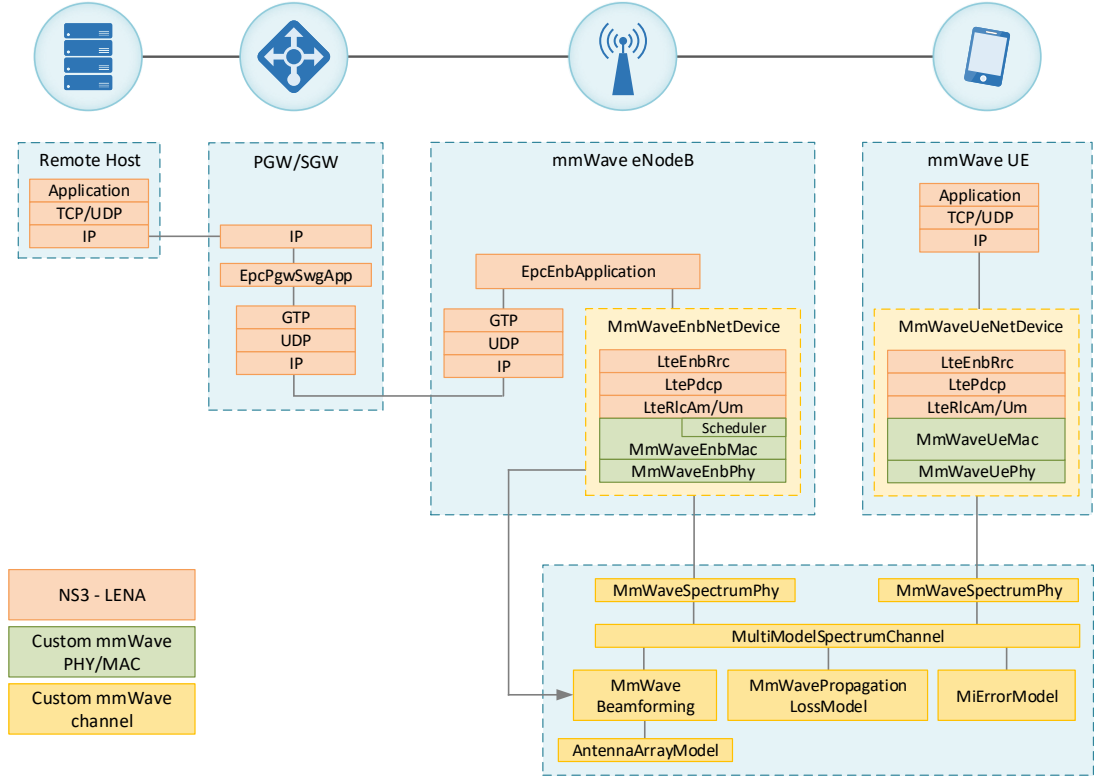


Fig. 6.1: Class diagram of the end-to-end mmWave module.

6.1.2 Physical Layer of mmWave Module

This section provides description of the key features of the PHY layer of the discussed mmWave module. More specifically, the authors implemented a new TDD frame and subframe structure that is similar to the TDD-LTE, but also offers more flexible allocation and placement of control and data channels inside the subframes and is compatible with the variable Transmission Time Interval (TTI) MAC scheme [91]. They also implemented a HARQ and error models, also based on their counterparts from LENA, but adjusted to be compatible with custom mmWave PHY and numerology (i.e., support for larger Transport Block (TB) and codeword sizes, and multiprocess UL and DL stop-and-wait HARQ)

The NS3 mmWave module utilizes a configurable TDD frame structure, which supports configurable and short slots to offer better utilization of wider bandwidths and to reduce radio link latency. The tunable parameters are shown in Tab. 6.1 and are accessible via attributes of the **MmWavePhyMacCommon** class. This class stores all PHY and MAC configuration parameters defined by the users. The frames and subframes are further divided into a number of subframes [91]. Each subframe

length can be adjusted in multiples of Orthogonal Frequency Division Multiplexing (OFDM) symbols. These variable-length subframes further contain symbols that can be assigned by the MAC scheduler and designated either for control or data channel transmission. This provides the MAC entity with full control over physical channels multiplexing within the subframe and also allows for the variable-length data slots to be assigned to different users for uplink or downlink transmission [91].

Tab. 6.1: mmWave PHY configuration parameters

Parameter name	Default Value	Description
SubframePerFrame	10	Number of subframes in one frame
SubframePeriod	100	Length of one subframe in microseconds
SymbolsPerSubframe	24	Number of OFDM symbols per slot
SymbolPeriod	4.16	Length of one OFDM symbol in microseconds
ChunkPerRB	72	Number of chunks comprising a resource block
ChunkWidth	13.89e6	Width of each chunk in Hz
SubcarriersPerChunk	48	Number of sub-carriers per chunk
CenterFreq	28e9	Possible carrier frequencies in GHz
NumRefScPerSymbol	864	Reference subcarriers per symbol
CtrlSymbols	1	Number of control symbols per sub-frame
GuardPeriod	4.16	Guard period for UL-to-DL mode switching in microseconds
NumHarqProcesses	20	Number of HARQ processes for both DL and UL

As it can be seen in Fig. 6.2, each frame takes 1 ms and is further divided into 10 subframes, each of length 100μ , consisted of 24 symbols of approximately $4.16\mu s$. The uplink and downlink control channels are fixed for all subframes, DL being first and UL last symbol, respectively [91]. Every time a switching from UL to DL occurs, a switching guard period of one symbol length is introduced. From the frequency domain point of view, the entire bandwidth of 1 GHz is splitted into 72 chunks of 13.89 MHz width, each composed of 48 subcarriers. Similarly to the OFDM in the LTE, it is possible to assign UE data to each of these subbands, but only TDMA operation is currently supported [91].

The `MmWaveUePhy` and `MmWaveEnbPhy` classes are used to model the mmWave UE and eNB PHY. Their three main purposes are therefore: (i) to manage the trans-

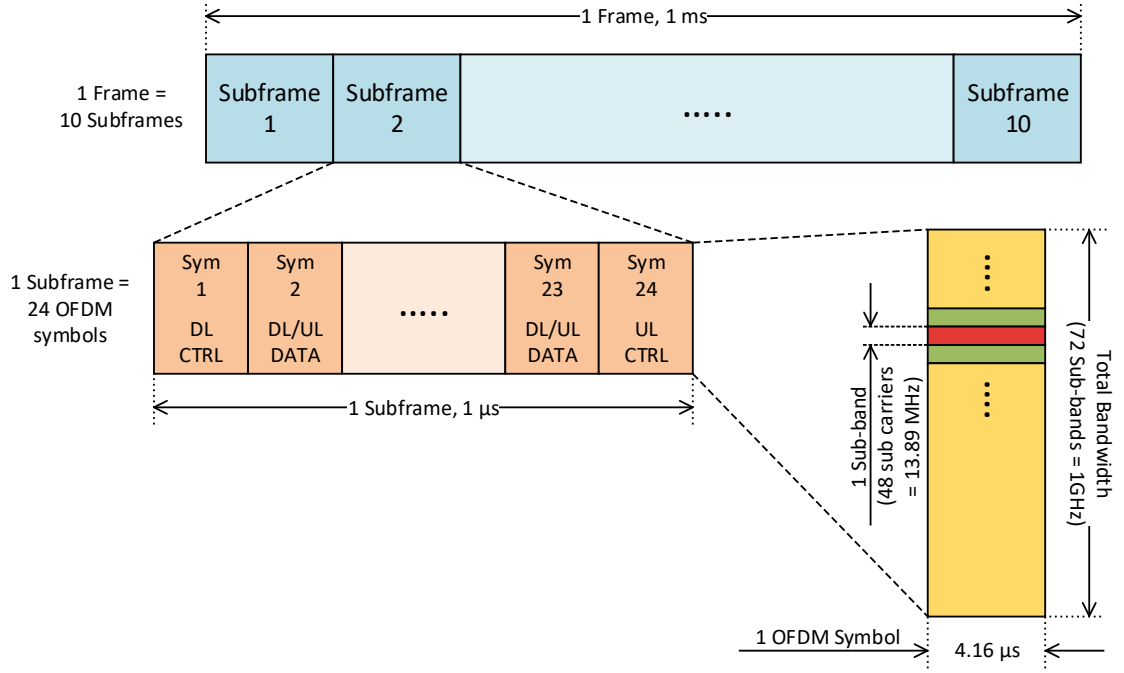


Fig. 6.2: Class diagram of the end-to-end mmWave module.

mission and reception of physical data and control channels, (ii) mimic the start and the end of slots, subframes and frames, and (iii) pass the received and successfully decoded data and control packets to the MAC layer. The `MmWaveUePhy` and `MmWaveEnbPhy` also contains `StartSubFrame()` and `EndSubFrame()` method calls. Their main purpose is to mark start and end of each subframe, and they are scheduled at fixed periods, which are derived from the user-specified subframe lengths [91]. The `SetSfAllocInfo()` method is used to enqueue `SfAllocInfo` allocation element for future subframe index that was specified by the MAC. This method is controlled by the MAC via the MAC-PHY SAP and is dynamically configuring the timing of variable-TTI by scheduling the `StartSlot()` and `EndSlot()` methods. A future subframe is allocated by triggering the scheduler at beginning of each subframe by the subframe indication to the MAC layer [91]. For the UE PHY, the `SfAllocInfo` objects are populated after successful reception of Downlink Control Information (DCI) messages. The current subframe allocation scheme, which is containing a variable amount of `SlotAllocInfo` objects, is dequeued at the beginning of each subframe. The `SlotAllocInfo` objects specify adjacent ranges of OFDM symbol indices occupied by given slot together with given type – either UL or DL and data or control. These control messages and data packets generated by the MAC are further linked to a specific subframe and slot index within the control message or packet burst maps, respectively [91]. To begin a data slot transmission, firstly the eNB PHY runs the `AtennaArrayModel::ChangeBeamformingVector` which updates both UE's and eNB's transmit and receive vectors. This is done to all slots except

the control ones, to which no beamforming is applied since authors assume “ideal” control channel. In the next step, `StartTxDataFrame()` or `StartTxCtrlFrame()` methods of the `MmWaveSpectrumPhy` are called to transmit data or control slot for both the UL and DL. Following the reception of the data packets by the PHY, it calculates the SINR for each subband using the MIMO beamforming gains, path loss and frequency-selective fading. The Channel Quality Information (CQI) reports that are further sent to the base station in the UL data or control slots are generated after the PHY layers calculations. Then, the error model instance is triggered to estimate whether the packet should be dropped by the receiver. This is done via probabilistic function that takes a SINR value as an input. Finally, the uncorrupted packets are processed by the `MmWavePhy` instance and forwarded to the MAC layer SAP [91].

6.1.3 MAC Layer of the mmWave Module

The `MmWaveEuMac` and `mmWaveEnbMac` classes contain MAC layer implementation and their primary roles is to coordinate the scheduling and retransmission procedures. Furthermore, they cooperate with PHY classes to transmit and receive packets and with RLC layer from which the receive buffer occupancy periodic reports. The `MmWaveAmc` class is dedicated to the Adaptive Modulation and Coding (AMC) mechanism, and takes over most of the code from the corresponding LENA module class. The only changes made to the source code were done to accommodate the dynamic TDMA MAC frame structure and scheme. The key role of the `MmWaveAmc` is to adapt the modulation and coding schemes based on the channel quality indicated by the CQIs.

The current version of the mmWave module contains full support for HARQ with soft combining. HARQ mechanism is critical for mmWave networks as it increases the probability of successful decoding of the data by fast retransmissions with incremental redundancy. These retransmissions have higher priority than new transmissions and therefore get the available resources first before the they are allocated to the data from the RLC buffers. Thanks to the nature of retransmissions, the HARQ mechanism introduces additional delay that has to be accounted for and mitigated as much as possible. Therefore the LENA HARQ module source code was adjusted. One of the changes was the option to create multiple HARQ processes for both UL and DL. Furthermore, users can configure the number of processes through the `NumHarqProcesses` attribute, which enables them to optimize the bandwidth utilization. Also, the integration with the flexible TTI physical layer offers a latency reduction of the retransmissions.

6.1.4 RLC Layer of mmWave Module

The mmWave module's RLC layer is directly inherited from the LENA module with all of its LTE RLC entities. Furthermore, the RLC AM entity was adjusted to provide compatibility with the mmWave MAC and PHY layers. Also, a new optional feature, which is providing Active Queue Management (AQM) for the RLC buffers was created.

Firstly, the `PollRetransmitTimer` was reduced from 20 ms to 2 ms as a result of reduced mmWave frame structure size. Furthermore, the option to perform segmentation for the retransmission process was added into the RLC AM layer to support an intermittent mmWave channel. This segmentation works as follows: if the amount of transmitted bytes that are ready to be sent in next opportunity is less than the number of bytes of the segment that should be retransmitted, the segment will be splitted into subsegments that will have a re-segment flag set to true. The receiver's side RLC layer then checks the subsegments' flags and waits for the final one when the flag is set to true. Then the original segment is reassembled from the subsegments. The segment is further checked if all the contained subsegments are received correctly and if so is forwarded to the upper Packet Data Convergence Protocol (PDCP) layer.

The RLC layer of the mmWave module enables users to choose between a default queue management (Drop-tail) or more elaborated AQM mechanism by setting the `EnableAQM` attribute to true. A CoDel scheme is set as a default AQM technique, but it is possible to utilize any of the NS3 queues via setting the queue attribute of the `LteRlcAm` class.

6.1.5 Advancements of the NS3 mmWave Module

Due to the aforementioned restrictions of the NS3 mmWave module, it was decided to update its structure. Firstly, the attention was given to the accuracy comparison of the NS3 mmWave channel models. In [156], it was identified that all the implemented channel models did not take into account the thickness of blockage objects. This lead to the overly optimistic propagation in case of strong block objects such as steel door. To mitigate this issue, a simple limit-power policy was proposed to simulate the outage events more accurately. This approach is further demonstrated in Fig. 6.3

This idea was further extended in [157], where the limit power policy was substituted by more sophisticated algorithm, which is accounting for the blockage object thickness. This extension enables users to simulate scenarios with multiple blockage objects of different thicknesses shadowing the LOS of the transmitter. As it can be seen in Fig. 6.4, the simulation results prove the importance of the accounting for the thickness of the object.

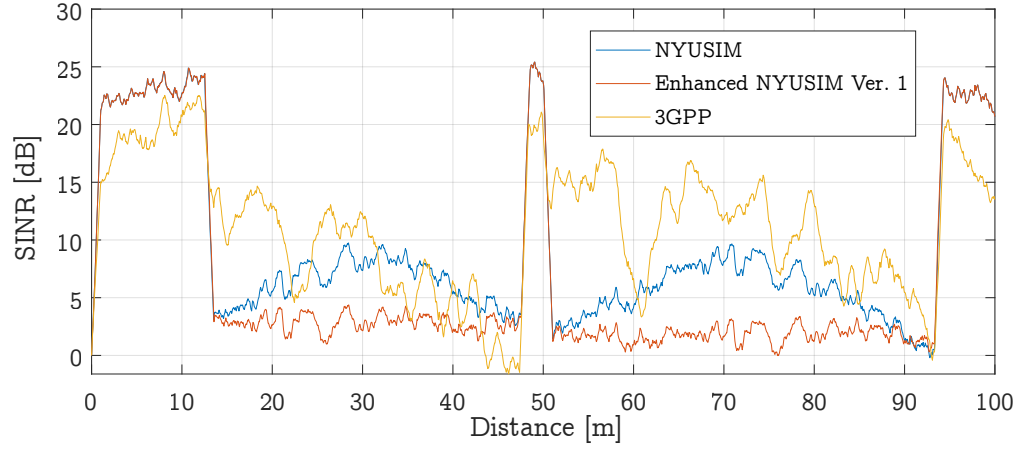


Fig. 6.3: SINR values based on the distance for two eNBss and two blockage objects.

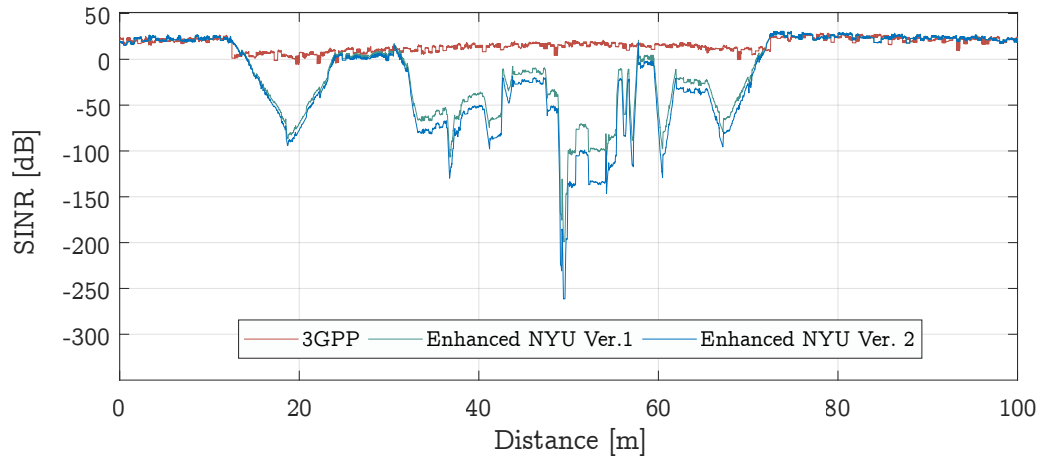


Fig. 6.4: Simulation results of complex building.

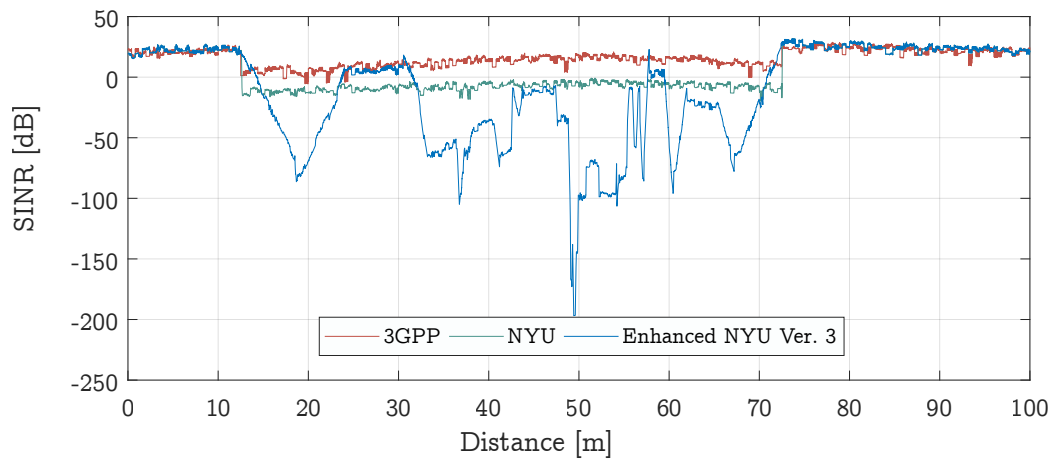


Fig. 6.5: Simulation results of complex building with different materials used for walls.

Finally, this model was further adjusted in [158] to account also for the material of the blocker. This enabled users to distinguish between not only thickness of the blocker, but also between the materials, from which was the blocker made. This is especially beneficial for diversification of the materials inside the room, where there are often metal or concrete walls, but the inside of the rooms is furnished with wooden closets. To further illustrate the importance of this approach, the results are depicted in Fig. 6.5.

6.1.6 Extension of the NS3 Propagation Model

To successfully implement our model into the NS3 simulator, the mmWave module had to be adjusted accordingly. Thanks to the modularity of the NS3 and its derived modules, the changes were made in the `BuildingsObstaclePropagationLossModel` class. This class, similarly to the whole mmWave module, was created by the authors from [85]. Its main purpose is to provide detailed propagation loss model for scenarios that take buildings into the account. It is further divided into three sub-scenarios based on the position of nodes: (i) outdoor scenario, where both UE and BS are outside the buildings, (ii) indoor to outdoor scenario, where either the UE or BS is inside and the other one is in the opposite environment, and (iii) indoor scenario, where both UE and BS are inside a building. As our model is primarily focused on the indoor off-body propagation channel, we added the option (iii) and modified its content to utilize our proposed model from Section 5.1.3.

6.2 Simulated Scenarios

As discussed in the Section 1.1, the need for accurate and reliable simulation of the mmWave networks is still unsatisfied. This section is proposing a model scenarios that are covering all tunable parameters of created channel model, providing a in-depth insights into how each parameter influences the simulation. If all these scenarios are combined, they simulate real-life scenarios as closely as possible.

6.2.1 Simulation Parameters

To effectively verify the validity of each of the setup parameters for selected simulation scenarios, it was needed to unify all remaining parameters that are not used to describe the scenarios' parameters. Therefore for all the simulations inside this section, the simulation settings were set as described in Tab. 6.2.

Tab. 6.2: Simulation scenarios' parameters

Parameter name	Set value
Center frequency	60 GHz
Tx power	1 dBm
Rx power	1 dBm
Tx gain	1 dBm
Rx gain	1 dBm
TCP segment size	1400 b
HARQ	Enabled
Chunk per RB	144
Bandwidth	2 GHz

This data was selected to simulate the current IEEE 802.11ad standard as closely as possible. The utilized bandwidth was setup to the similar size of 2 GHz and the rest of the settings are set as described in Tab. 6.1.

6.2.2 Different Room Dimensions

The biggest disadvantage of mmWave spectrum is its high atmospheric loss, which effectively attenuates the signals over bigger distances. This effect is especially strong around the 60 GHz frequency (see Fig. 2.1 for more detailed information), which, in combination with the reflection loss can be critical inside a larger rooms such as airport lounges or seminar rooms. This subsection is dedicated to modeling the effect of different room sizes on the propagation attenuation and transmission speed.

Utilizing the created channel model, we have tasted three different room sizes to evaluate the impact on the network performance. The room sizes, which are illustrated in Fig. 6.6, were: (4x2 m, 10x6 m and 20x12 m). The user was moving towards the BS positioned at the middle of the furthest wall (see Fig. 6.6 for reference). By taking this approach, it was possible to simulate the pathloss decay for all three rooms, effectively preserving the baseline for the comparison. The channel coefficients, corresponding to each room size were taken from Section 5.1.4.

The simulation results are depicted in Fig. 6.7. It can clearly be seen that the room sizes up to 20 m do play a minor role in the signal attenuation, resulting usually in about less than half of dB difference. On the contrary, the antenna location and the reflection coefficient can play a significant role, providing bigger loss when the location is incorrect. For example, the SINR difference between the two antenna placements inside a room of 20x12 m is almost a 1 dB. If a stronger reflection loss is

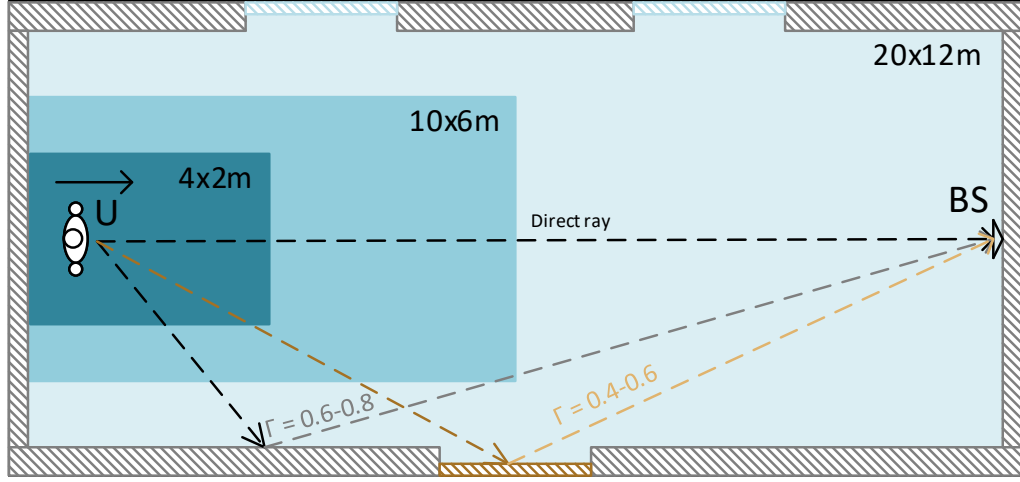


Fig. 6.6: SINR value estimates based on our proposed channel model.

added to this scenario, the SINR will be better by more than 2 dB. Even though all aforementioned differences may seem negligible in comparison to the variance shown in Fig. 6.7, it has to be noted that with much larger rooms and communication on greater distances, the attenuation will increase drastically. This trend is visible from the Fig. 6.7 as well, showing the difference between the smallest room with smaller reflection coefficients and the largest room with the stronger reflection coefficients to be almost 10 dB.

To further illustrate the impact of the propagation attenuation on the users' QoE, we provide a throughput and RTT figures for the aforementioned scenario in Fig. 6.8, and Fig. 6.10. These values can be taken as a baseline for the QoE estimation.

The visible ramp up in the beginning of the Fig. 6.8 is caused by the Transmission Control Protocol (TCP) initialization. Then, for the rest of the simulation, the data is stable due to the strong enough signal (high SINR). This is an expected result based on the data from the model optimization in Section 5.1.4 and the set up parameters of the currently presented scenario (the transmitting powers, antenna gains, etc.). Very similar results are, as expected, for the RTT, which can be seen in Fig. 6.9. Also, for the initialization process, there is a slight delay and initially higher RTT and from 0.5 m further, the value is stabilized around 0.0225 s.

Furthermore, if we take the same models and add an attenuation of 20 dB, which was measured as a average attenuation done by blocking human body, and increase the transmission distance, the results are much more interesting. This behavior can be seen in Fig. 6.10, where the ramp up in the beginning is again caused by the

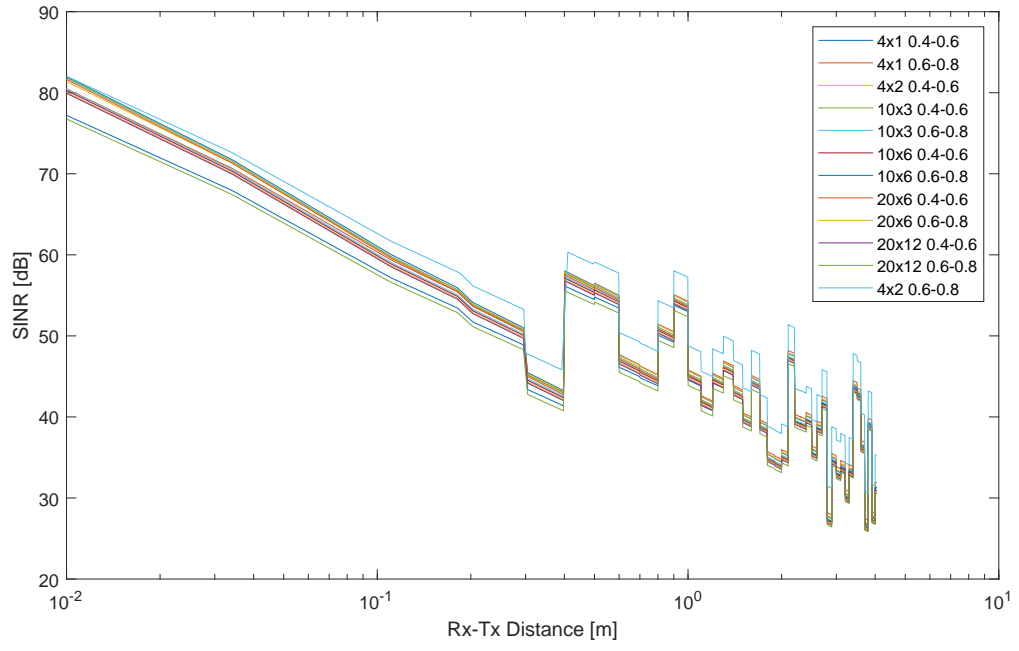


Fig. 6.7: SINR value estimates based on our proposed channel model.

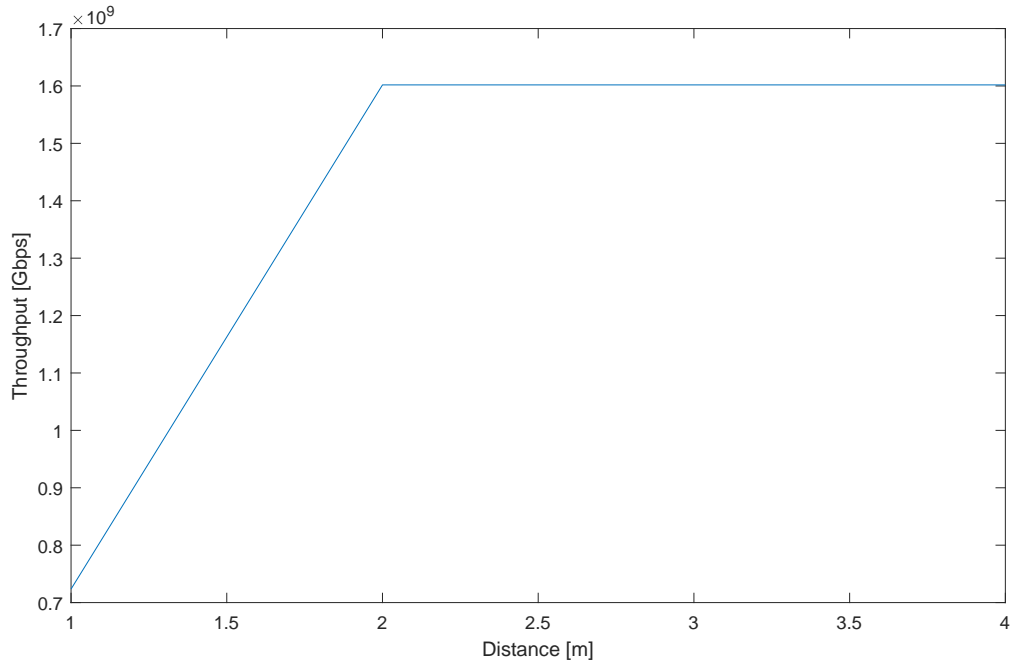


Fig. 6.8: Throughput of scenario with one UE and one BS.

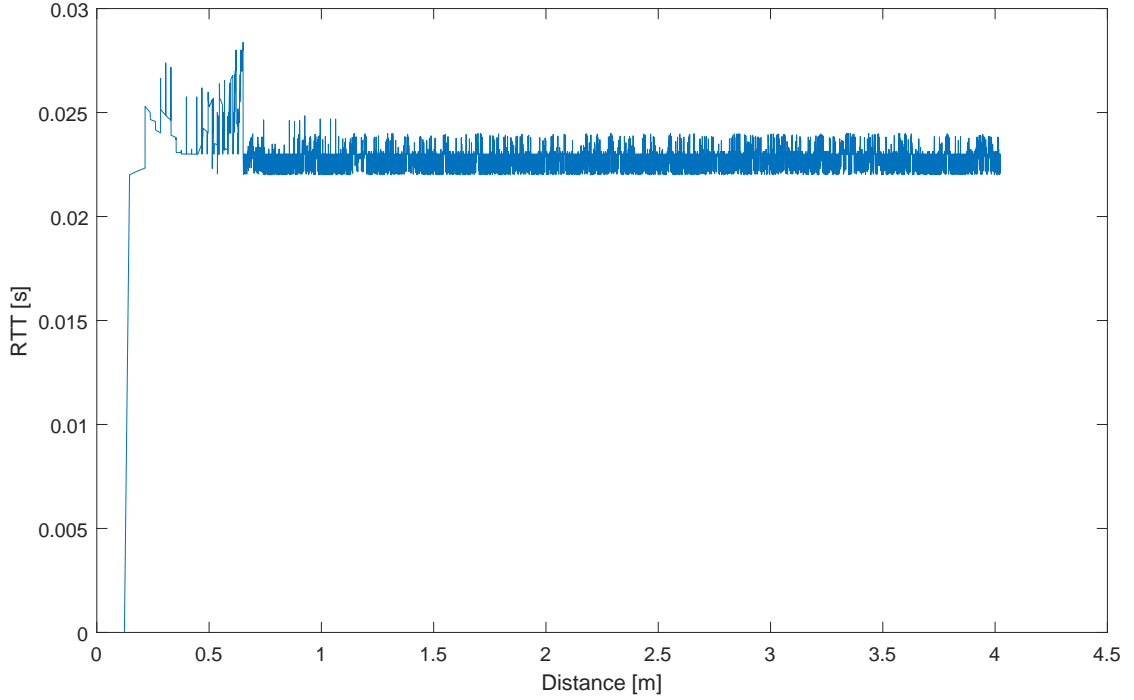


Fig. 6.9: RTT of scenario with one UE and one BS.

TCP initialization process, where it adjusts the transmission parameters to fully utilize the available bandwidth. Also, it can be seen that the throughput begins to decrease after 9 m, based on which it can be concluded that for larger rooms with a random human blockage (i.e., airport halls, larger offices, etc.), it will be vital to utilize higher gain antennas together with complex beamforming algorithms.

Based on all the aforementioned simulation results, it can be stated that for the fast prediction of channel behavior inside a rooms up to size of 20x12 m, all the developed channel parameters can be used. Furthermore, if they will be approximated into the single value, it can be used for a even faster, rough estimation of the channel quality. For more detailed and accurate simulation, the correct parameters from Section 5.1.4 have to be taken. Also, it should be noted that the model is not in the final state and further development is planned to provide more flexible simulation and more accurate results.

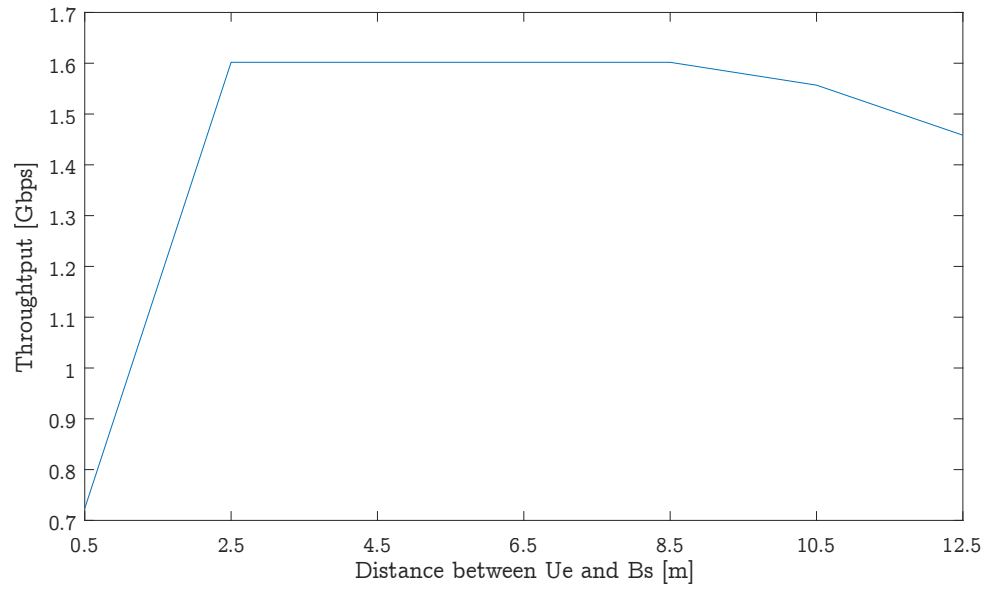


Fig. 6.10: RTT of scenario with one UE and one BS.

7 Conclusion

The rapid evolution of BANs caused by the new revolutionary applications such as AR and VR is driving the next stage of wireless networks. These networks are expected to be interconnected with the cellular systems, together creating a next-generation (5G) wireless systems. Their main advantage lies in the manifold increase in data rates, latency and overall QoE. This, as aforementioned, will be extremely beneficial for the novelty applications in healthcare, industry and entertainment fields. However, to be able to unleash the full potential of these systems, a new frequencies, mainly from the millimeter-wave spectrum need to be utilized. This poses a challenges in the propagation modeling, which was dealt with in this thesis.

The signal propagation at mmWaves is comprehensively described in Chapter 2. The first part of this chapter is dedicated to large scale propagation channel effects, which are vital part of the whole propagation channel. More precisely, the insight into four main channel effects is given. Starting with the log-distance propagation models that are widely used for pathloss decay characterization, the insight into the pathloss exponent estimation and utilization is given. Furthermore, the atmospheric and weather effects are discussed to highlight the importance of the attenuation caused by the water molecules in the air, which is very pronounced especially around the 60 GHz frequencies. This topic is followed by the signal phenomena caused by objects in the signal path. This phenomena becomes much more stronger at higher frequencies, completely changing the material parameters (at lower frequencies, the surface roughness did not play such a significant role in terms of reflection and scattering). In the second part of this chapter, the small scale propagation channel effects are discussed. Beginning with the delay spread, which, as aforementioned, is much higher due to the higher reflection coefficients and much stronger multipath propagation. Lastly, the attention is given to the Doppler effect, which is expected to be 15-30 times greater than at microwave frequencies.

The Chapter 3 is offering a comprehensive overview of the most advanced mmWave propagation Models. These models are further divided into three groups, creating a complete description of currently available propagation models for any type of scenario. Firstly, the attention is given to the most well-known and used models – the outdoor propagation channel models. Here, the detailed description of the 3GPP style models, from which the 3GPP statistical channel model is the most complex. It is defined for frequencies from 6 to 100 GHz with bandwidths up to 10 % of the carrier frequency. The second mentioned model is the New York University model, which is heavily based on the extensive measurements done by the NYU team. This model is composed of two propagation models (LOS and NLOS) to provide more accurate results. Further, the vehicle-to-vehicle channel models are discussed to

provide an understanding of the vehicular network specifics. The second part of this chapter is dedicated to indoor propagation models, with attention given to the ray-tracing and Rayleigh, Rician and multiwave fading models that are considered a baseline in indoor channel propagation. These models are followed by the IEEE 802.15.3c and IEEE 802.11ad models, which are currently the most advanced models used for mmWave channel modeling. The last section of this chapter is dedicated to the state-of-the-art simulation tools used for mmWave simulation. This section starts with the WSnet simulator, which is very flexible simulation tool, that can be interfaced with many other modules and simulators to provide a complex wireless network nodes simulation. It is followed by the comprehensive overview of Riverbed Modeler and OMNeT++ simulators, which are widely used throughout the scientific and industrial communities. Lastly, the attention is given to NS3 simulator, which is open-source, community backed simulator containing a lot of modules used for wide variety of simulations. This simulator was chosen to be utilized in this thesis for the simulations that are utilizing custom developed channel model.

To be able to provide a valuable channel model for the off-body communication, a profound knowledge of the BANs was necessary. Therefore the Chapter 4 is dedicated to this topic, providing a thorough description of the peculiarities of BAN channel modeling. Firstly, a deep investigation of three different BAN channels is provided. This complete overview of the on-body, off-body and body-to-body channel modeling provides a strong knowledge base for further simulations. Similarly, the human blockage modeling, which is described in detail in following section, provides an insight into the main areas of the body blockage channel models. The last section of this chapter is dedicated to the BAN antennas, which are an essential part of the whole BAN channel modeling.

Utilizing the knowledge from Chapters 2, 3, and 4, a custom channel model was designed in Chapter 5. This model is based on the first order reflections ray tracing principle enhanced by the body shadowing function to more accurately simulate the off-body communication scenarios. The model itself was implemented in MATLAB to provide fast and accurate computations. Furthermore, the model was optimized and fitted to a log-distance pathloss formula to allow easy implementation into the simulation tools such as NS3. After the optimization process, the model was verified against three field measurement campaigns that were conducted by the best scientists in the field and their teams (e.g., prof. S.L.Cotton). This verification proved the accuracy of the proposed model, together with the need of having the pathloss parameters created for different simulation scenarios.

The successfully developed and verified model from the Chapter 5 was further implemented into the NS3 simulator in Chapter 6. Before the analysis of the developed model is presented, the detailed description of the NS3 mmWave module

is given, focusing on the core parts module, together with PHY, MAC, and RLC layers. Furthermore, a short overview of the advancements of the NS3 mmWave module enhancements proposed by the author of this thesis is given. Following these enhancements, the extension which is utilizing the developed indoor off-body channel model is laid out. The last section of the Chapter 6 is providing an in-depth description of plethora of simulations, which were carefully selected in order to provide a complete understanding of how the channel model parameters affect the channel. Based on these results, we can conclude that all the goals of this thesis were successfully accomplished.

As it was aforementioned in previous paragraph, the main goals of the thesis, were successfully completed. The key contributions are summarized as follows:

- The extensive overview and study of currently available and state-of-the-art high speed wireless BAN standards and technologies was performed.
- An in-depth analysis of currently utilized mmWave network standards were studied, with close attention given to the channel modeling sections.
- Creation of custom channel model, aimed at the simulation accuracy was performed. The developed channel model is offering not only higher accuracy, but also easy implementability into currently available network simulators.
- The developed model was further evaluated against currently available field measurements. Furthermore, its parameters were adjusted to provide even more accurate simulation.
- To improve the usability and user-friendliness, the model was implemented into the NS3 simulator.
- Utilizing the newly available model in the NS3, which was added in previous step, and extensive simulation of selected scenarios was performed. The results provided great insight into the influence of the rooms sizes, reflection coefficients and antenna position on the propagation loss and overall system performance.

Bibliography

- [1] “Cisco Visual Networking Index: Forecast and Trends, 2017–2022 White Paper,” 2018. Available at <https://www.cisco.com/c/en/us/solutions/collateral/service-provider/visual-networking-index-vni/white-paper-c11-741490.html>.
- [2] P. Masek, E. Mokrov, K. Zeman, A. Ponomarenko-Timofeev, A. Pyattaev, S. Nesterov, S. Andreev, J. Hosek, K. Samouylov, and Y. Koucheryavy, “A practical perspective on 5g-ready highly dynamic spectrum management with lsa,” *Wireless Communications and Mobile Computing*, vol. 2018, 2018.
- [3] J. Rantakokko, J. Rydell, P. Strömbäck, P. Händel, J. Callmer, D. Törnqvist, F. Gustafsson, M. Jobs, and M. Grudén, “Accurate and reliable soldier and first responder indoor positioning: multisensor systems and cooperative localization,” *IEEE Wireless Communications*, vol. 18, no. 2, pp. 10–18, 2011.
- [4] K. Zeman, P. Masek, J. Hosek, P. Dvorak, R. Josth, and T. Jankech, “Experimental evaluation of technology enablers for cutting edge wearables’ applications,” in *2016 8th International Congress on Ultra Modern Telecommunications and Control Systems and Workshops (ICUMT)*, pp. 89–93, IEEE, 2016.
- [5] K. Zeman, M. Stusek, J. Pokorny, P. Masek, J. Hosek, S. Andreev, P. Dvorak, and R. Josth, “Emerging 5G applications over mmWave: Hands-on assessment of WiGig radios,” in *2017 40th International Conference on Telecommunications and Signal Processing (TSP)*, pp. 86–90, IEEE, 2017.
- [6] T. S. Rappaport, J. N. Murdock, and F. Gutierrez, “State of the art in 60-GHz integrated circuits and systems for wireless communications,” *Proceedings of the IEEE*, vol. 99, no. 8, pp. 1390–1436, 2011.
- [7] H. T. Friis, “A note on a simple transmission formula,” *Proceedings of the IRE*, vol. 34, no. 5, pp. 254–256, 1946.
- [8] F. Gutierrez, S. Agarwal, K. Parrish, and T. S. Rappaport, “On-chip integrated antenna structures in CMOS for 60 GHz WPAN systems,” *IEEE Journal on Selected Areas in Communications*, vol. 27, pp. 1367–1378, October 2009.

- [9] Z. Pi and F. Khan, "A millimeter-wave massive MIMO system for next generation mobile broadband," in *2012 Conference Record of the Forty Sixth Asilomar Conference on Signals, Systems and Computers (ASILOMAR)*, pp. 693–698, Nov 2012.
- [10] S. Rajagopal, S. Abu-Surra, Z. Pi, and F. Khan, "Antenna Array Design for Multi-Gbps mmWave Mobile Broadband Communication," in *2011 IEEE Global Telecommunications Conference - GLOBECOM 2011*, pp. 1–6, Dec 2011.
- [11] T. S. Rappaport, S. Sun, R. Mayzus, H. Zhao, Y. Azar, K. Wang, G. N. Wong, J. K. Schulz, M. Samimi, and F. Gutierrez, "Millimeter Wave Mobile Communications for 5G Cellular: It Will Work!," *IEEE Access*, vol. 1, pp. 335–349, 2013.
- [12] E. Ben-Dor, T. S. Rappaport, Y. Qiao, and S. J. Lauffenburger, "Millimeter-Wave 60 GHz Outdoor and Vehicle AOA Propagation Measurements Using a Broadband Channel Sounder," in *2011 IEEE Global Telecommunications Conference - GLOBECOM 2011*, pp. 1–6, Dec 2011.
- [13] T. S. Rappaport, E. Ben-Dor, J. Murdock, and Y. Qiao, "38 GHz and 60 GHz angle-dependent propagation for cellular & peer-to-peer wireless communications," in *ICC*, pp. 4568–4573, 2012.
- [14] Y. Azar, G. N. Wong, K. Wang, R. Mayzus, J. K. Schulz, H. Zhao, F. Gutierrez, D. Hwang, and T. S. Rappaport, "28 GHz propagation measurements for outdoor cellular communications using steerable beam antennas in New York City," in *Communications (ICC), 2013 IEEE International Conference on*, pp. 5143–5147, IEEE, 2013.
- [15] M. Samimi, K. Wang, Y. Azar, G. N. Wong, R. Mayzus, H. Zhao, J. K. Schulz, S. Sun, F. Gutierrez, and T. S. Rappaport, "28 GHz angle of arrival and angle of departure analysis for outdoor cellular communications using steerable beam antennas in New York City," in *Vehicular Technology Conference (VTC Spring), 2013 IEEE 77th*, pp. 1–6, IEEE, 2013.
- [16] T. Rappaport, *Wireless communications: Principles and practice*. Prentice Hall communications engineering and emerging technologies series, Prentice Hall, 2nd ed., 2002. Includes bibliographical references and index.
- [17] M. Fryziel, C. Loyez, L. Clavier, N. Rolland, and P. A. Rolland, "Path-loss model of the 60-GHz indoor radio channel," *Microwave and optical technology letters*, vol. 34, no. 3, pp. 158–162, 2002.

- [18] S.-K. Yong, "TG3c channel modeling sub-committee final report," *IEEE802.15-06-0195-07-003c*, 2006.
- [19] T. S. Rappaport, R. W. Heath, R. C. Daniels, and J. N. Murdock, *Millimeter wave wireless communications*. 1 ed., 2015.
- [20] D. Rogers, "Propagation considerations for satellite broadcasting at frequencies above 10 GHz," *IEEE journal on selected areas in communications*, vol. 3, no. 1, pp. 100–110, 1985.
- [21] F. Giannetti, M. Luise, and R. Reggiannini, "Mobile and personal communications in the 60 GHz band: A survey," *Wireless Personal Communications*, vol. 10, no. 2, pp. 207–243, 1999.
- [22] H. Xu, V. Kukshya, and T. Rappaport, "Spatial and temporal characterization of 60 GHz channels," in *Proc. IEEE VTC'2000*, pp. 24–28, 2000.
- [23] H. Xu, T. S. Rappaport, R. J. Boyle, and J. H. Schaffner, "Measurements and models for 38-GHz point-to-multipoint radiowave propagation," *IEEE Journal on Selected Areas in Communications*, vol. 18, no. 3, pp. 310–321, 2000.
- [24] H. Zhao, R. Mayzus, S. Sun, M. Samimi, J. K. Schulz, Y. Azar, K. Wang, G. N. Wong, F. Gutierrez, and T. S. Rappaport, "28 GHz millimeter wave cellular communication measurements for reflection and penetration loss in and around buildings in New York city," in *2013 IEEE International Conference on Communications (ICC)*, pp. 5163–5167, June 2013.
- [25] T. S. Rappaport, F. Gutierrez, E. Ben-Dor, J. N. Murdock, Y. Qiao, and J. I. Tamir, "Broadband millimeter-wave propagation measurements and models using adaptive-beam antennas for outdoor urban cellular communications," *IEEE transactions on antennas and propagation*, vol. 61, no. 4, pp. 1850–1859, 2013.
- [26] S. Nie, G. R. MacCartney, S. Sun, and T. S. Rappaport, "72 GHz millimeter wave indoor measurements for wireless and backhaul communications," in *Personal Indoor and Mobile Radio Communications (PIMRC), 2013 IEEE 24th International Symposium on*, pp. 2429–2433, IEEE, 2013.
- [27] P. Smulders and A. Wagemans, "Wideband indoor radio propagation measurements at 58 GHz," *Electronics letters*, vol. 28, no. 13, pp. 1270–1272, 1992.

- [28] C. P. Ho, T. S. Rappaport, and M. P. Koushik, "Antenna effects on indoor obstructed wireless channels and a deterministic image-based wide-band propagation model for in-building personal communication systems," *International Journal of Wireless Information Networks*, vol. 1, no. 1, pp. 61–76, 1994.
- [29] T. Zwick, T. J. Beukema, and H. Nam, "Wideband channel sounder with measurements and model for the 60 GHz indoor radio channel," *IEEE transactions on Vehicular technology*, vol. 54, no. 4, pp. 1266–1277, 2005.
- [30] C. Lim, R. Burkholder, J. Volakis, and R. Marhefka, "Propagation modeling of indoor wireless communications at 60 ghz," in *Antennas and Propagation Society International Symposium 2006, IEEE*, pp. 2149–2152, IEEE, 2006.
- [31] L. M. Correia and J. R. Reis, "Wideband characterisation of the propagation channel for outdoors at 60 GHz," in *Proceedings of PIMRC '96 - 7th International Symposium on Personal, Indoor, and Mobile Communications*, vol. 2, pp. 752–755 vol.2, Oct 1996.
- [32] K. L. Blackard, M. J. Feuerstein, T. S. Rappaport, S. Y. Seidel, and H. H. Xia, "Path loss and delay spread models as functions of antenna height for microcellular system design," in *Vehicular Technology Conference, 1992, IEEE 42nd*, pp. 333–337, IEEE, 1992.
- [33] J. Meredith, "Study on channel model for frequency spectrum above 6 GHz," tech. rep., 3GPP TR 38.900, Jun, 2016.
- [34] M. R. Akdeniz, Y. Liu, M. K. Samimi, S. Sun, S. Rangan, T. S. Rappaport, and E. Erkip, "Millimeter Wave Channel Modeling and Cellular Capacity Evaluation," *IEEE Journal on Selected Areas in Communications*, vol. 32, pp. 1164–1179, June 2014.
- [35] W. Schafer and E. Lutz, "Propagation characteristics of short-range radio links at 60 GHz for mobile intervehicle communication," in *SBT/IEEE International Symposium on Telecommunications*, pp. 212–216, Sep. 1990.
- [36] T. S. Rappaport, S. DiPierro, and R. Akturan, "Analysis and simulation of interference to vehicle-equipped digital receivers from cellular mobile terminals operating in adjacent frequencies," *IEEE Transactions on Vehicular Technology*, vol. 60, no. 4, pp. 1664–1676, 2011.
- [37] A. Zajic, *Mobile-to-Mobile Wireless Channels*. Norwood, MA, USA: Artech House, Inc., 2013.

- [38] H. Yang, M. H. Herben, and P. F. Smulders, "Impact of antenna pattern and reflective environment on 60 GHz indoor radio channel characteristics," *IEEE Antennas and wireless propagation letters*, vol. 4, pp. 300–303, 2005.
- [39] M. Williamson, G. Athanasiadou, and A. Nix, "Investigating the effects of antenna directivity on wireless indoor communication at 60 GHz," in *Personal, Indoor and Mobile Radio Communications, 1997. Waves of the Year 2000. PIMRC'97., The 8th IEEE International Symposium on*, vol. 2, pp. 635–639, IEEE, 1997.
- [40] T. Manabe, Y. Miura, and T. Ihara, "Effects of antenna directivity on indoor multipath propagation characteristics at 60 GHz," in *Personal, Indoor and Mobile Radio Communications, 1995. PIMRC'95. Wireless: Merging onto the Information Superhighway., Sixth IEEE International Symposium on*, vol. 3, p. 1035, IEEE, 1995.
- [41] C. R. Anderson and T. S. Rappaport, "In-building wideband partition loss measurements at 2.5 and 60 GHz," *IEEE Transactions on Wireless Communications*, vol. 3, pp. 922–928, May 2004.
- [42] S. Y. Seidel and T. S. Rappaport, "Site-specific propagation prediction for wireless in-building personal communication system design," *IEEE transactions on Vehicular Technology*, vol. 43, no. 4, pp. 879–891, 1994.
- [43] G. Durgin, N. Patwari, and T. S. Rappaport, "An advanced 3D ray launching method for wireless propagation prediction," in *Vehicular Technology Conference, 1997, IEEE 47th*, vol. 2, pp. 785–789, IEEE, 1997.
- [44] R. R. Skidmore, T. S. Rappaport, and A. L. Abbott, "Interactive coverage region and system design simulation for wireless communication systems in multifloored indoor environments: SMT Plus," in *Universal Personal Communications, 1996. Record., 1996 5th IEEE International Conference on*, vol. 2, pp. 646–650, IEEE, 1996.
- [45] G. D. Durgin, T. S. Rappaport, and H. Xu, "Partition-based path loss analysis for in-home and residential areas at 5.85 GHz," in *Global Telecommunications Conference, 1998. GLOBECOM 1998. The Bridge to Global Integration. IEEE*, vol. 2, pp. 904–909, IEEE, 1998.
- [46] V. Degli-Esposti, G. Falciasacca, M. Frullone, G. Riva, and G. E. Corazza, "Performance evaluation of space and frequency diversity for 60 GHz wireless LANs using a ray model," in *Vehicular Technology Conference, 1997, IEEE 47th*, vol. 2, pp. 984–988, IEEE, 1997.

- [47] S. Seidel, K. Schaubach, T. Tran, and T. Rappaport, "Research in site-specific propagation modeling for PCS system design," in *Vehicular Technology Conference, 1993., 43rd IEEE*, pp. 261–264, IEEE, 1993.
- [48] H. Xu, V. Kukshya, and T. S. Rappaport, "Spatial and temporal characteristics of 60-GHz indoor channels," *IEEE Journal on selected areas in communications*, vol. 20, no. 3, pp. 620–630, 2002.
- [49] G. Allen and A. Hammoudeh, "Outdoor narrow band characterisation of millimetre wave mobile radio signals," in *Radiocommunications in the Range 30-60 GHz, IEEE Colloquium*, pp. 4–1, IET, 1991.
- [50] D. Dardari, L. Minelli, V. Tralli, and O. Andrisano, "Wideband indoor communication channels at 60 GHz," in *Personal Indoor and Mobile Radio Communications, 1996. PIMRC'96., Seventh IEEE International Symposium*, vol. 3, pp. 791–794, IEEE, 1996.
- [51] D. Polydorou, P. Babalis, and C. Capsalis, "Statistical characterization of fading in LOS wireless channels with a finite number of dominant paths. Application in millimeter frequencies," *International journal of infrared and millimeter waves*, vol. 20, no. 3, pp. 461–472, 1999.
- [52] G. D. Durgin, T. S. Rappaport, and D. A. De Wolf, "More complete probability density functions for fading in mobile communications," in *Vehicular Technology Conference, 1999 IEEE 49th*, vol. 2, pp. 985–989, IEEE, 1999.
- [53] G. D. Durgin, T. S. Rappaport, and D. A. De Wolf, "New analytical models and probability density functions for fading in wireless communications," *IEEE Transactions on Communications*, vol. 50, no. 6, pp. 1005–1015, 2002.
- [54] G. D. Durgin, *Space-time wireless channels*. Prentice Hall Professional, 2003.
- [55] S. A. Saberali and N. C. Beaulieu, "New expressions for TWDP fading statistics," *IEEE Wireless Communications Letters*, vol. 2, no. 6, pp. 643–646, 2013.
- [56] S. Sun and T. S. Rappaport, "Wideband mmwave channels: Implications for design and implementation of adaptive beam antennas," in *Microwave Symposium (IMS), 2014 IEEE MTT-S International*, pp. 1–4, IEEE, 2014.
- [57] S. Yong, "TG3c channel modeling sub-committee final report," 2007.
- [58] T. Baykas, C. Sum, Z. Lan, J. Wang, M. A. Rahman, H. Harada, and S. Kato, "IEEE 802.15.3c: the first IEEE wireless standard for data rates over 1 Gb/s," *IEEE Communications Magazine*, vol. 49, pp. 114–121, July 2011.

- [59] S.-K. Yong, P. Xia, and A. Valdes-Garcia, *60GHz Technology for Gbps WLAN and WPAN: from Theory to Practice*. John Wiley & Sons, 2011.
- [60] A. Maltsev, R. Maslennikov, A. Sevastyanov, A. Lomayev, and A. Khoryaev, "Statistical channel model for 60 GHz WLAN systems in conference room environment," in *2010 Proceedings of the Fourth European Conference on Antennas and Propagation (EuCAP)*, pp. 1–5, IEEE, 2010.
- [61] E. Hamida, "Wsnnet Simulator for Large Scale Wireless Sensor Networks," 2018. Available at <http://wsnet.gforge.inria.fr/>.
- [62] OpenSim Ltd.N, "OMNeT++ Discrete Event Simulator," 2018. Available at <https://omnetpp.org/>.
- [63] R. Technology, "Riverbed Modeler," 2018. Available at <https://www.riverbed.com/gb/products/steelcentral/steelcentral-riverbed-modeler.html>.
- [64] Nsnam, "The Network Simulator - NS-2," 2018. Available at http://nsnam.sourceforge.net/wiki/index.php/User_Information.
- [65] NS-3 Consortium, "NS-3 Simulator," 2018. Available at <https://www.nsnam.org/>.
- [66] "CORMORAN – Exploring ways to Improve Cooperation In and Between Wireless Body Area Networks (WBAN)," 2018. Available at <http://pylayers.github.io/pylayers/cormoran.html>.
- [67] I. PyLayers developer team, "Propagation and Localisation Simulator," 2018. Available at <http://pylayers.github.io/pylayers/>.
- [68] M. M. Alam, E. Ben Hamida, O. Berder, D. Menard, and O. Sentieys, "A Heuristic Self-adaptive Medium Access Control for Resource-constrained WBAN Systems," *IEEE Access*, vol. 4, pp. 1287–1300, 2016.
- [69] R. Technology, "Riverbed Modeler," 2018. Available at <https://support.riverbed.com/content/support/software/steelcentral-npm/modeler-index.html>.
- [70] E. Seven and A. CALHAN, "Priority Based Wireless Body Area Network with Cognitive Radio," *Balkan Journal of Electrical and Computer Engineering*, vol. 3, no. 4, 2015.

- [71] F. Aktas, C. Ceken, and Y. E. Erdemli, “IoT-based Healthcare Framework for Biomedical Applications,” *Journal of Medical and Biological Engineering*, 2017.
- [72] X.-P. Chen, K. Wu, L. Han, and F. He, “Low-cost High Gain Planar Antenna Array for 60-GHz Band Applications,” *IEEE transactions on Antennas and Propagation*, vol. 58, no. 6, pp. 2126–2129, 2010.
- [73] T. Zhang and N. Jaber, “Aeronautical Channel Simulation in Network Simulators for Incorporation into Opnet,” in *International Telemetry Conference Proceedings*, International Foundation for Telemetry, 2010.
- [74] S. R. Ramyah, “3D Visualization of UMTS/WLAN Integration Using Opnet Modeler,” *Wireless Sensor Network*, vol. 04, no. 12, pp. 281–285, 2012.
- [75] J. Mohorko, M. Fras, and S. Klampfer, “Advanced Modelling and Simulation Methods for Communication Networks,” *Microwave Review*, vol. 14, pp. 41–46, 2008. Available at <http://www.mwr.medianis.net/pdf/Vol14No1-09-JMohorko.pdf>.
- [76] X. Zhang, L. Zhao, and K. Liang, “Heterogeneous Control and Data Sub-network for Millimeter-wave Communications,” *China Communications*, vol. 12, pp. 58–66, Dec. 2015.
- [77] “Castalia,” 2018. Available at <https://github.com/boulis/Castalia>.
- [78] OMNeT++ team, “INET Framework,” 2018. Available at <https://inet.omnetpp.org/Introduction.html>.
- [79] O. Ltd., “OMNeT++ Simulation Models,” 2018. Available at <https://omnetpp.org/models/>.
- [80] M. Stehlik, “Comparison of Simulators for Wireless Sensor Networks,” Master’s thesis, Masaryk university, Faculty of informatics, 2011.
- [81] C. Pham, “A Video Sensor Simulation Model with Omnet++, Castalia Extension,” 2015. Available at <http://cpham.perso.univ-pau.fr/WSN-MODEL/wvsn-castalia.html>.
- [82] M. Nabi, M. Geilen, and T. Basten, “MoBAN: A Configurable Mobility Model for Wireless Body Area Networks,” in *Proceedings of the 4th International ICST Conference on Simulation Tools and Techniques*, SIMUTools ’11, (ICST, Brussels, Belgium, Belgium), pp. 168–177, ICST (Institute for Computer Sciences, Social-Informatics and Telecommunications Engineering), 2011. Available at <http://dl.acm.org/citation.cfm?id=2151054.2151088>.

- [83] J. Mahapatro, S. Misra, M. Manjunatha, and N. Islam, “Interference Mitigation between Wban Equipped Patients,” *Ninth International Conference on Wireless and Optical Communications Networks (WOCN)*, 2012.
- [84] W. Yue, C. Li, Y. Song, L. Yang, and X. Yuan, “WBAN on Ns-3: Novel Implementation with High Performance of IEEE 802.15.6,” *IEEE Wireless Communications and Networking Conference*, 2016.
- [85] M. Mezzavilla, S. Dutta, M. Zhang, M. R. Akdeniz, and S. Rangan, “5G mmWave Module for the NS-3 Network Simulator,” *Proceedings of the 18th ACM International Conference on Modeling, Analysis and Simulation of Wireless and Mobile Systems - MSWiM '15*, 2015.
- [86] “Lena,” 2018. Available at <http://networks.cttc.es/mobile-networks/software-tools/lena/>.
- [87] 3GPP, *Study on Channel Model for Frequency Spectrum above 6 Ghz*. 2017. Available at <https://portal.3gpp.org/desktopmodules/Specifications/SpecificationDetails.aspx?specificationId=2991>.
- [88] Altairhyperworks, “WinProp - Propagation Modeling,” 2018. Available at <https://altairhyperworks.com/product/FEKO/WinProp-Propagation-Modeling>.
- [89] S. Jaeckel, L. Raschkowski, K. Börner, and L. Thiele, “Quadriga: A 3-D Multi-cell Channel Model with Time Evolution for Enabling Virtual Field Trials,” *IEEE Transactions on Antennas and Propagation*, vol. 62, no. 6, pp. 3242–3256, 2014.
- [90] S. Zhang, X. Chen, I. Syrytsin, and G. F. Pedersen, “A planar switchable 3-D-coverage phased array antenna and its user effects for 28-GHz mobile terminal applications,” *IEEE Transactions on Antennas and Propagation*, vol. 65, no. 12, pp. 6413–6421, 2017.
- [91] M. Mezzavilla, M. Zhang, M. Polese, R. Ford, S. Dutta, S. Rangan, and M. Zorzi, “End-to-End Simulation of 5G mmWave Networks,” *CoRR*, vol. abs/1705.02882, 2017. Available at <http://arxiv.org/abs/1705.02882>.
- [92] Altair, “WinProp - Propagation Modeling,” 2019. Available at <https://altairhyperworks.com/product/Feko/WinProp-Propagation-Modeling>.
- [93] Remcom, “Wireless InSite,” 2019. Available at <https://www.remcom.com/wireless-insite-em-propagation-software>.

- [94] S. Alipour, F. Parvaresh, H. Ghajari, and F. K. Donald, "Propagation Characteristics for a 60 GHz Wireless Body Area Network (WBAN)," in *Military communications Conference, 2010-MILCOM 2010*, pp. 719–723, IEEE, 2010.
- [95] Ali, K. and Pellegrini, A. and Brizzi, A. and Hao, Y., "Full Wave and Ray - Based Analysis of a Body-centric Scenario at V Band," in *Proc. of EuCAP'13 - 7th European Conference on Antennas and Propagation*, pp. 780–783, Apr. 2013.
- [96] Brizzi, Alessio and Pellegrini, Alice and Zhang, Lianhong and Hao, Yang, "Statistical Path-loss Model for On-body Communications at 94 GHz," *IEEE Transactions on Antennas and Propagation*, vol. 61, no. 11, pp. 5744–5753, 2013.
- [97] N. Chahat, M. Zhadobov, R. Sauleau, and S. I. Alekseev, "New method for determining dielectric properties of skin and phantoms at millimeter waves based on heating kinetics," *IEEE Transactions on Microwave Theory and Techniques*, vol. 60, no. 3, pp. 827–832, 2012.
- [98] Y. I. Nechayev, X. Wu, C. C. Constantinou, and P. S. Hall, "Millimetre-wave Path-loss Variability between Two Body-mounted Monopole Antennas," *IET Microwaves, Antennas & Propagation*, vol. 7, no. 1, pp. 1–7, 2013.
- [99] Y. I. Nechayev, X. Wu, C. C. Constantinou, and P. S. Hall, "Effect of Body Motion on Propagation Path Gain at 60 GHz," in *6th European Conference on Antennas and Propagation (EUCAP)*, pp. 3397–3401, IEEE, 2012.
- [100] L. Petrillo, T. Mavridis, J. Sarrazin, A. Benlarbi-Delai, and P. De Doncker, "Statistical On-body Measurement Results at 60 GHz," *IEEE Transactions on Antennas and Propagation*, vol. 63, no. 1, pp. 400–403, 2015.
- [101] L. Petrillo, T. Mavridis, J. Sarrazin, D. Lautru, A. Benlarbi-Delai, and P. De Doncker, "Analytical Creeping Wave Model and Measurements for 60 GHz Body Area Networks," *IEEE transactions on antennas and propagation*, vol. 62, no. 8, pp. 4352–4356, 2014.
- [102] S. L. Cotton, Y. J. Chun, W. G. Scanlon, and G. A. Conway, "Path Loss Models for Indoor Off-body Communications at 60 GHz," in *IEEE International Symposium on Antennas and Propagation (APSURSI)*, pp. 1441–1442, IEEE, 2016.
- [103] S. K. Yoo, S. L. Cotton, Y. J. Chun, W. G. Scanlon, and G. A. Conway, "Channel Characteristics of Dynamic Off-Body Communications at 60 GHz

- Under Line-of-Sight (LOS) and Non-LOS Conditions,” *IEEE Antennas Wireless Propag. Lett.*, vol. 16, pp. 1553–1556, Feb. 2017.
- [104] S. K. Yoo and S. L. Cotton, “Composite Fading in Non-Line-of-Sight Off-Body Communications Channels,” in *Proc. of EuCAP’17 - 11th European Conference on Antennas and Propagation*, (Paris, France), Mar. 2017.
 - [105] S. K. Yoo, S. L. Cotton, R. W. Heath, and Y. J. Chun, “Measurements of the 60 GHz UE to eNB Channel for Small Cell Deployments,” *IEEE Wireless Commun. Lett.*, vol. 6, pp. 178–181, Apr. 2017.
 - [106] S. K. Yoo, S. L. Cotton, Y. J. Chun, and W. G. Scanlon, “Fading Characterization of UE to Ceiling-Mounted Access Point Communications at 60 GHz,” in *Proc. of EuCAP’18 - 12th European Conference on Antennas and Propagation*, (London, UK), Apr. 2018.
 - [107] T. Mavridis, L. Petrillo, J. Sarrazin, D. Lautru, A. Benlarbi-Delai, and P. De Doncker, “Near-Body Shadowing Analysis at 60 GHz,” *IEEE Trans. Antennas Propag.*, vol. 63, pp. 4505–4511, Oct. 2015.
 - [108] D. Kim, H. Lee, and J. Kang, “Comments on "Near-Body Shadowing Analysis at 60 GHz",” *IEEE Trans. Antennas Propag.*, vol. 65, pp. 3314–3314, June 2017.
 - [109] L. Petrillo, T. Mavridis, J. Sarrazin, A. Benlarbi-Delaï, and P. De Doncker, “Wideband Off-Body Measurements and Channel Modeling at 60 GHz,” *IEEE Antennas Wireless Propag. Lett.*, vol. 16, pp. 1088–1091, Oct. 2017.
 - [110] S. L. Cotton, W. G. Scanlon, and B. K. Madahar, “Millimeter-Wave Soldier-to-Soldier Communications for Covert Battlefield Operations,” *IEEE Commun. Mag.*, vol. 47, pp. 72–81, Oct. 2009.
 - [111] S. L. Cotton, W. G. Scanlon, and B. K. Madahar, “Simulation of Millimetre-Wave Channels for Short-Range Body to Body Communications,” in *Proc. of EuCAP’10 - 4th European Conference on Antennas and Propagation*, (Barcelona, Spain), Apr. 2010. Available at <http://ieeexplore.ieee.org/stamp/stamp.jsp?arnumber=5504917>.
 - [112] S. L. Cotton, W. G. Scanlon, and P. S. Hall, “A Simulated Study of Co-Channel Inter-BAN Interference at 2.45 GHz and 60 GHz,” in *Proc. of EuWIT’10 - 3rd European Wireless Technology Conference*, (Paris, France), Sept. 2010. Available at <http://ieeexplore.ieee.org/stamp/stamp.jsp?arnumber=5615120>.

- [113] M. Jacob, C. Mbianke, and T. Kürner, “A dynamic 60 GHz radio channel model for system level simulations with MAC protocols for IEEE 802.11ad,” in *IEEE International Symposium on Consumer Electronics (ISCE 2010)*, pp. 1–5, June 2010.
- [114] M. Peter, M. Wisotzki, M. Raceala-Motoc, W. Keusgen, R. Felbecker, M. Jacob, S. Priebe, and T. Kürner, “Analyzing human body shadowing at 60 GHz: Systematic wideband MIMO measurements and modeling approaches,” in *2012 6th European Conference on Antennas and Propagation (EUCAP)*, pp. 468–472, March 2012.
- [115] C. Gustafson and F. Tufvesson, “Characterization of 60 GHz shadowing by human bodies and simple phantoms,” in *2012 6th European Conference on Antennas and Propagation (EUCAP)*, pp. 473–477, March 2012.
- [116] M. Ghaddar, L. Talbi, T. A. Denidni, and A. Sebak, “A Conducting Cylinder for Modeling Human Body Presence in Indoor Propagation Channel,” *IEEE Transactions on Antennas and Propagation*, vol. 55, pp. 3099–3103, Nov 2007.
- [117] T. Mavridis, L. Petrillo, J. Sarrazin, D. Lautru, A. Benlarbi-Delaï, and P. De Doncker, “Theoretical and Experimental Investigation of a 60 GHz Off-Body Propagation Model,” *IEEE Trans. Antennas Propag.*, vol. 62, pp. 393–402, Jan. 2014.
- [118] T. Mavridis, L. Petrillo, J. Sarrazin, D. Lautru, A. Benlarbi-Delaï, and P. De Doncker, “Creeping Wave Model of Diffraction of an Obliquely Incident Plane Wave by a Circular Cylinder at 60 GHz,” *IEEE Trans. Antennas Propag.*, vol. 62, pp. 1372–1377, Mar. 2014.
- [119] “5G; Study on Channel Model for Frequencies from 0.5 to 100 GHz,” Tech. Rep. TR 138 901 V14.0.0, ETSI, Valbonne, France, May 2017. 3GPP TR 38.901 version 14.0.0 Release 14.
- [120] I. Syrytsin, S. Zhang, G. Pedersen, K. Zhao, T. Bolin, and Z. Ying, “Statistical investigation of the user effects on mobile terminal antennas for 5G applications,” *IEEE Transactions on Antennas and Propagation*, 2017.
- [121] X. Zhao, Q. Wang, S. Li, S. Geng, M. Wang, S. Sun, and Z. Wen, “Attenuation by human bodies at 26-and 39.5-GHz millimeter wavebands,” *IEEE Antennas and Wireless Propagation Letters*, vol. 16, pp. 1229–1232, 2016.

- [122] K. Zhao, J. Helander, D. Sjöberg, S. He, T. Bolin, and Z. Ying, “User Body Effect on Phased Array in User Equipment for the 5G mmWave Communication System,” *IEEE Antennas and Wireless Propagation Letters*, vol. 16, pp. 864–867, 2017.
- [123] J. D. Parsons, *The Mobile Radio Propagation Channel*. London, UK: John Wiley & Sons, 2 ed., 2000.
- [124] D. A. McNamara, C. W. I. Pistorius, and J. A. G. Malherbe, *Introduction to the Uniform Geometrical Theory of Diffraction*. Norwood, MA, USA: Artech House, 1990.
- [125] G. L. James, *Geometrical Theory of Diffraction for Electromagnetic Waves*. Electromagnetic Waves, Herts, UK: Institution of Engineering and Technology, 3 ed., 1986.
- [126] J. Kunisch and J. Pamp, “Ultra-Wideband Double Vertical Knife-Edge Model for Obstruction of a Ray by a Person,” in *2008 IEEE International Conference on Ultra-Wideband*, vol. 2, (Hannover, Germany), Sept. 2008.
- [127] M. Jacob, S. Priebe, A. Maltsev, A. Lomayev, V. Erceg, and T. Kürner, “A Ray Tracing Based Stochastic Human Blockage Model for the IEEE 802.11ad 60 GHz Channel Model,” in *Proc. of EuCAP’11 - 5th European Conference on Antennas and Propagation*, (Rome, Italy), Apr. 2011. Available at <http://ieeexplore.ieee.org/document/5782233/>.
- [128] L. Raschkowski, P. Kyösti, K. Kusume, and T. Jämsä, “METIS Channel Models, Deliverable 1.4 v.1.3,” techreport ICT-317669-METIS/D1.4, ICT-317669 METIS project, 2015. Available at https://www.metis2020.com/wp-content/uploads/METIS_D1.4_v3.pdf.
- [129] G. R. MacCartney, S. Deng, S. Sun, and T. S. Rappaport, “Millimeter-Wave Human Blockage at 73 GHz with a Simple Double Knife-Edge Diffraction Model and Extension for Directional Antennas,” in *Proc. of VTC’16-Fall - 84th IEEE Vehicular Technology Conference*, (Montreal, QC, Canada), Sept. 2016. Available at <https://arxiv.org/abs/1607.00226v3>.
- [130] W. Qi, J. Huang, J. Sun, Y. Tan, C. X. Wang, and X. Ge, “Measurements and Modeling of Human Blockage Effects for Multiple Millimeter Wave Bands,” in *Proc. of IWCMC’17 - 13th International Wireless Communications and Mobile Computing Conference*, (Valencia, Spain), June 2017.

- [131] F. Villanese, N. E. Evans, and W. G. Scanlon, "Pedestrian-Induced Fading for Indoor Channels at 2.45, 5.7 and 62 GHz," in *Proc. of VTC'00-Fall - 52th IEEE Vehicular Technology Conference*, vol. 1, (Boston, MA, USA), Sept. 2000.
- [132] B. R. Levy and J. B. Keller, "Diffraction by a Smooth Object," *Communications on Pure and Applied Mathematics*, vol. 12, pp. 159–209, Feb. 1959.
- [133] P. Pathak, W. Burnside, and R. Marhefka, "A Uniform GTD Analysis of the Diffraction of Electromagnetic Waves by a Smooth Convex Surface," *IEEE Trans. Antennas Propag.*, vol. 28, pp. 631–642, Sept. 1980.
- [134] M. Jacob, T. Priebe, S. and Kürner, M. Peter, M. Wisotzki, R. Felbecker, and W. Keusgen, "Fundamental Analyses of 60 GHz Human Blockage," in *Proc. of EuCAP'13 - 7th European Conference on Antennas and Propagation*, (Gothenburg, Sweden), Apr. 2013. Available at <http://ieeexplore.ieee.org/document/6546811/>.
- [135] M. Gapeyenko, A. Samuylov, M. Gerasimenko, D. Moltchanov, S. Singh, E. Aryafar, S.-p. Yeh, N. Himayat, S. Andreev, and Y. Koucheryavy, "Analysis of Human-Body Blockage in Urban Millimeter-Wave Cellular Communications," in *Proc. of ICC'16 - IEEE International Conference on Communications*, (Kuala Lumpur, Malaysia), May 2016. Available at <https://arxiv.org/pdf/1604.04743.pdf>.
- [136] K. Venugopal and R. W. Heath, "Millimeter Wave Networked Wearables in Dense Indoor Environments," *IEEE Access*, vol. 4, pp. 1205–1221, Mar. 2016.
- [137] B. Sanz-Izquierdo, L. Wu, J. C. Batchelor, and P. R. Young, "Textile integrated waveguide slot antenna," in *Antennas and Propagation Society International Symposium (APSURSI), 2010 IEEE*, pp. 1–4, IEEE, 2010.
- [138] B. Sanz-Izquierdo and J. C. Batchelor, "A dual band belt antenna," in *Antenna Technology: Small Antennas and Novel Metamaterials, 2008. iWAT 2008. International Workshop on*, pp. 374–377, IEEE, 2008.
- [139] B. Sanz-Izquierdo, J. C. Batchelor, and M. Sobhy, "UWB wearable button antenna," in *2006 First European Conference on Antennas and Propagation*, pp. 1–4, Nov 2006.
- [140] B. Sanz-Izquierdo, J. C. Batchelor, and M. Sobhy, "Button antenna on textiles for wireless local area network on body applications," *IET microwaves, antennas & propagation*, vol. 4, no. 11, pp. 1980–1987, 2010.

- [141] N. Ojaroudiparchin, M. Shen, G. Fr, *et al.*, “Multi-layer 5G mobile phone antenna for multi-user MIMO communications,” in *Telecommunications Forum Telfor (TELFOR), 2015 23rd*, pp. 559–562, IEEE, 2015.
- [142] B. Sanz-Izquierdo and S. Jun, “WLAN antenna on 3D printed bracelet and wrist phantom,” in *Antennas and Propagation Conference (LAPC), 2014 Loughborough*, pp. 372–375, IEEE, 2014.
- [143] S. Jun, B. Sanz-Izquierdo, and M. Summerfield, “UWB antenna on 3D printed flexible substrate and foot phantom,” in *Antennas & Propagation Conference (LAPC), 2015 Loughborough*, pp. 1–5, IEEE, 2015.
- [144] S. Jun, J. Heirons, and B. Sanz-Izquierdo, “Inkjet printed dual band antenna for paper UAVs,” in *Antennas and Propagation (EUCAP), 2017 11th European Conference on*, pp. 3452–3456, IEEE, 2017.
- [145] K. X. Wang and H. Wong, “A wideband CP millimeter wave antenna by using 3D printed technology,” in *Applied Computational Electromagnetics Society Symposium (ACES), 2017 International*, pp. 1–2, IEEE, 2017.
- [146] A. Vorobyov, J. R. Farserotu, and J.-D. Decotignie, “3D printed antennas for Mm-wave sensing applications,” in *Medical Information and Communication Technology (ISMICT), 2017 11th International Symposium on*, pp. 23–26, IEEE, 2017.
- [147] M. Fawaz, S. Jun, W. Oakey, C. Mao, A. Elibiary, B. Sanz-Izquierdo, D. Bird, and A. McClelland, “3D printed patch Antenna for millimeter wave 5G wearable applications,” 2018.
- [148] N. Ojaroudiparchin, M. Shen, S. Zhang, and G. F. Pedersen, “A switchable 3-D-coverage-phased array antenna package for 5G mobile terminals,” *IEEE Antennas and Wireless Propagation Letters*, vol. 15, pp. 1747–1750, 2016.
- [149] I. Syrytsin, S. Zhang, and G. F. Pedersen, “Finger Ring Phased Antenna Array for 5G IoT and Sensor Networks at 28 GHz,” in *12th European Conference on Antennas and Propagation European Conference on Antennas and Propagation*, 2018.
- [150] K. Sato, H. Kozima, H. Masuzawa, T. Manabe, T. Ihara, Y. Kasashima, and K. Yamaki, “Measurements of reflection characteristics and refractive indices of interior construction materials in millimeter-wave bands,” in *1995 IEEE 45th Vehicular Technology Conference. Countdown to the Wireless Twenty-First Century*, vol. 1, pp. 449–453 vol.1, July 1995.

- [151] K. Turbic, S. J. Ambroziak, and L. M. Correia, “A body-shadowing model for off-body and body-to-body communications,” in *2018 Baltic URSI Symposium (URSI)*, pp. 53–54, May 2018.
- [152] K. Zeman, J. Hosek, and L. M. Correia, “Designing Off-Body Propagation Channel Model for mmWave Indoor Communications,” *IEEE Access; Under the review (Submitted 07/2019)*, vol. XX, no. X, pp. 1–8, 2017.
- [153] M. Khatun, H. Mehrpouyan, and D. Matolak, “60-GHz Millimeter-Wave Pathloss Measurements in Boise Airport,” in *2018 IEEE Global Conference on Signal and Information Processing (GlobalSIP)*, pp. 1276–1280, Nov 2018.
- [154] S. K. Yoo, S. L. Cotton, R. W. Heath, and Y. J. Chun, “Measurements of the 60 GHz UE to eNB Channel for Small Cell Deployments,” *IEEE Wireless Communications Letters*, vol. 6, pp. 178–181, April 2017.
- [155] S. L. Cotton, Y. J. Chun, W. G. Scanlon, and G. A. Conway, “Path loss models for indoor off-body communications at 60 GHz,” in *2016 IEEE International Symposium on Antennas and Propagation (APSURSI)*, pp. 1441–1442, June 2016.
- [156] K. Zeman, P. Masek, M. Stusek, J. Hosek, and P. Silhavy, “Accuracy comparison of propagation models for mmWave communication in NS-3,” in *2017 9th International Congress on Ultra Modern Telecommunications and Control Systems and Workshops (ICUMT)*, pp. 334–340, Nov 2017.
- [157] K. Zeman, M. Stusek, P. Masek, J. Hosek, and J. Sedova, “Enhanced 3D Propagation Loss Model for mmWave Communications,” in *2018 10th International Congress on Ultra Modern Telecommunications and Control Systems and Workshops (ICUMT)*, pp. 1–7, IEEE, 2018.
- [158] K. Zeman, M. Stusek, P. Masek, and J. Hosek, “Improved NLOS Propagation Models for Wireless Communication in mmWave bands,” in *2018 8th International Conference on Localization and GNSS (ICL-GNSS)*, pp. 1–6, IEEE, 2018.
- [159] N. Guo, R. C. Qiu, S. S. Mo, and K. Takahashi, “60-GHz millimeter-wave radio: Principle, technology, and new results,” *EURASIP journal on Wireless Communications and Networking*, vol. 2007, no. 1, pp. 48–48, 2007.
- [160] J. B. Andersen, T. S. Rappaport, and S. Yoshida, “Propagation measurements and models for wireless communications channels,” *IEEE Communications Magazine*, vol. 33, pp. 42–49, Jan 1995.

- [161] C. Balanis, *Antenna theory*. Wiley-Interscience, 2016.

BIBLIOGRAPHY OF AUTHOR

- [1] K. Zeman, P. Masek, J. Hosek, P. Dvorak, R. Josth, and T. Jankech, “Experimental evaluation of technology enablers for cutting edge wearables’ applications,” in *2016 8th International Congress on Ultra Modern Telecommunications and Control Systems and Workshops (ICUMT)*, pp. 89–93, IEEE, 2016.
- [2] K. Zeman, P. Masek, M. Stusek, J. Hosek, and P. Silhavy, “Accuracy comparison of propagation models for mmwave communication in ns-3,” in *2017 9th International Congress on Ultra Modern Telecommunications and Control Systems and Workshops (ICUMT)*, pp. 334–340, Nov 2017.
- [3] K. Zeman, M. Stusek, J. Pokorny, P. Masek, J. Hosek, S. Andreev, P. Dvorak, and R. Josth, “Emerging 5g applications over mmwave: Hands-on assessment of wigg radios,” in *2017 40th International Conference on Telecommunications and Signal Processing (TSP)*, pp. 86–90, IEEE, 2017.
- [4] K. Zeman, M. Stusek, P. Masek, and J. Hosek, “Improved nlos propagation models for wireless communication in mmwave bands,” in *2018 8th International Conference on Localization and GNSS (ICL-GNSS)*, pp. 1–6, IEEE, 2018.
- [5] K. Zeman, M. Stusek, P. Masek, J. Hosek, and J. Sedova, “Enhanced 3d propagation loss model for mmwave communications,” in *2018 10th International Congress on Ultra Modern Telecommunications and Control Systems and Workshops (ICUMT)*, pp. 1–7, IEEE, 2018.
- [6] K. Zeman, J. Hosek, and L. M. Correia, “Designing Off-Body Propagation Channel Model for mmWave Indoor Communications,” *IEEE Access; Under the review (Submitted 07/2019)*, vol. XX, no. X, pp. 1–8, 2017.
- [7] P. Masek, E. Mokrov, K. Zeman, A. Ponomarenko-Timofeev, A. Pyattaev, S. Nesterov, S. Andreev, J. Hosek, K. Samouylov, and Y. Koucheryavy, “A practical perspective on 5g-ready highly dynamic spectrum management with lsa,” *Wireless Communications and Mobile Computing*, vol. 2018, 2018.

Abbreviations

3DNV 3D Network Visualized.

3GPP Third Generation Partnership Project.

AM Additive Manufacturing.

AM Acknowledged Mode.

AMC Adaptive Modulation and Coding.

AP Access Point.

AQM Active Queue Management.

AR Augmented Reality.

B2B Body to Body.

BAN Body Area Network.

BER Bit Error Rate.

BS Base Station.

COST European Cooperation in Science and Technology.

CQI Channel Quality Information.

CSMA/CA Carrier-Sense Multiple Access with Collision Avoidance.

CTO Czech Telecommunication Office.

DCE Direct Code Execution.

DCI Downlink Control Information.

DL Downlink.

ECG Electrocardiogram.

ECIT Electronics, Communications and Information Technology.

EEG Electroencephalography.

EIRP Equivalent Isotropically Radiated Power.

eNB Evolved Node B.

EPC Evolved Packet Core.

ETSI European Telecommunications Standards Institute.

FSPL Free Space Path Loss.

GCS Global Coordinate System.

GPS Global Positioning System.

GSM Global System for Mobile Communications.

GTD Geometrical Theory of Diffraction.

HARQ Hybrid Automatic Repeat Request.

HD High Definition.

IEEE Institute of Electrical and Electronics Engineers.

IP Internet Protocol.

ISM Industrial, Scientific and Medical.

ITU International Telecommunication Union.

KED Knife-Edge Diffraction.

LAN Local Area Network.

LENA LTE-EPC Network Simulator.

LOS Line of Sight.

LTE Long Term Evolution.

MAC Media Access Control.

MCS Modulation and Coding Scheme.

MI Mutual Information.

MIMO Multiple Input Multiple Output.

MPC Multipath Component.

MPL Mean Path Loss.

NLOS Non Line Of Sight.

NS3 Network Simulator 3.

NYU New York University.

OFDM Orthogonal Frequency Division Multiplexing.

OOBE Out of Band Emission.

PDCP Packet Data Convergence Protocol.

PHY Physical Layer.

PLE Pathloss Exponent.

POSIX Portable Operating System Interface.

QoE Quality of Experience.

RCS Radar Cross Section.

RF Radio Frequency.

RLC Radio Link Control.

RMS Root Mean Square.

RRC Radio Resource Control.

RTT Round Trip Time.

Rx Receiver.

SAP Service Access Point.

SINR Signal to Interference plus Noise Ratio.

SM Saturation Mode.
STA-AP Station-to-Access Point.
STA-STA Station-to-Station.

TB Transport Block.
TCP Transmission Control Protocol.
TCP/IP Transport Control Protocol/Internet Protocol.
TDD Time Division Duplex.
TDMA Time Division Multiple Access.
TM Transparent Mode.
TR Technical Report.
TTI Transmission Time Interval.
TWDP Two Wave with Diffuse Power.
Tx Transceiver.

UE User Equipment.
UHF Ultra High Frequency.
UL Uplink.
UM Unacknowledged Mode.
UMTS Universal Mobile Telecommunication System.
UTD Uniform Theory of Diffraction.

VNA Vector Network Analyzer.
VR Virtual Reality.

WAN Wide Area Network.
WBAN Wireless Body Area Network.
WLAN Wireless Local Area Network.
WSN Wireless Sensor Network.

List of appendices

A Attachments

98

A Attachments

On the attached DVD, the whole simulation data, together with all utilized scripts for MATLAB can be found. The archive structure is as follows:

```
/ ..... root folder of attached DVD
├── Campaigns ..... results from simulations of real-world measurements campaigns
│   ├── SmallCellDep1 ..... results data for Small Cell Deployments scenario
│   ├── Ecit ..... results data for Queen's University Belfast
│   └── Boise ..... results data for Boise Airport scenario
├── NS-3 ..... results from NS3 simulations
│   ├── 4x1x0608 ..... result for room 4x1 m with refl. coeff. between 0.6 and 0.8
│   ├── 4x2x0406 ..... result for room 4x2 m with refl. coeff. between 0.4 and 0.6
│   ├── 4x2x0608 ..... result for room 4x2 m with refl. coeff. between 0.6 and 0.8
│   ├── 10x3x0406 ..... result for room 10x3 m with refl. coeff. between 0.4 and 0.6
│   ├── 10x6x0608 ..... result for room 10x6 m with refl. coeff. between 0.6 and 0.8
│   ├── 20x6x0608 ..... result for room 20x6 m with refl. coeff. between 0.4 and 0.6
│   └── 20x12x0608 ..... result for room 20x12 m with refl. coeff. between 0.6 and 0.8
├── Scripts ..... developed MATLAB scripts
└── Simulation ..... results from MATLAB simulations
    ├── 0406 ..... data for reflection coefficients between 0.4 and 0.6
    │   ├── 4x1 ..... results for room size 4x1 m
    │   ├── 4x2 ..... results for room size 4x2 m
    │   ├── 10x3 ..... results for room size 10x3 m
    │   ├── 10x6 ..... results for room size 10x6 m
    │   ├── 20x6 ..... results for room size 20x6 m
    │   └── 20x12 ..... results for room size 20x12 m
    └── 0608 ..... data for reflection coefficients between 0.6 and 0.8
        ├── 4x1 ..... results for room size 4x1 m
        ├── 4x2 ..... results for room size 4x2 m
        ├── 10x3 ..... results for room size 10x3 m
        ├── 10x6 ..... results for room size 10x6 m
        ├── 20x6 ..... results for room size 20x6 m
        └── 20x12 ..... results for room size 20x12 m
```

Table 1: Distribution fitting results for the room size of 4x2m with reflection coefficients of 0.4-0.6 Part A

Y position [m]	Num_samples	Distribution	Parameters	Chi2_passed	Corr_passed	KS_passed	LogLik_order	AIC_order	Chi2_order	Corr_order	KS_order	Mean_data	Mean_fit	Error_means	Std_dev_data	Std_dev_fit	Error_Std_devs	Neg_LogLikLhood	AIC	Chi2_statistic	Chi2_crit_value	Chi2_pvalue	Significance	Corr	Corr_th	KS_statistic	KS_crit_value
0.125	3040	Normal	1;0.25	×	×	×	3	2	2	1	2	1.00	1.00	0.00	0.25	0.25	0.00	53.79	111.58	330.98	64.00	2.43E-44	0.05	0.89	0.95	0.05	0.02
	3040	Rayleigh	0.73	×	×	×	7	7	7	7	7	1.00	0.91	0.09	0.25	0.48	-0.23	1215.30	2432.61	2106.39	65.17	0	0.05	0.31	0.95	0.23	0.02
	3040	Logistic	1.01;0.15	×	×	×	5	5	5	5	1	1.00	1.01	-0.01	0.25	0.27	-0.02	162.57	329.15	504.37	64.00	6.72E-78	0.05	0.86	0.95	0.05	0.02
	3040	Stable	2;-0.99;0.17;1	×	×	×	2	3	3	2	3	1.00	1.00	1.26E-07	0.25	NaN	NaN	53.79	115.59	331.07	61.66	3.15E-45	0.05	0.89	0.95	0.05	0.02
	3040	Rice	0.97;0.25	×	×	×	1	1	1	3	4	1.00	1.00	-4.20E-06	0.25	0.25	5.76E-05	53.30	110.59	330.17	64.00	3.45E-44	0.05	0.88	0.95	0.05	0.02
	3040	Nakagami	4.14;1.06	×	×	×	4	4	4	4	5	1.00	1.00	0.00	0.25	0.25	0.00	69.42	142.85	358.48	64.00	5.47E-50	0.05	0.87	0.95	0.06	0.02
	3040	Lognormal	-0.14;1.16	×	×	×	6	6	6	6	6	1.00	1.00	0.00	0.25	0.27	-0.03	187.38	378.76	566.29	64.00	7.08E-92	0.05	0.81	0.95	0.08	0.02
0.25	3040	Normal	1;0.24	×	×	×	2	1	1	1	2	1.00	1.00	0.00	0.24	0.24	0.00	-34.10	-64.20	429.27	64.00	3.69E-63	0.05	0.83	0.95	0.06	0.02
	3040	Rayleigh	0.73	×	×	×	7	7	7	7	7	1.00	0.91	0.09	0.24	0.48	-0.24	1199.56	2401.12	2416.05	65.17	0	0.05	0.27	0.95	0.24	0.02
	3040	Logistic	1.01;0.14	×	×	×	5	5	5	5	1	1.00	1.01	-0.01	0.24	0.26	-0.02	78.53	161.07	611.72	64.00	2.48E-99	0.05	0.80	0.95	0.06	0.02
	3040	Stable	2;0.54;0.17;1	×	×	×	1	3	2	2	3	1.00	1.00	-1.38E-07	0.24	NaN	NaN	-34.10	-60.19	429.36	61.66	3.69E-64	0.05	0.83	0.95	0.06	0.02
	3040	Rice	0.97;0.24	×	×	×	3	2	3	3	4	1.00	1.00	-2.15E-06	0.24	0.24	4.84E-05	-33.98	-63.96	429.56	64.00	3.25E-63	0.05	0.83	0.95	0.06	0.02
	3040	Nakagami	4.36;1.06	×	×	×	4	4	4	4	5	1.00	1.00	0.00	0.24	0.24	0.00	-10.77	-17.54	469.10	64.00	1.88E-71	0.05	0.82	0.95	0.07	0.02
	3040	Lognormal	-0.14;1.13	×	×	×	6	6	6	6	6	1.00	1.00	0.00	0.24	0.26	-0.03	116.79	237.58	704.62	64.00	6.27E-120	0.05	0.76	0.95	0.09	0.02
0.375	3040	Normal	1;0.23	×	×	×	3	2	2	1	1	1.00	1.00	0.00	0.23	0.23	0.00	-94.90	-185.79	301.37	64.00	8.03E-39	0.05	0.89	0.95	0.05	0.02
	3040	Rayleigh	0.73	×	×	×	7	7	7	7	7	1.00	0.91	0.09	0.23	0.48	-0.24	1190.12	2382.24	2295.19	65.17	0	0.05	0.25	0.95	0.25	0.02
	3040	Logistic	1.01;0.14	×	×	×	5	5	5	5	4	1.00	1.01	0.00	0.23	0.25	-0.02	12.35	28.71	471.01	64.00	2.55E-71	0.05	0.86	0.95	0.05	0.02
	3040	Stable	2;1;0.17;1	×	×	×	2	3	3	2	2	1.00	1.00	7.17E-07	0.23	NaN	NaN	-94.90	-181.78	301.46	61.66	1.15E-39	0.05	0.89	0.95	0.05	0.02
	3040	Rice	0.97;0.24	×	×	×	1	1	1	3	3	1.00	1.00	-2.17E-06	0.23	0.23	4.78E-05	-95.18	-186.35	300.83	64.00	3.92E-39	0.05	0.89	0.95	0.05	0.02
	3040	Nakagami	4.57;1.06	×	×	×	4	4	4	4	5	1.00	1.00	0.00	0.23	0.24	0.00	-79.61	-155.22	324.85	64.00	4.71E-44	0.05	0.88	0.95	0.06	0.02
	3040	Lognormal	-0.13;1.09	×	×	×	6	6	6	6	6	1.00	1.00	0.00	0.23	0.26	-0.02	29.72	63.44	512.48	64.00	1.22E-81	0.05	0.84	0.95	0.08	0.02
0.5	3040	Normal	1;0.23	×	×	×	3	2	2	1	1	1.00	1.00	0.00	0.23	0.23	0.00	-199.14	-394.27	308.54	64.00	1.44E-40	0.05	0.90	0.95	0.05	0.02
	3040	Rayleigh	0.73	×	×	×	7	7	7	7	7	1.00	0.91	0.09	0.23	0.48	-0.25	1176.16	2354.31	2479.07	65.17	0	0.05	0.30	0.95	0.27	0.02
	3040	Logistic	1.01;0.14	×	×	×	5	5	5	5	4	1.00	1.01	0.00	0.23	0.25	-0.02	-93.18	-182.36	482.52	64.00	1.38E-73	0.05	0.86	0.95	0.05	0.02
	3040	Stable	2;1;0.16;1	×	×	×	2	3	3	2	2	1.00	1.00	-3.62E-07	0.23	NaN	NaN	-199.14	-390.26	308.62	61.66	1.97E-41	0.05	0.90	0.95	0.05	0.02
	3040	Rice	0.97;0.23	×	×	×	1	1	1	3	3	1.00	1.00	-1.24E-06	0.23	0.23	4.28E-05	-199.26	-394.51	308.21	64.00	1.66E-40	0.05	0.90	0.95	0.05	0.02
	3040	Nakagami	4.9;1.06	×	×	×	4	4	4	4	5	1.00	1.00	0.00	0.23	0.23	0.00	-183.16	-362.32	332.58	64.00	1.63E-45	0.05	0.89	0.95	0.06	0.02
	3040	Lognormal	-0.11;1.05	×	×	×	6	6	6	6	6	1.00	1.00	0.00	0.23	0.25	-0.02	-77.65	-151.29	514.06	64.00	5.87E-82	0.05	0.85	0.95	0.08	0.02
0.625	3040	Normal	1;0.22	×	×	×	2	1	1	1	2	1.00	1.00	0.00	0.22	0.22	0.00	-304.36	-604.71	291.76	64.00	4.75E-37	0.05	0.88	0.95	0.05	0.02
	3040	Rayleigh	0.73	×	×	×	7	7	7	7	7	1.00	0.91	0.09	0.22	0.48	-0.26	1161.05	2324.10	2685.67	65.17	0	0.05	0.16	0.95	0.27	0.02
	3040	Logistic	1.01;0.13	×	×	×	5	5	5	5	1	1.00	1.01	-0.01	0.22	0.24	-0.02	-200.91	-397.82	455.26	64.00	3.12E-68	0.05	0.85	0.95	0.05	0.02
	3040	Stable	2;0.95;0.15;1	×	×	×	1	3	2	2	3	1.00	1.00	-1.23E-07	0.22	NaN	NaN	-304.36	-600.70	291.83	61.66	7.06E-38	0.05	0.88	0.95	0.05	0.02
	3040	Rice	0.98;0.22	×	×	×	3	2	3	3	4	1.00	1.00	-5.29E-07	0.22	0.22	3.84E-05	-304.16	-604.31	292.16	64.00	4.01E-37	0.05	0.88	0.95	0.05	0.02
	3040	Nakagami	5.23;1.05	×	×	×	4	4	4	4	5	1.00	1.00	0.00	0.22	0.22	0.00	-283.86	-563.71	325.08	64.00	1.16E-43	0.05	0.87	0.95	0.06	0.02
	3040	Lognormal	-0.1;1.02	×	×</																						

Table 1: Distribution fitting results for the room size of 4x2m with reflection coefficients of 0.4-0.6

Y position [m]	Num_samples	Distribution	Parameters	Chi2_passed	Corr_passed	KS_passed	LogLik_order	AIC_order	Chi2_order	Corr_order	KS_order	Mean_data	Mean_fit	Error_means	Std_dev_data	Std_dev_fit	Error_Std_devs	Neg_LogLikLhood	AIC	Chi2_statistic	Chi2_crit_value	Chi2_pvalue	Significance	Corr	Corr_th	KS_statistic	KS_crit_value
1.125	3040	Normal	1.01;0.19	×	×	×	2	1	1	1	1	1.01	1.01	0.00	0.19	0.19	0.00	-799.27	-1594.53	171.83	64.00	1.04E-16	0.05	0.94	0.95	0.04	0.02
	3040	Rayleigh	0.72	×	×	×	7	7	7	7	7	1.01	0.91	0.10	0.19	0.47	-0.29	1109.59	2221.19	3495.47	65.17	0	0.05	0.18	0.95	0.33	0.02
	3040	Logistic	1.01;0.11	×	×	×	5	5	5	5	4	1.01	1.01	0.00	0.19	0.20	-0.01	-713.87	-1423.75	310.68	64.00	5.75E-41	0.05	0.91	0.95	0.05	0.02
	3040	Stable	2;-0.26;0.13;1.01	×	×	×	1	3	2	2	2	1.01	1.01	3.92E-07	0.19	NaN	NaN	-799.27	-1590.52	171.87	61.66	2.52E-17	0.05	0.94	0.95	0.04	0.02
	3040	Rice	0.99;0.19	×	×	×	3	2	3	3	3	1.01	1.01	6.58E-08	0.19	0.19	3.02E-05	-798.95	-1593.90	172.47	64.00	8.16E-17	0.05	0.94	0.95	0.04	0.02
	3040	Nakagami	7.29;1.05	×	×	×	4	4	4	4	5	1.01	1.01	0.00	0.19	0.19	0.00	-779.64	-1555.28	208.09	64.00	3.66E-23	0.05	0.93	0.95	0.05	0.02
	3040	Lognormal	-0.05;0.85	×	×	×	6	6	6	6	6	1.01	1.01	0.00	0.19	0.20	-0.01	-689.98	-1375.96	358.65	64.00	7.22E-52	0.05	0.91	0.95	0.07	0.02
1.25	3040	Normal	1;0.18	×	×	×	2	1	1	1	1	1.00	1.00	0.00	0.18	0.18	0.00	-967.52	-1931.04	172.77	64.00	1.79E-17	0.05	0.94	0.95	0.04	0.02
	3040	Rayleigh	0.72	×	×	×	7	7	7	7	7	1.00	0.90	0.10	0.18	0.47	-0.29	1071.60	2145.20	3833.78	65.17	0	0.05	0.33	0.95	0.34	0.02
	3040	Logistic	1;0.1	×	×	×	5	5	5	5	4	1.00	1.00	0.00	0.18	0.19	-0.01	-886.04	-1768.08	303.46	64.00	3.30E-39	0.05	0.92	0.95	0.05	0.02
	3040	Stable	2;1;0.12;1	×	×	×	1	3	2	2	2	1.00	1.00	4.97E-08	0.18	NaN	NaN	-967.52	-1927.03	172.80	61.66	4.12E-18	0.05	0.94	0.95	0.04	0.02
	3040	Rice	0.98;0.18	×	×	×	3	2	3	3	3	1.00	1.00	2.84E-08	0.18	0.18	2.88E-05	-967.31	-1930.62	173.34	64.00	1.43E-17	0.05	0.94	0.95	0.04	0.02
	3040	Nakagami	8.03;1.03	×	×	×	4	4	4	4	5	1.00	1.00	0.00	0.18	0.18	0.00	-951.55	-1899.09	199.42	64.00	2.41E-22	0.05	0.94	0.95	0.05	0.02
	3040	Lognormal	-0.08;0.8	×	×	×	6	6	6	6	6	1.00	1.00	0.00	0.18	0.19	-0.01	-873.99	-1743.98	368.10	64.00	3.20E-53	0.05	0.92	0.95	0.07	0.02
1.375	3040	Normal	1;0.16	×	✓	×	2	1	1	1	1	1.00	1.00	0.00	0.16	0.16	0.00	-1167.24	-2330.47	130.35	64.00	3.07E-11	0.05	0.96	0.95	0.03	0.02
	3040	Rayleigh	0.72	×	×	×	7	7	7	7	7	1.00	0.90	0.10	0.16	0.47	-0.30	1055.63	2113.27	4279.46	65.17	0	0.05	0.29	0.95	0.36	0.02
	3040	Logistic	1;0.1	×	×	×	5	5	5	5	5	1.00	1.00	0.0	0.16	0.17	-0.01	-1101.92	-2199.84	243.29	64.00	2.14E-29	0.05	0.94	0.95	0.04	0.02
	3040	Stable	2;0.99;0.12;1	×	✓	×	1	3	2	2	2	1.00	1.00	-6.82E-07	0.16	NaN	NaN	-1167.24	-2326.46	130.37	61.66	8.94E-12	0.05	0.96	0.95	0.03	0.02
	3040	Rice	0.99;0.17	×	✓	×	3	2	3	3	3	1.00	1.00	2.17E-08	0.16	0.16	2.70E-05	-1167.07	-2330.14	130.74	64.00	2.67E-11	0.05	0.96	0.95	0.04	0.02
	3040	Nakagami	9.17;1.03	×	✓	×	4	4	4	4	4	1.00	1.00	0.00	0.16	0.17	0.00	-1153.06	-2302.12	158.67	64.00	4.65E-16	0.05	0.96	0.95	0.04	0.02
	3040	Lognormal	-0.07;0.75	×	×	×	6	6	6	6	6	1.00	1.00	0.00	0.16	0.17	-0.01	-1083.19	-2162.38	284.07	64.00	4.15E-38	0.05	0.94	0.95	0.05	0.02
1.5	3040	Normal	1.01;0.15	×	×	×	2	1	2	2	2	1.01	1.01	0.00	0.15	0.15	0.00	-1416.41	-2828.82	180.65	64.00	8.88E-20	0.05	0.95	0.95	0.05	0.02
	3040	Rayleigh	0.72	×	×	×	7	7	7	7	7	1.01	0.91	0.10	0.15	0.47	-0.32	1067.87	2137.74	5031.77	65.17	0	0.05	0.04	0.95	0.38	0.02
	3040	Logistic	1.01;0.09	×	×	×	5	5	5	5	3	1.01	1.01	0.00	0.15	0.16	-0.01	-1344.02	-2684.04	301.52	64.00	5.85E-41	0.05	0.92	0.95	0.05	0.02
	3040	Stable	1.99;-1;0.11;1.01	×	×	×	1	3	1	1	1	1.01	1.01	0.00	0.15	NaN	NaN	-1416.64	-2825.26	179.55	61.66	2.87E-20	0.05	0.95	0.95	0.04	0.02
	3040	Rice	1;0.15	×	×	×	3	2	3	3	4	1.01	1.01	5.88E-08	0.15	0.15	2.46E-05	-1416.02	-2828.04	181.31	64.00	6.84E-20	0.05	0.95	0.95	0.05	0.02
	3040	Nakagami	10.96;1.04	×	×	×	4	4	4	4	5	1.01	1.01	0.00	0.15	0.15	0.00	-1393.02	-2782.03	219.11	64.00	6.18E-27	0.05	0.94	0.95	0.05	0.02
	3040	Lognormal	-0.01;0.68	×	×	×	6	6	6	6	6	1.01	1.01	0.00	0.15	0.16	-0.01	-1312.63	-2621.25	360.30	64.00	4.01E-54	0.05	0.92	0.95	0.07	0.02
1.625	3040	Normal	0.99;0.14	×	✓	×	2	1	1	1	1	0.99	0.99	0.00	0.14	0.14	0.00	-1639.27	-3274.53	135.52	64.00	1.37E-12	0.05	0.96	0.95	0.03	0.02
	3040	Rayleigh	0.71	×	×	×	7	7	7	7	7	0.99	0.89	0.10	0.14	0.46	-0.32	1000.14	2002.27	5314.32	65.17	0	0.05	0.26	0.95	0.40	0.02
	3040	Logistic	0.99;0.08	×	×	×	6	6	6	6	5	0.99	0.99	0.00	0.14	0.15	-0.01	-1574.36	-3144.71	256.85	64.00	1.22E-32	0.05	0.94	0.95	0.04	0.02
	3040	Stable	2;0.99;0.1;0.99	×	✓	×	1	3	2	2	2	0.99	0.99	1.47E-06	0.14	NaN	NaN	-1639.27	-3270.53	135.54	61.66	3.65E-13	0.05	0.96	0.95	0.03	0.02
	3040	Rice	0.98;0.14	×	✓	×	3	2	3	3	3	0.99	0.99	-1.09E-09	0.14	0.14	2.32E-05	-1639.26	-3274.51	135.57	64.00	1.35E-12	0.05	0.96	0.95	0.03	0.02
	3040	Nakagami	12.37;1	×	✓	×	4	4	4	4	4	0.99	0.99	7.95E-05	0.14	0.14	0.00	-1632.86	-3261.71	147.98	64.00	1.					

Ing. Krystof Zeman

Affiliation

Date of birth: 17.2.1991
Address: Domamysl 39, Czech Republic
E-mail: xzeman43@vutbr.cz
xzeman43@stud.feec.vutbr.cz
krystof.zeman@gmail.com
Tel: +420 541 146 964
+420 602 468 470
WWW: <https://www.vutbr.cz/lide/krystof-zeman-134671>
<https://www.linkedin.com/in/krystof-zeman-21615a96/>

QUALIFICATION AND PROFESSIONAL CAREER

Current position

2015–up to now Junior researcher with the Department of Telecommunications,
Faculty of Electrical Engineering and Communication (FEEC),
Brno University of Technology (BUT)

Qualification

2015–2019 (planned) Ph.D. in Teleinformatics, BUT, Doctoral thesis:
*Modeling of mmWave Propagation Channel for
Off-body Communication Scenarios*
2013–2015 MSc. in Telecommunication and Information Technology, BUT,
Diploma thesis: *Implementation of the Wireless M-Bus protocol
into the NS-3 simulation environment*
2010–2013 Bc. in Teleinformatics, BUT,
Bachelor thesis: *Designing desktop applications using the
windows workflow foundation library*

Professional career

2014–up to now Member of the research group WISLAB (Wireless System
Laboratory of Brno)
Link: <http://www.wislab.cz>
2013–up to now Junior researcher within the SIX Research Centre
Link: <http://www.six.feec.vutbr.cz/>

PROFESSIONAL ACTIVITIES

Specialization

Research and development in the area of ultra-high speed wireless
networks (Millimeter Wave), M2M / H2H communication, Industry 4.0,
next-generation (5G) networks, Internet of Things and energy
constrained devices

Author / co-author of experimental prototypes developed within the
contractual research for premier ICT companies (Konica Minolta,
Vodafone, Telekom Austria Group, etc.).

Scientific internships

Tampere University of Technology, Tampere, Finland, Ph.D. exchange
stay; (10/2014 – 11/2015)
Instituto Superior Tecnico, Lisbon, Portugal, Ph.D. exchange
stay; (4/2018 – 9/2018)

Membership in scientific and technical program

International Congress on Ultra-Modern Telecommunications and
Control Systems ICUMT (workshop chair, 2015 - up to now).

committee international conferences

Designated reviewer

- International Conference on Telecommunications and Signal Processing (WoS/Scopus, Conference)
- IEEE Wireless Communications Letters (IF: 2.449, Journal; ISSN: 2162-2337)

Teaching activities

- | | |
|-------------|---|
| 2015 – 2018 | Assistant lecturer, Computers and Programming 1 (laboratories, BUT) |
| 2015 – 2018 | Assistant lecturer, Computers and Programming 2 (laboratories, BUT) |

OTHER QUALIFICATIONS AND KNOWLEDGE

- | | |
|---------------------------|---------------------------------|
| Language knowledge | Czech language (native speaker) |
| | English language (level C1) |
| | German language (level A1) |

Certifications

- HCSP: Hillstone Certified Security Professional (Aug 2017)
- CCNA Exploration: LAN Switching and Wireless, Brno University of Technology, FEEC (May 2012)
- CCNA Exploration: Accessing the WAN, Brno University of Technology, FEEC (May 2012)
- CCNP ROUTE: Implementing IP Routing, Brno University of Technology, FEEC (December 2012)

Awards

- 1st Place at Inter-university Student Competition (MUNISS 2016). Topic: *Realization of Smart City Vision for City District Nový Liskovec*

RESEARCH PROJECTS

Project participant (selected projects)

- 29840 iAuto5 – 2017
- 26610 Smart Multi-Purpose Home Gateway 2.0 – proof of concept demonstrator 2015
- 28457 Vyzkum informacních a komunikačních systému a jejich bezpečnost
- 30854 Zarizení pro vzdálené odcety fyzikálních veličin

SELECTED PUBLICATIONS (2013 – 2017)

Selected publications in scientific journals with impact factor according to Web of Science

- MASEK, P.; HOSEK, J.; ZEMAN, K.; STUSEK, M.; KOVAC, D.; CIKA, P.; MASEK, J.; ANDREEV, S.; KROPFL, F. Implementation of True IoT Vision: Survey on Enabling Protocols and Hands-on Experience. *International Journal of Distributed Sensor Networks*, 2016, vol. 2016, no. 4, p. 1-18. ISSN: 1550-1329. (VaV ID 122369)
- MALEK, P.; MOKROV, E.; ZEMAN, K.; PONOMARENKO-TIMOFEEV, A.; PYATTAEV, A.; NESTEROV, S.; ANDREEV, S.; HOLÉK, J.; SAMOUYLOV, K.; KOUCHERYAVY, Y. A Practical Perspective on 5G-Ready Highly Dynamic Spectrum Management with LSA. *Wireless Communications and Mobile Computing*, 2018, vol. 2018, no. 1, p. 1-9. ISSN: 1530-8677. (VaV ID 148947)

SELECTED PRODUCTS (2013 – 2017)

- MASEK, P.; STUSEK, M.; ZEMAN, K.; MASEK, J.; KREJCI, J.; HOSEK, J.: G-WMBUS-02; Univerzální testovací zařízení pro přenos Wireless M-BUS dat. T12, SE5.118.. URL: <http://wislab.cz/our-work/universal-tester-for-wireless-m-bus-data-transmissions>. (prototyp) <http://wislab.cz/our-work/universal-tester-for-wireless-m-bus-data-transmissions>.
- ZEMAN, K.; STUSEK, M.; POKORNY, J.; MASEK, P.; HOSEK, J.: Home 4.0; Voice-assisted Smart Home within the Internet of Things Platform. Kancelář SE5.124, Technická 12, 616 00 Brno. URL: <http://www.wislab.cz>. (funkční vzorek) <http://www.wislab.cz>
- MASEK, P.; STUSEK, M.; ZEMAN, K.; MASEK, J.; KREJCI, J.; HOSEK, J.: R-WMBUS-01; Generator M2M dat bezdrátového komunikačního protokolu Wireless M-BUS v sítích SmartGrid. T12, SE5.118. URL: <http://wislab.cz/our-work/m2m-data-generator-utilizing-communication-protocol-wireless-m>

bus-within-the-smartgrid-infrastructure. (software) <http://wislab.cz/our-work/m2m-data-generator-utilizing-communication>

- HOSEK, J.; MASEK, P.; KOVAC, D.; CIKA, P.; STUSEK, M.; ZEMAN, K.: OSGi Smart Hub 1.0; OSGi-based Smart Hub Platform. Ustav Telekomunikaci, Technicka 12, Brno.
URL: <http://wislab.cz/our-work/>. (software) <http://wislab.cz/our-work/>

SUMMARY OF PUBLICATION ACTIVITIES

- Scientific journals with impact factor according to Web of Science: **2**
- International conferences indexed in Web of Science or Scopus: **14**
- Total number of citations according to Web of Science: **26**
- Total number of citations according to Scopus: **62**
- H-index according to Scopus: **4**
- H-index according to Web of Science: **3**
- Number of released products: **4**

REFERENCES

Prof. Luis M. Correia

Vice-President of IST; Coordinating Researcher of INOV-INESC
Department of Electrical and Computer Engineering (DEEC)
Av. Rovisco Pais 1, 1049-001 Lisboa, Portugal
Email: luis.m.correia@tecnico.ulisboa.pt

Prof. Yevgeni Koucheryavy

Head of W.I.N.T.E.R research lab & Senior IEEE Member
Department of Electronics and Communication Engineering
Tampere University of Technology, Korkeakoulunkatu 1, 33720
Email: yk@cs.tut.fi